Self-Assembly of Lyotropic Chromonic Liquid Crystal Mixtures

by

Akihiro Yamaguchi

Department of Physics

Primary Thesis Advisor

Noel A. Clark | Department of Physis

Committee Members

John P. Cumalat | Department of Physics

David M. Walba | Department of Chemistry and Biochemistry

University of Colorado at Boulder

October 2015

Abstract

Molecular self-assembly in the formation of lyotropic chromonic liquid crystals (LCLCs) offers potential for generating novel materials and biomedical applications, because of their similarity to DNA liquid crystals. In order to better understand the phase behavior of LCLCs, we investigated the mixture of two LCLCs (Sunset Yellow FCF (SSY) and disodium cromoglycate (DSCG)). Properties of interest include orientational and positional order as well as the potential dependence of LC phases on concentration and temperature. These mixtures exhibited nematic and columnar phases.

Keywords: Liquid crystals (LCs), lyotropic chromonic liquid crystals (LCLCs), Sunset Yellow FCF (SSY), disodium cromoglycate (DSCG), self-assembly, orientational template effect

Acknowledgements

I would like to thank all the people who provided me great supports and advice for
my work and life at the University of Colorado Boulder.
This work could never have accomplished without your help and kindness.

Professor Noel A. Clark, Dr. Youngwoo Yi, Greg Smith
Professor Joseph Maclennan
Professor Matthew Glaser
Professor David M. Walba
Artuhr Klittnick
Annett Baumgartner, Dakota Nanton, Lauren Moreno
University of Colorado Boulder and Soft Materials Research Group

Professor Jun Ye, Professor John Cumalat, Professor James K. Thompson
Professor Steven Pollock
Martin Black, Marilyn Ratcliff Mensing, Kristen Apodaca
University of Colorado Boulder

Charles Xu, Silvia Biffi, Francesca Serra, and Professor Tommasso Bellini
Colleagues in SSY and DSCG mixture work

Justin Latici, Daniel Johnston, Scott Holman, Dr. Adriane Genette

People in Writing Center

Dr. Mochizuki Akihiro, Dr. Le Van Khoa

And my friends and family

Contents

List of Figures

List of Tables

List of Abbreviations and Symbols

LC ………………….…... Liquid Crystal

LLC……………………..Lyotropic Liquid Crystal

LCLC …………………..Lyotropic Chromonic Liquid Crystal

SSY ………….................Sunset Yellow FCF

DSCG ……….…………. Disodium Cromoglycate

DNA …………..……….Deoxyribonucleic Acid

LD ……………..……… Linear Dichroism

UV-Vis microscopy …….Ultra-Violet – Visible microscopy

DTLM ……………......... Depolarized Transmitted Light Microscopy

TPD ……………............Ternary Phase Diagram

a.u. ……………………...Arbitrary Unit

I ……………….............. Isotropic

N ……………….............Nematic

N_S ……………….……. SSY-rich Nematic

N_D ……………….............DSCG-rich Nematic

C or M ………………….Columnar

c_S ……………….…….. Weight Concentration (wt%) of SSY

c_D ……………….............Weight Concentration of DSCG

c_W ……………….............. Weight Concentration of water

S ……………….............. Scalar Order Parameter

$A_{//}$…….Absorption (when the direction of the analyzer and that of the aggregates are parallel)

$A_{\perp}$…….Absorption (when the direction of the analyzer and the aggregates are perpendicular)

Chapter 1

Introduction

Molecular self-assembly in the formation of lyotropic liquid crystals (LLCs) is of particular interest because of its potential in generating novel materials and biomedical applications [1]. While the study of LLCs has a potential of developing a novel drug delivery system as a therapeutic agent, studying lyotropic chromonic liquid crystals (LCLCs) also has a potential to deepen basic scientific interests, such as the formation of the primordial form of biological information carriers like DNA by studying the similarities between DNA LCs and LCLCs [2,3]. Therefore, the process of self-assembly in LC systems has been widely studied due to its relevance in a wide range of areas in science.

The primary focus of this project is to better understand the behavior of self-assembly of disk-like molecules in LCs under various conditions. This project is potentially relevant to DNA LCs because both chromonics and DNA are the same type of LCs called lyotropic chromonic LCs. Therefore, if the mixture of LCLCs are able to form long aggregates, this novel LC is expected to advance our understanding of the DNA-like LCs.

In order to better understand the mechanisms of molecular self-assembly in LC phases, extensive studies of LC systems are necessary. While the molecular behaviors of pure LCLC phases have been extensively studied (especially Sunset Yellow FCF (SSY) and disodium cromoglycate (DSCG) [4–11]), no study has yet shown the molecular interaction between two LCLCs when they are mixed in water. Therefore, the study of the molecular interaction between two LCLCs is expected to provide with new insights into the process of molecular self-assembly.

This thesis describes the experiments with the mixture of two LCLCs in water. Further analysis and additional experiments are also described. This chapter provides background information about LC systems in general and the features of LCLCs in particular. Chapter 2 explains the theoretical background necessary for studying LC systems. Chapter 3 provides background for the two LCLCs (SSY and DSCG) used in this study. Experimental methods and the results are described in chapter 4 and 5, respectively. Chapter 6 discusses the results of the observations, and Chapter 7 describes the conclusion of this project.

1.1 Background

This section introduces the basic physical backgrounds that help to explain the primary experimental methods used throughout the project and introduces the basics of LCs and LCLCs.

1.1.1 Polarization of Light and Birefringence

Throughout the project, LCs and their phase behaviors were observed visually with a depolarized transmitted light microscopy (explained more fully in Sec. 4.4), which uses the polarization effect of light and the unique optical property of the LCs called birefringence. This optical property is the basis of most visual observations of LCs, and is therefore very important for the study of molecular behavior in LCs. Thus, it is important to understand *polarization of light* and *birefringence* in order to understand the relationship between the observed phases and the behaviors of molecules.

Polarization of Light

The phenomena of polarization depends on the fact that the light is described as a vector field, or an oscillating electric field. This vector field oscillates in a plane perpendicular to the direction of propagation, and the direction of oscillation can be described as a vector field that has a direction of x- and y-components, as shown in Fig. 1.1.
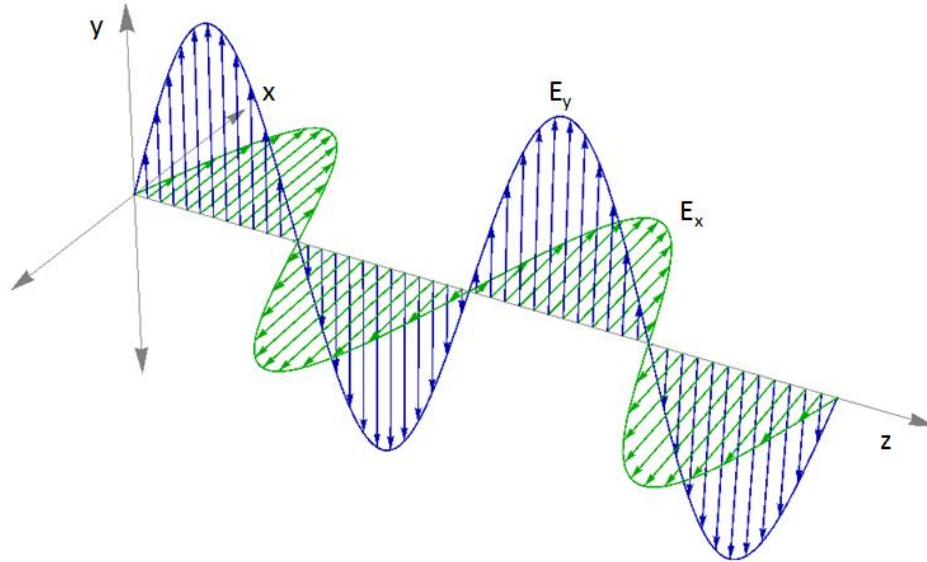
Fig. 1.1 Light is considered a transverse wave of an electric field oscillating in a direction (x- and y-axis) perpendicular to the direction of propagation (z-axis). Since the xy-plane is always perpendicular to the direction of propagation, the light can oscillate in any direction on the xy-plane.

Since an electron experiences Lorentz Force under the electric field, the oscillating electric field affects the motion of the substance as the field propagates. Moreover, the transmitted electric field is also affected by the motion of the electron. Therefore, depending on the structure of the molecule, the electron in the substance responds more easily to oscillation in a direction parallel to the axis of the molecules than the electron would respond if the electric field (light) tried to push the electron at right angles to the molecular axis. This direction of the axis of the molecule is called the optical axis (Fig. 1.2).

When the light is transmitted through a polarizing material, which is composed of ordered unsymmetrical molecules, the direction of oscillation of the electric field transmitted through the polarizer is limited in the direction of the optical axis of the material. When the electric field oscillates on a straight line along with the optical axis of the polarizer, the light is called linearly polarized (Fig. 1.3).

Asymmetric molecules

Optical Axis
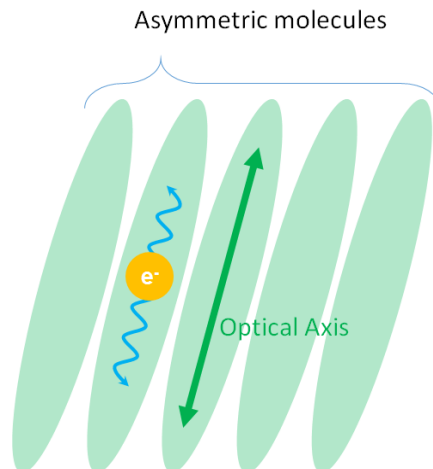
Fig. 1.2 Molecular model of birefringent substances composed of asymmetric molecules. The electron in a molecule (represented by a yellow circle) responds more easily to the external electric field (i.e., light) in a direction parallel to the axis of the molecule.

Polarizer (Vertical)
Analyzer (Horizontal)
Incident Light (Unpolarized)
Linearly Polarized Light (Vertical)
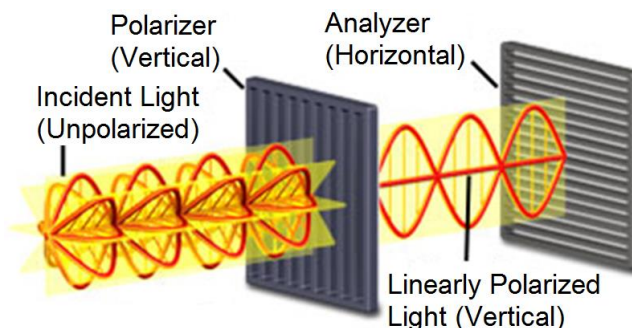
Fig. 1.3 Unpolarized incident light is linearly polarized by the polarizer in the direction of the optical axis. The transmitted light is oscillating only in the linear direction parallel to the direction of the polarizer. If there is another polarizer (called *analyzer* to distinguish 1st and 2nd polarizer), in which the direction of polarization is perpendicular to that of the polarizer, then no light will be transmitted after the analyzer.
(Figure is obtained and modified from https://www.microscopyu.com/articles/polarized/polarizedlightintro.html)

Furthermore, there are substances for which the index of refraction is different for linearly polarized light in one direction and linearly polarized light in a different direction. Such a substance is called birefringent and has two or more indices of refractions or refrangibilities. Birefringent substances can polarize the incident light depending on the direction of the molecules that constitute the birefringent substance.

A cubic crystal with the symmetry of a cube cannot be birefringent because of a lack of asymmetry. However, crystals composed of well-ordered asymmetric (or long needlelike)

molecules can be birefringent. This phenomena is easily observed in a calcite crystal, as shown in Fig. 1.4 (a).
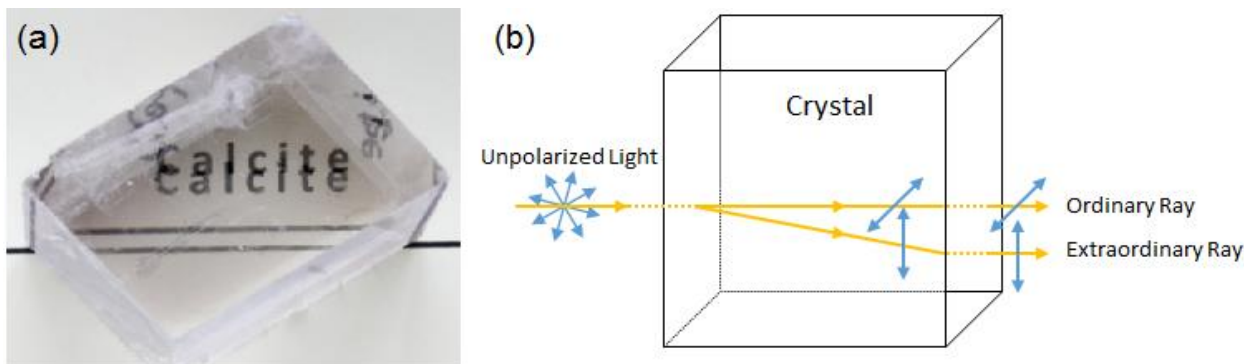
Fig. 1.4 (a) A calcite crystal showing birefringence. The light transmitted through a crystal is polarized in two orthogonal directions both parallel and perpendicular to the optical axis of the crystal, and we see two images as shown. (b) Each polarized light is called *ordinary ray* or *extraordinary ray*, corresponding to the polarization components perpendicular and not perpendicular to the optical axis.
(The figure of a calcite is obtained from http://www.newvisiondisplay.com/re_polarization.html)

Since the intensity and color of transmitted light depends on the birefringent substance that transmits light, the observation of transmitted light enables us to determine the macroscopic molecular ordering of the substance. The next section describes how LCs can become birefringent and the method for determining the macroscopic molecular ordering in LC phases.

1.1.2   Liquid Crystals

The LC phase, also called the mesomorphic phase, is an intermediate phase of matter between isotropic liquids (i.e., molecules with no preferred orientation) and crystalline solids (i.e., molecules with both orientational and positional ordering) (Fig. 1.5 (b)). LCs are ordered fluids formed by anisotropic objects, such as elongated or disk-like molecules. LCs can flow like liquids, but their molecules or stacks of molecules exhibit some degree of ordering in their arrangement [12,13].
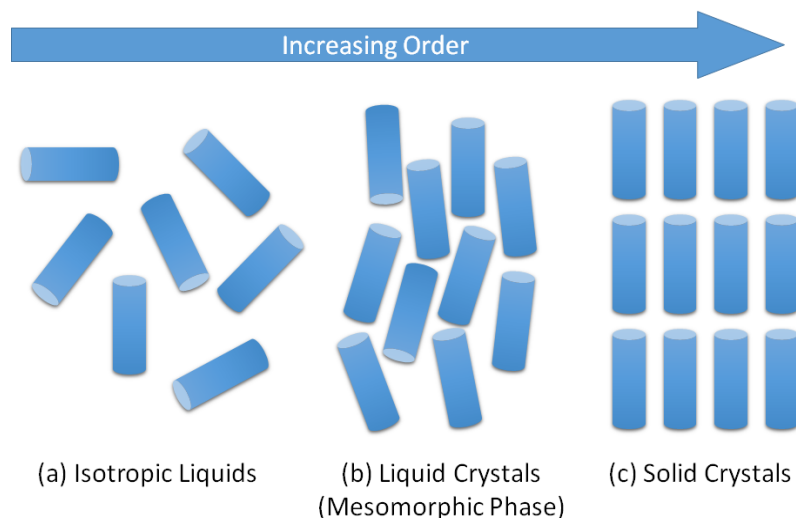
Fig. 1.5 Schematics of three distinct phases of matter. Blue rod represents asymmetric molecules. (a) The isotropic liquid has no order. If the molecules have no preferred orientation, such a substance is called isotropic. (b) The liquid crystal (mesomorphic phase) distinguishes itself from other phases because they have fluidity but also an ordered structure (orientational and/or positional orders). (c) The solid crystal has orientational and positional order but no fluidity.
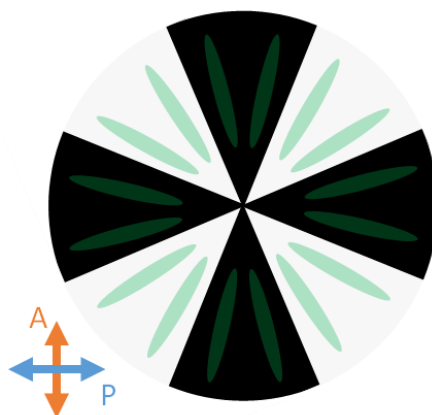
Fig. 1.6 Model of a LC domain and composing molecules. The arrows on the lower left represent the direction of the analyzer and polarizer.

By observing the intensity of the transmitted light through the crossed analyzer and polarizer, the direction of the molecules in LCs can be macroscopically determined. For example, if a set of molecules form a LC domain in which the molecules are radially oriented, we observe a circular domain with four brushes of dark and bright regions, as shown in Fig. 1.6. In the dark regions, the molecules are aligned either parallel or perpendicular to the direction of the analyzer or polarizer. Similarly, the bright regions indicate that the molecules are not aligned well to the direction of the analyzer or polarizer.

6

In addition, there are several types of LCs that depend on the structure of the constituent molecules and several LC phases that depend on the ordering of the molecules. The next section introduces one type of LC studied in this project.

1.1.3 Lyotropic Chromonic Liquid Crystals (LCLCs)

As briefly mentioned in the previous section, the structure of the constituent molecules creates various types of LCs. There are mainly two types of LCs, classified as *thermotropic* and *lyotropic* LCs. As the term implies, thermotropic LCs consist of pure or mixed substances that exhibit various LC phases that depend only on temperature. In contrast, LLCs consist of one or more substances known as mesogens[1] and solvents such as water. In addition, LLCs exhibit LC phases that depend on both the temperature and the ratio of constituent substances (Fig. 1.7).

Lipid bilayers[2] are one of the well-known substances that form LLCs. Moreover, many *disk-like* or *plank-like* molecules are also known to form LLCs, and the LLCs composed of disk-like molecules are called Lyotropic Chromonic Liquid Crystals (Fig. 1.7). LCLCs' fluidic but ordered structure of molecules in water is very similar to biological cell membranes and many other biological systems. Furthermore, DNA also exhibits LC phase as a LCLC and there are many similarities between DNA and other LCLC materials. Therefore, LCLCs have been extensively studied due to their potential in biomedical applications [1,12].

---

[1] a compound or the fundamental unit of LCs that induces structural ordering
[2] a biomaterial that constitutes cell membranes
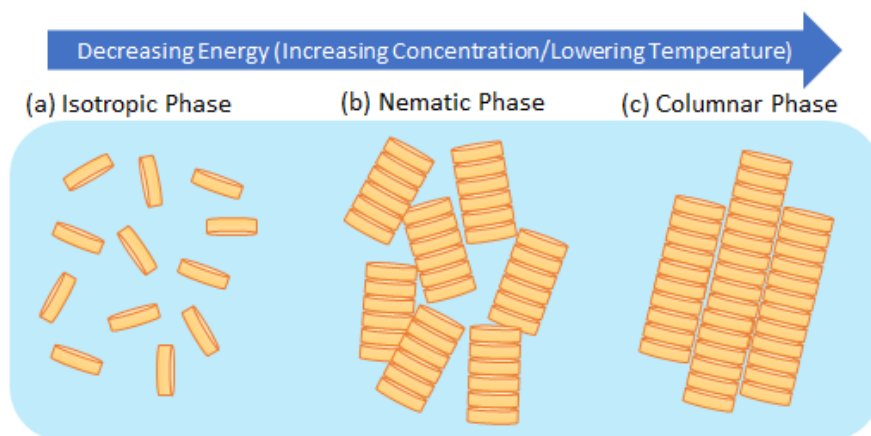
Fig. 1.7 Typical structures of LCLC phases. (a) In the isotropic phase, the molecules are randomly oriented due to the low concentration of molecules or high thermal energy. Therefore, the substance has no birefringence. (b) In the nematic phase, the concentration of molecules in a solvent is higher or the thermal energy is lower than that in the isotropic phase. The molecules start forming aggregates and the aggregates tend to be orientationally ordered but not positionally ordered. Therefore, the mixture of mesogens and solvent has birefringence, and this phase can be visually observed under a polarizing microscope. In the columnar phase (c), molecules have both orientational and positional order and the mixture is birefringent.

LCLCs exhibit three types of phases called the isotropic phase (I), nematic phase (N), and columnar phase (C) (also known as middle phase (M)). These phases are formed depending on the degrees of positional and/or orientational ordering of the molecules that are influenced by the concentration of molecules and thermal condition. In the isotropic phase, molecules have random motion, and neither long-range positional nor orientational ordering. In the nematic phase, molecules have orientational, but not positional ordering. In the columnar phase, molecules have both positional and orientational ordering. These structures and observed phases are schematically shown in Figures 1.7 and 1.8.
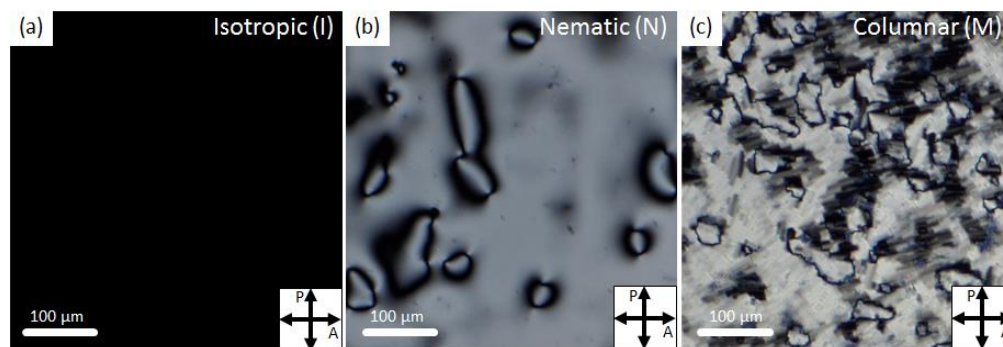
Fig. 1.8 Micrographs of typical LCLC phases. (a) Isotropic (I), (b) nematic (N), and (c) columnar phase (C) are observed under a polarized microscope. The arrows on the lower right corner represents the direction of polarizer and analyzer.

The LCLC phases are visually determined by the observation of the texture. For example, the substance is classified as isotropic phase if no birefringence is observed under a crossed polarizer and analyzer as shown in Fig. 1.8 (a). On the other hand, the phase is considered a nematic phase if a texture called *Schlieren texture*[3] is observed under the crossed polarizer and analyzer, as we can see in Fig. 1.8 (b). The columnar phase is birefringent, but this phase does not have Schlieren texture and usually has smaller domains, or the texture is more rigid than that in the nematic phase.

1.2 Goals

The primary goals of this project is to advance the understanding of the behavior of self-assembly of disk-like molecules in LCLCs. In order to achieve this goal, we study the optical properties and phase behaviors of a mixture of two LCLCs (the food dye SSY and the anti-asthmatic drug DSCG). In order to understand the molecular self-assembly of LCs in further detail, we observe optical textures and dichroism of LCLC mixtures and measure the order parameters of LCs.

---

[3] the singular points called noyaux (or node) are connected by black stripes, showing the regions where the optical axis is parallel to either polarizer or analyzer, and the general texture resulting from those points

Chapter 2

Theoretical Background

In order to qualitatively understand the behavior of molecules in LC phases, such as the orientational and positional orderings of the molecules, mathematical representation of the molecular orderings is necessary because it generalizes the molecular configuration. In addition, understanding the correlation between the molecular behavior and the concentration of the molecules in a solvent is essential because the LCLC molecules change their configurations or behaviors depending on their concentration in water.

This chapter provides a theoretical background of the mathematical representation of molecular orderings (Sec. 2.1), which is important to understand the behaviors of molecules in terms of orientational and positional ordering in LC phases. In addition, Sec. 2.2 explains a theory that can be applied to determine the local concentration of SSY based on the characteristic absorption spectrum of SSY.

2.1 Order Parameter

When molecules form LC phases, they are called anisotropic, and they can have an orientational and/or positional order. Based on the statistical theory of the molecules, the degree of order illustrates the molecular ordering in the LC phases. In order to develop the theory, it is assumed that the LC is composed of rod-like molecules, which are symmetric at the axis of the preferred orientation, and have no polarity (i.e., the preferred orientation **n** and –**n** are equivalent) [14].

Based on these assumptions, the degree of molecular ordering is described by the order parameter (also called long-range orientational order) (Eq. 2.1). The order parameter is denoted

by *S* and is the average of the function of the angle between the director (i.e., preferred

orientation of the aggregates) and the direction of the long axis of the molecule (Fig. 2.1), which

is given by:

$$S \equiv \langle P_2(\cos\theta) \rangle \equiv \langle \tfrac{1}{2}(3\cos^2\theta - 1) \rangle, \tag{2.1}$$

where $P_2(x)$ is the second Legendre polynomial. For instance, if all the molecules are aligned in

the same direction, as in the case of a perfect crystal, the angle θ (theta) is 0 since the direction of

the director and the molecules are the same. In this case, the order parameter *S* becomes 1. On

the other hand, if all the molecules are randomly oriented, then the order parameter is 0. Since

LCLCs depend on both the temperature of the system and the concentration of the material, the

order parameter also depends on the temperature and concentration (Fig. 2.2).
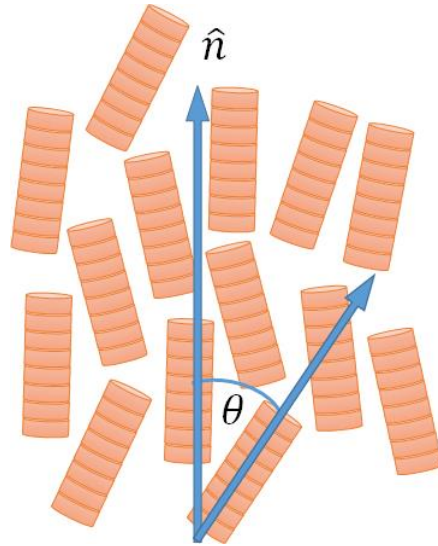
Fig. 2.1 The snapshot of the aggregates in the LC phase. This figure illustrates the direction of preferred orientation of the aggregates (called a director, denoted by $\hat{\boldsymbol{n}}$ (n-hat)) and the direction of an aggregate of disk-like molecules. θ is the angle between the director and the long axis of each aggregate.
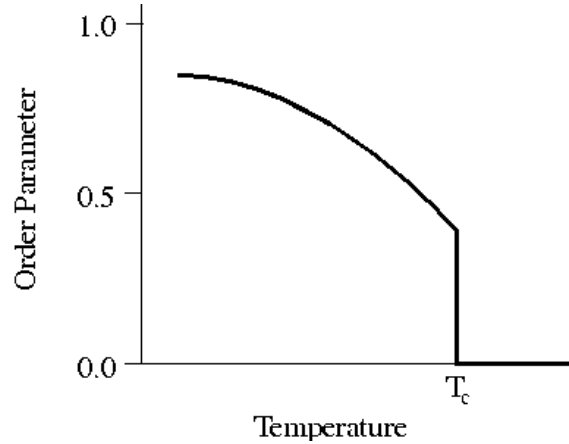
Fig. 2.2 This graph shows the relationship between the order parameter and temperature in the LC phase at constant concentration of a mesogen in a solvent. T_c represents the critical temperature, and the limit to which LCs can have orientational order. Above T_c, the molecules lose directional order and the system becomes isotropic [1].

Although the order parameter is defined by equation 2.1, it is not clear how to determine S from the value for θ in terms of optically measurable quantities. In order to determine the order parameter, various methods can be used. For instance, the order parameter can be related to the optical anisotropy of a given material, such as linear dichroism or birefringence. In other words, the S can be found from the index of refractions ($n_\parallel$ and $n_\perp$) and the absorption of lights ($A_\parallel$ and $A_\perp$), which are measured when the director is parallel ($\parallel$) and perpendicular ($\perp$) to the polarization [6]. In this case, the order parameter can be given by:

$$S = \frac{n_\parallel A_\parallel - A_\perp}{n_\parallel A_\parallel + 2n_\perp A_\perp}. \tag{2.2}$$

When the index of refractions are considered the same, this equation can be further simplified into the following equation [15]:

$$S = \frac{A_\parallel - A_\perp}{A_\parallel + 2A_\perp}, \tag{2.3}$$

which can be determined purely by the absorption of light ($A_\parallel$ and $A_\perp$) for the LCs with linear dichroism. This equation is used to determine the order parameter in Sec. 5.4 from the measurements of the absorption of light.

2.2 Beer-Lambert Law

In order to study the correlation between the order parameter (molecular ordering) and the concentration of LCLC molecules in water, it is important to accurately measure the local concentration of the sample with known order parameter. The system called μ(micro)-spectroscopy was developed to measure the concentration of an LCLC (i.e., SSY) based on the law that describes the relationship between the attenuation of light, the concentration, and the path length of a sample (Beer-Lambert law) (also see Chapter 4.4).

The Beer-Lambert law is used to determine the concentration of isotropic SSY and the order parameter of SSY LC with ultraviolet-visible light (UV-Vis) spectroscopy by measuring the light absorption at different wavelengths (Fig. 2.4). The Beer-Lambert law is given by:

$$A = -\log_{10}\left(\frac{I_1}{I_0}\right) = \varepsilon c l, \tag{2.4}$$

where A is the absorption (an arbitrary unit (a.u.)), I_1 is the intensity of transmitted light, I_0 is the intensity of incident light, ε is the extinction coefficient or molar absorptivity ((wt%)$^{-1}$·cm^{-1} or m^2·mol^{-1}), c is the concentration of the solution (wt%), and l is the path length of a sample (cm).

Equation 2.4 shows that the absorption of light is proportional to the concentration and/or path length of a sample when the extinction coefficient is constant. The extinction coefficient is experimentally determined for different samples. In particular, the extinction coefficient of SSY is determined to measure the concentration of SSY in the mixtures (see Chapter 4.3).
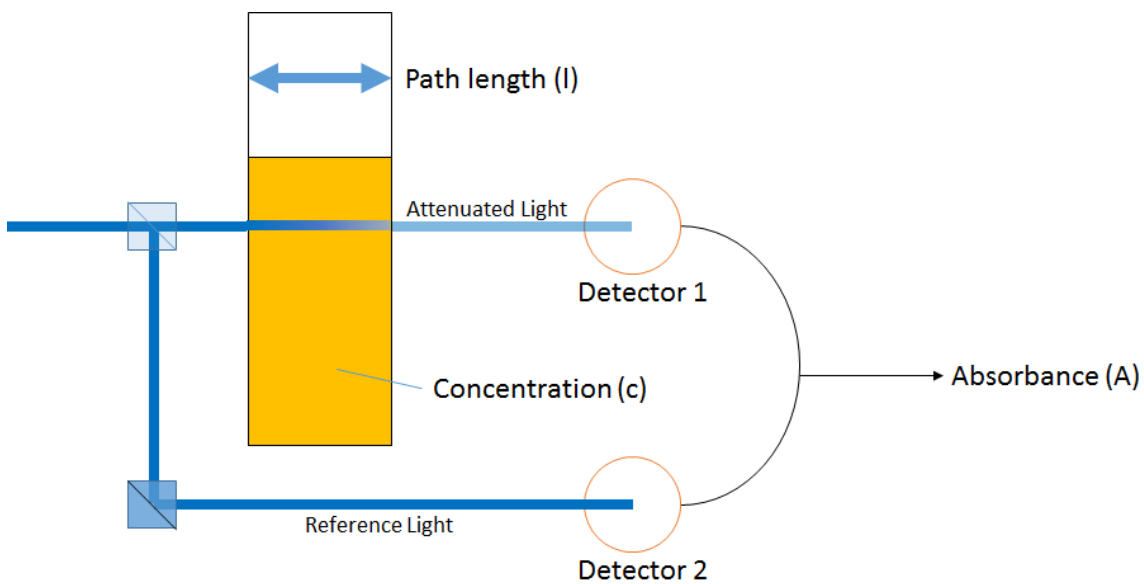
Fig. 2.4 Mechanism of UV-Vis spectroscopy. In addition to the concentration of the reagent and the path length, the absorption of light also depends on the preferred wavelength of the sample. For example, the peak absorption of SSY is at around 480 nm. In other word, the absorption value of the attenuated light is lower if other wavelength was chosen. A good example of the absorption spectrum for SSY is shown in Fig. 3.8.

Chapter 3

Background and Previous Studies of two LCLCs

It is essential to understand the aggregate structure of disk-like LCLC molecules and the detailed LC phases prior to studying the mixture of two LCLCs. Having this knowledge is important to better understand the molecular interactions between the two LCLCs. Based on the extensive previous studies of the aggregate structure and LC phases, we selected two LCLCs, Disodium Cromoglycate (DSCG) and Sunset Yellow FCF (SSY), as reagents for the experiment. This chapter introduces previous work investigating the featured LCLCs for DSCG and SSY.

3.1 Disodium Cromoglycate (DSCG)

The anti-asthmatic drug, disodium cromoglycate (DSCG), also known as *Cromolyn* or *INTAL*, is the first chromonic LC to have been examined in detail using optical and X-ray diffraction techniques [4,5,10,12,16]. In the 1970s, the two liquid crystalline phases, nematic (N) and columnar (C or M), of DSCG were first reported, and the phase diagram (Fig. 3.1), optical textures (Fig. 3.2), and X-ray diffraction patterns were investigated [9,17].

The molecular structure of DSCG is shown in Figure 3.3. The molecule of DSCG is composed of rigid aromatic cores connected by a flexible bridge, and the molecule is symmetric about the center. This structure is considered a disk-like molecule because of the aromatic cores that form aggregates when mixed in water (Fig. 3.2). The structure of the aggregate of DSCG is under investigation, and three models have been proposed: (1) simple π-π stacking model, (2) chimney-like model, and (3) thread-like model (Fig. 3.3). A study by Agra-Kooijman *et al.* [18] supports the simple π-π staking arrangement shown in Figure 3.3 (a) with the spacing 3.4 Å between the molecules [9,18].
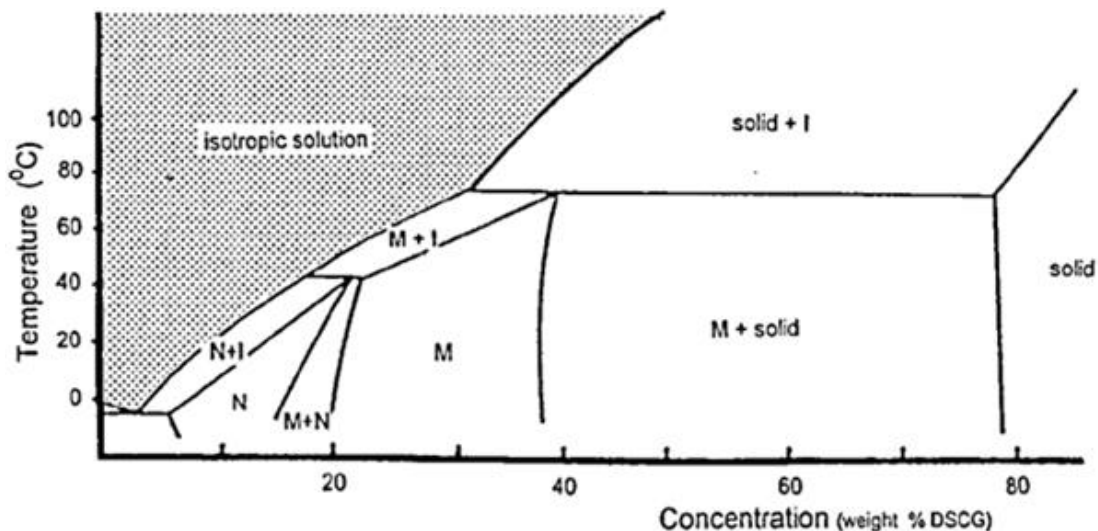
Fig. 3.1 Phase Diagram of DSCG **[11]**. The LC phase of DSCG depends on the concentration (weight concentration (wt%) in horizontal axis) and temperature (°C in vertical axis). The two-phase coexistences are denoted by N + I (nematic and isotropic), M + I (columnar and isotropic), M + N (columnar and nematic), M + solid (columnar and solid crystal), and solid + I (solid crystal and isotropic). DSCG exhibits lower order phases as the concentration decreases and/or the temperature increases.
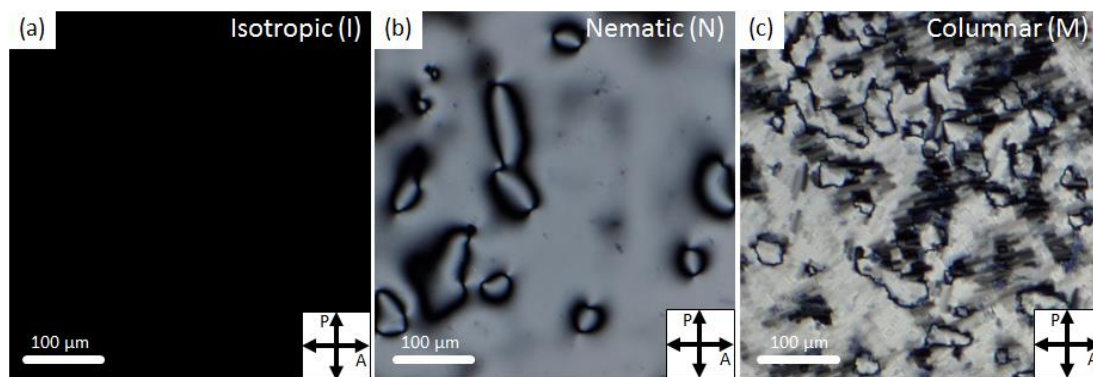
Fig. 3.2 Typical optical textures of DSCG LC observed under a polarized microscope. (a) Isotropic phase shows no birefringence effect, and thus no transmitted light is observed. (b) Schlieren texture appears in nematic phase. Dark regions in nematic phase correspond to the orientation of the aggregates that are oriented either parallel or perpendicular to the axes of polarizer or analyzer. (c) Columnar phase shows birefringence, but the singular points are not as clear as in the nematic phase and the contrast of the black stripes are higher than that can be seen in nematic phase.

16
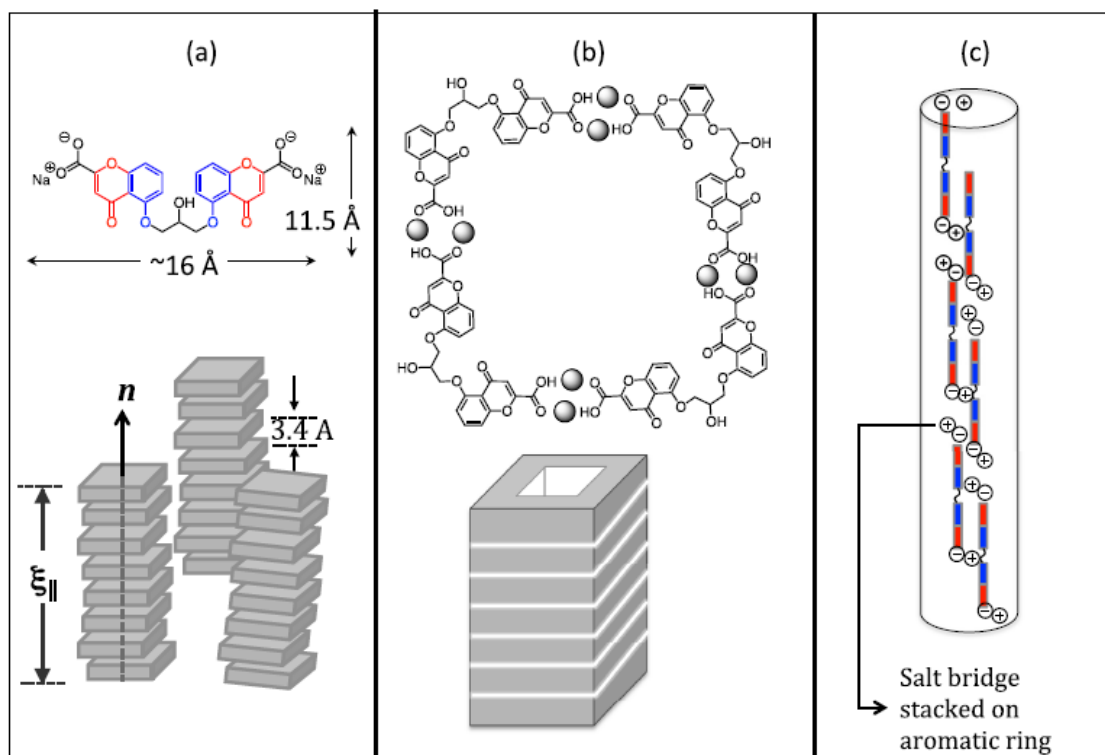
Fig. 3.3 Molecular structure (a) and stacking models (a - c) of DSCG obtained from Agra-Kooijman *et al.* [18] The molecule is composed of symmetric rigid aromatic cores connected by a flexible bridge at the center. This molecule is considered to be a bent disk-like molecule because of rigid aromatic rings connected by a flexible bridge.

(a) Simple π-π stacking model by Hartshorne and Woodard [9]; (b) chimney-like stacking proposed by Lydon [10], and (c) thread-like model by Wu *et al.* [19]. The colors in (c) correspond to the colors of the DSCG molecular structure in (a).

3.2 Sunset Yellow FCF (SSY)

A widely-used food colorant and an anionic monoazo[4] dye, Sunset Yellow FCF (also known as Edicol Sunset Yellow or food dye Yellow 6) was the next chromonic system to be examined in detail after DSCG. Extensive studies of aggregation behavior and LC properties of SSY include optical observations, X-ray diffraction measurements, and analysis using NMR techniques [6,7,20–22].

Figure 3.4 shows the molecular structure of two forms of SSY that contains hydrophilic ionic ends (Na^+) and hydrophobic aromatic rings. While NH hydrazone tautomer of SSY has a flexible chain at N-N binding, Park *et al.* and Chami and Wilson consider OH azo tautomer of SSY to be a planar and a disk-like molecule because of the N=N double bond [8,22]. When the molecule is mixed with water, both tautomers are expected to form aggregates in order to minimize their hydrophobic aromatic rings' exposure to water. Chami and Wilson showed that the structure of the aggregate is a simple π-π staking using the computer simulation model (Fig. 3.5) [8].
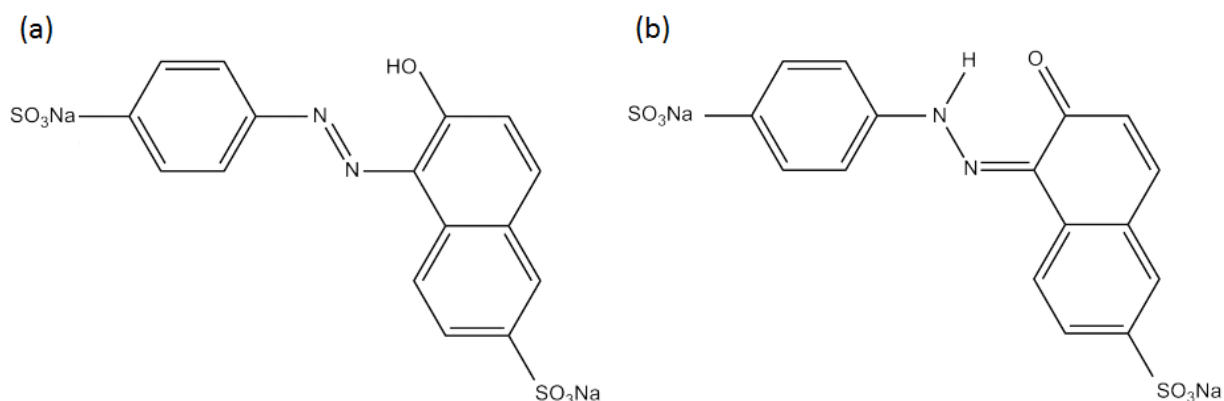
Fig. 3.4 Molecular structure of (a) OH azo tautomer and (b) NH hydrazone tautomer of Sunset Yellow FCF (chemical name: the disodium salt of 6-hydroxy-5-[(4-sulfophenyl) azo]-2-naphthalenesulfonic acid) **[22]**. OH azo tautomer is considered as a planar molecule composed of rigid hydrophobic aromatic rings connected by the double bond of two nitrogen (N=N bonding). The dimension of the molecule is 13.7 Å **[23]**.

---

[4] Monoazo is an azo compound composed of diazene (also called diimide) (HN=NH) or azobenzene (two phenyl rings linked by an N=N double bond). Azo compounds exhibit yellow or red color by the N=N double bond by absorbing ultraviolet-visual range spectrum (480 nm for SSY) of light.
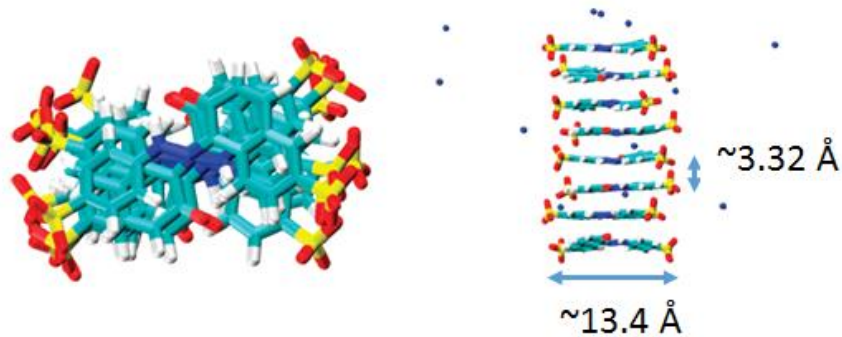
Fig. 3.5 Computer simulated structure of an eight-molecule SSY aggregate by F. Chami and M. R. Wilson **[8]**. The molecules form an aggregate of simple π-π staking. The aggregate diameter (13.4 Å) and the intermolecular separation (3.32 Å) were studied by Joshi *et al.* **[23]**.

In 2008, the nematic (N) and columnar (M or C) phases of SSY were reported by Park *et al.* [22] and the phase diagram (Fig. 3.6), optical textures (Fig. 3.7), and x-ray diffraction patterns were investigated [23].
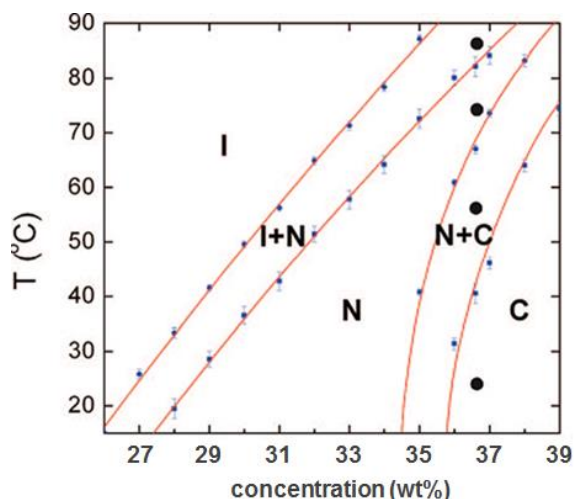
Fig. 3.6 Phase Diagram of SSY modified from Park *et al*. **[22]**. The LC phase of SSY depends on the concentration (wt% in horizontal axis) and temperature (°C in vertical axis). The two-phase coexistences are denoted by I +N (isotropic and nematic), N + C (nematic and columnar).
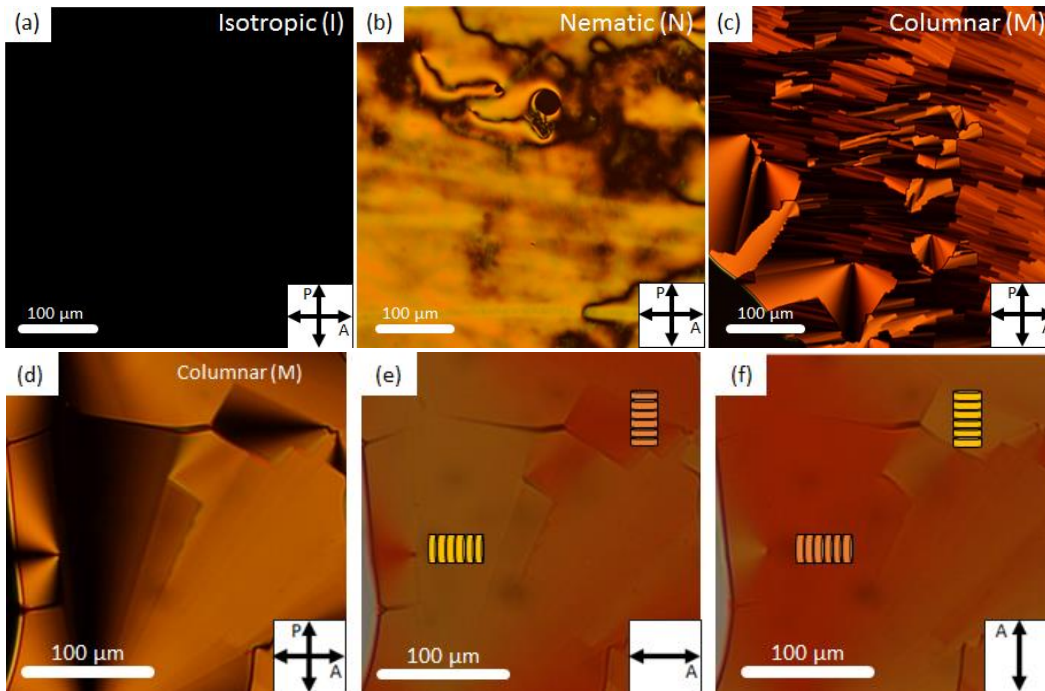
Fig. 3.7 Typical optical textures of SSY LC observed under polarized microscope. The images correspond to the isotropic phase (a), nematic phase (b), and columnar phase (c) and (d). Linear dichroism is shown in (e) and (f); the color depends on the orientation of the molecules relative to the direction of the axis of the polarizer.

In 2005, Horowitz *et al*. extensively studied the aggregation process and LC phases of SSY using X-ray scattering and various optical techniques [6]. One of their experimental results showed that the peak of the spectroscopy curve of the absorption coefficient of SSY in various concentration stays at around 480 nm (Fig. 3.8) [6]. In our experiment, this information is used to determine the local concentration of SSY when mixed with DSCG in water.
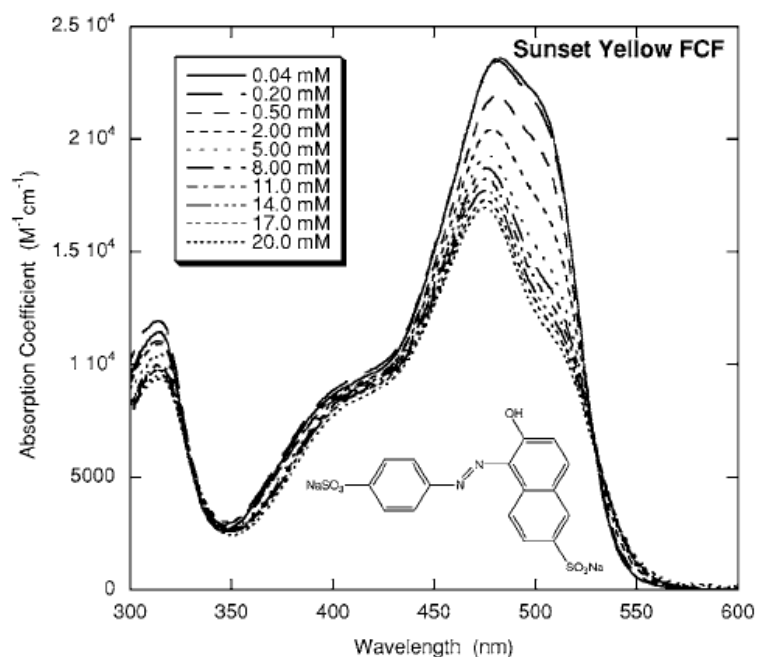
Fig. 3.8 Absorption spectrum of SSY using UV-Vis spectroscopy by Horowitz *et al.* **[6]**. This spectrum curve shows the absorption peak of SSY at around 480 nm at various concentrations. The change of absorbed light intensity is used to determine the order parameter and the concentration of SSY.

3.2.1 Linear Dichroism (LD)

SSY not only exhibits LC phases, but it also exhibits an optical property called linear dichroism (LD) because of the azobenzene (R'-N=N-R) in its molecule. LD is an optical property of a LC that changes the intensity of transmitted light when the SSY LC is placed under a polarizer without an analyzer, depending on the relative orientation between the direction of the polarizer and that of the molecules. Therefore, LD can appear only when SSY forms LC phases and the observation of LD is used to verify the appearance of SSY LC phase (Fig. 3.7 (e) and (f)).

Chapter 4

Experimental Methods: SSY and DSCG

4.1 Introduction

Based on the previous studies of SSY [7,8,20,22] and DSCG [9,10,17,18] and the assumptions that the molecules of DSCG and SSY are flat disk-like shapes, we hypothesized that the molecules of SSY and DSCG can form mixed aggregates, as shown in Fig. 4.1. Hence, we were initially interested in observing the uniform molecular stacking of DSCG and SSY, and the initial goal of observing the mixture of DSCG and SSY was to verify whether or not the mixtures of the molecules can form mixed stacks and uniform LC phases.
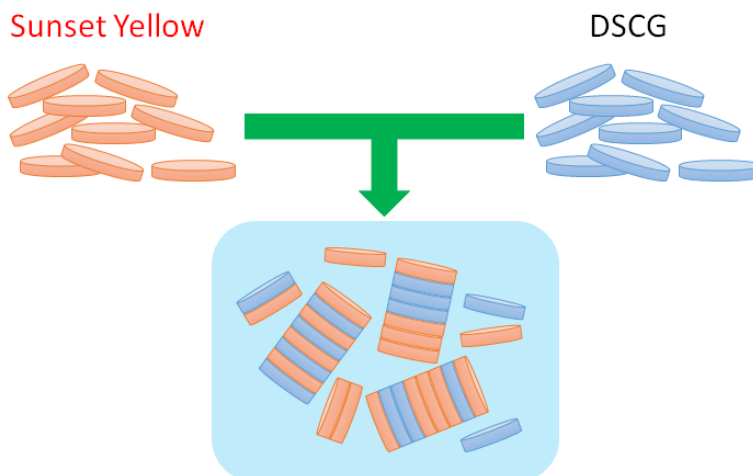
Fig. 4.1 Initial hypothesis of the molecular behavior of SSY and DSCG in water. Based on the simple molecular model of SSY and DSCG as flat-disk-like molecules, we hypothesized that the molecules of SSY and DSCG can form mixed aggregates, as shown below the arrow.

The first several observations of the mixtures showed, however, that the mixed solutions exhibit clear separations between the SSY-rich and DSCG-rich domains. Based on the observed tendency of the phase separation, we concluded that these different molecules tend to expel each other (further detail is described in Ch. 6). Moreover, the observed phases and phase

coexistences exhibit novel LC phases that have the potential to deepen the understanding of the mixture of two LCLCs, thus we studied the behavior of the mixed molecules in more detail.

Prior to describing the observed phases of the mixture of two LCLCs, this chapter introduces the experimental methods, including sample preparation methods (Sec. 4.2), cell preparation methods (Sec. 4.3), and the observation techniques (Sec. 4.4 – 4.6). The limitations of each method and technique are described in each section.

4.2 Preparation of the Mixed Samples

SSY and DSCG samples were purchased from Sigma-Aldrich (See Appendix I for detail). The samples were prepared from the dried powder of each material in a plastic conical vial. The amount of each reagent was determined based on the desired ratio of the samples and measured by weight using a weight scale. After the two LCLC materials were measured in a vial by weight, deionized (DI) water was added using a micro pipet (Fig. 4.2). The amount of water was also determined based on the desired concentration; the weight concentrations (wt%) of SSY and DSCG are denoted by (c_S, c_D) respectively.
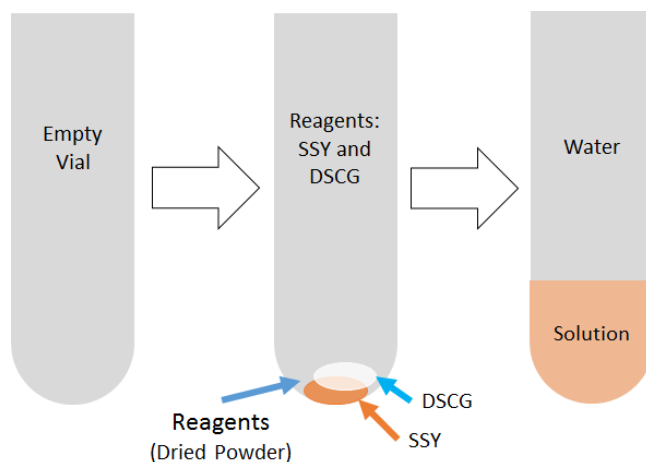
Fig. 4.2 Sample preparation steps. The steps of the sample preparation were as follows: (i) The dried powder of SSY and DSCG were put into a plastic conical vial. (ii) After the weights of each material were measured, DI water was added to make a mixed solution. (iii) The vial was centrifuged several times before adding ID water in order to minimize the residual of reagents on the wall of the vial. (iv) After the water was added, the vial was placed in an oven at a temperature of 60 ~ 80 °C in order to homogenize the sample.

After adding water, the vial was placed in a heat oven (typically around 60-80 °C) for 5

~ 10 minutes in order for the samples to be uniformly mixed in water. If a sample contained very

small amounts of water (i.e., 40 or 50 wt%), then the sample needed to be heated for a longer

time at higher temperature in order to disperse the molecules and homogenize the sample. The

prepared samples were taken by micro-pipette and placed on or inserted into a glass cell. The

details of the glass cells are described in the next section.

4.3 Cell Preparation

In order to make detailed observations of the prepared samples using the depolarized

transmitted light microscopy (DTLM), a flat and thin cell that kept the desired phase for a long

enough time was very important. Furthermore, it is important to have a cell that allows quick

water evaporation in order to observe various LC phases in a short period of time. Therefore, we

designed three different types of cells using flat and thin glass plates for visual observation of LC

phases under DTLM (See Fig. 22 (a – c)). Furthermore, in order to study the structure of the LC

phases in detail, an additional cell was designed for X-ray crystallography (See Fig. 22 (d)).

In particular, in order to determine the local concentration of SSY in sample mixtures,

we designed a cell with a known thickness. The cell was filled with a sample mixture by

capillary force and sealed with mineral oil. The thickness of the cell was determined by

measuring the interference of incoming light by the μ-spectroscopy (Sec. 4.6).

24
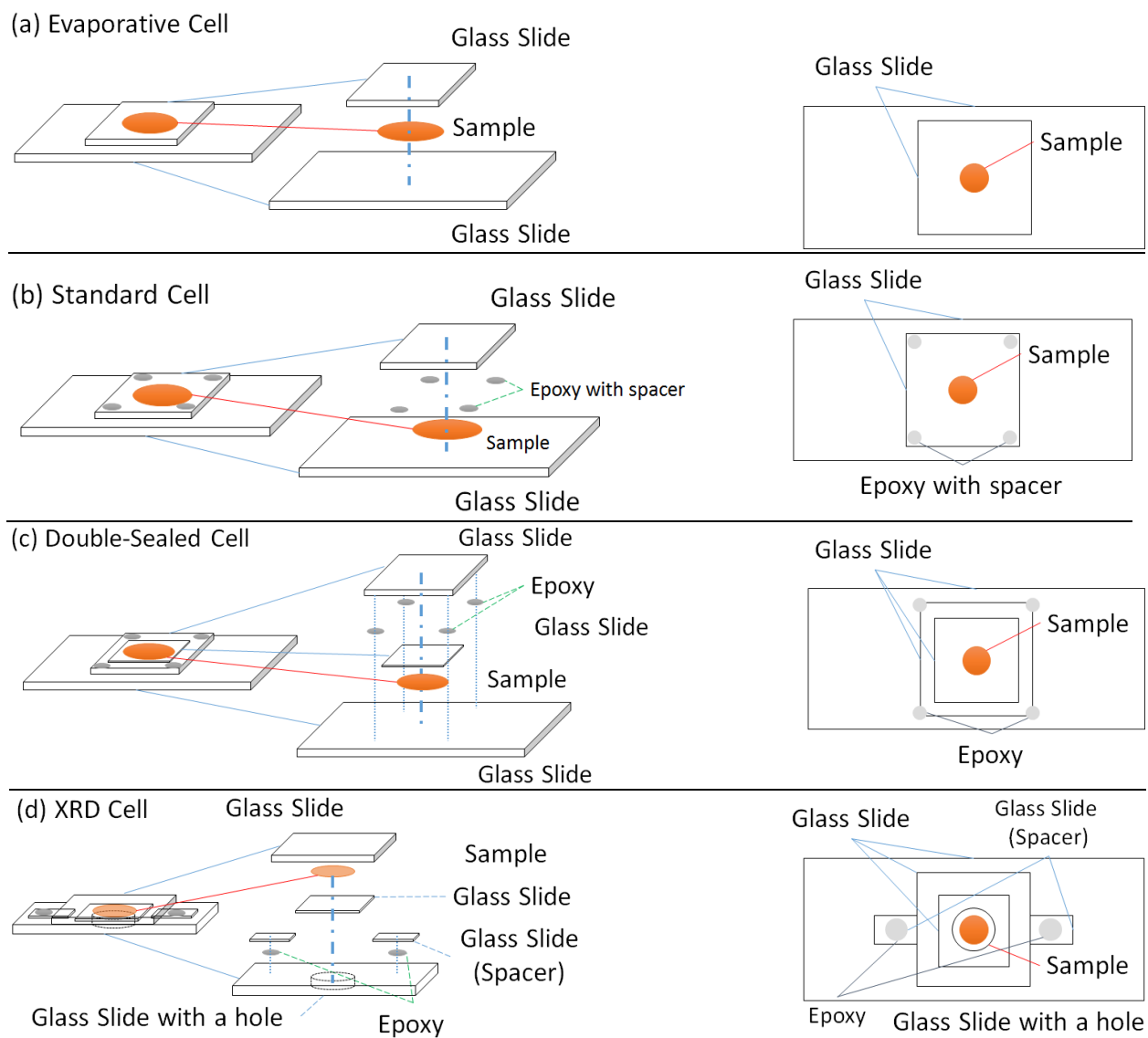
Fig. 4.3 Four types of cells for sample observation. The cell type (a), (b), and (c) were designed for visual observation of LC phases under polarized microscope and cell. The stability of the LC phase in the cell type (a) and (b) were typically about 3-4 days, while (c) was about a month. The cell type (d) was designed for a X-ray diffraction experiment. Mineral oil was filled after loading the sample between the glass slides. The top and the bottom glass slides have a thickness of about 1 mm. For cell (b), the thickness of the glass slide in the middle is about 50 µm. The thickness of the middle glass slide in cell (c) is about 15 µm. These cells were designed by Greg Smith and Youngwoo Yi.

Four different types of cells were prepared as follows: (1) Evaporative Cell (Fig. 4.3 (a)) that has two 1 mm-thick glasses that allows the water in the solution to evaporate in typically less than 1 ~ 2 hours, depending on the amount of water in the sample and the condition in the surrounding environment. (2) Standard Cell (Fig. 4.3 (b)) had the same configuration as the

25

Evaporative Cell, but the sample is covered by mineral oil, which prevents quick water evaporation. The LC phase in this type of cell normally stays for 3 ~ 4 days. (3) Standard Cell with spacers (Fig. 4.3 (b)) has the same configuration as the Evaporative Cell, but the thickness between the two glass plates was predetermined by the spacer that is mixed in epoxy. This cell was designed to be able to measure the local concentration of SSY using UV-vis spectroscopy by measuring the absorption spectra of the transmitted light. The fluidic LC sample was inserted into the Standard Cell (shown in Fig. 4.3 (b)) from the edge by the capillary force effect. The use of this cell was limited for low-concentration fluidic samples because of the viscous samples, which have high-concentrations of the reagents compared to water and cannot be inserted into the cell. (4) Well Sealed Cell (Fig. 4.3 (c)) has an additional thin glass plate between the two glass plates. The top and the bottom glass plates were fixed by epoxy. The LC sample normally stayed stable for a few weeks to a month because of the slow evaporation of water. (5) XRD Cell (Fig. 4.3 (d)) has three glass plates, similar to Well Sealed Cell, but the bottom glass plate has a hole in order to optimize the cell for X-ray diffraction experiments. In the XRD cell, two additional thin glass plates are used as spacers.

The basic configurations of cell type (a), (c), and (d) are as follows: (1) A small amount of the mixture (0.3 ~ 1.0 μl) was dropped on a glass plate and covered with another glass plate. (2) The sandwiched sample was sealed with mineral oil. (3) The cell size is typically less than 2.5×3.5 cm (base/bottom glass) and 1.0×1.0 cm (cover/top glass). For the KT-cell, a small amount of sample was inserted from the side of the cell by the capillary effect.

4.4 Depolarized Transmitted Light Microscopy (DTLM)

A depolarized transmitted light microscopy (DTLM) was used in order to observe birefringence and the LC phases of the samples (Fig. 4.4). Sample vials and the cells were placed

on a heat stage of DTLM, and the LC phases were observed. The polarizer below the sample stage

was detachable. The analyzer on top of the sample was rotatable for 180 degrees but not detachable.

The LC phases were observed by eyepieces or on a computer display and recorded by

taking a micrograph with a camera that was placed on top of the microscope. Moreover, the

absorption spectra were measured with a μ-spectrometer (Fig. 4.4). The temperature of the heat

stage can be raised above the room temperature, and this enables observations of the LC phases

under various temperatures. The lowest possible temperature was around 22 ~ 25 °C, room

temperature, and the highest temperature was restricted to around 100 °C in order to prevent a

bubble formation and rapid water evaporation during observation.
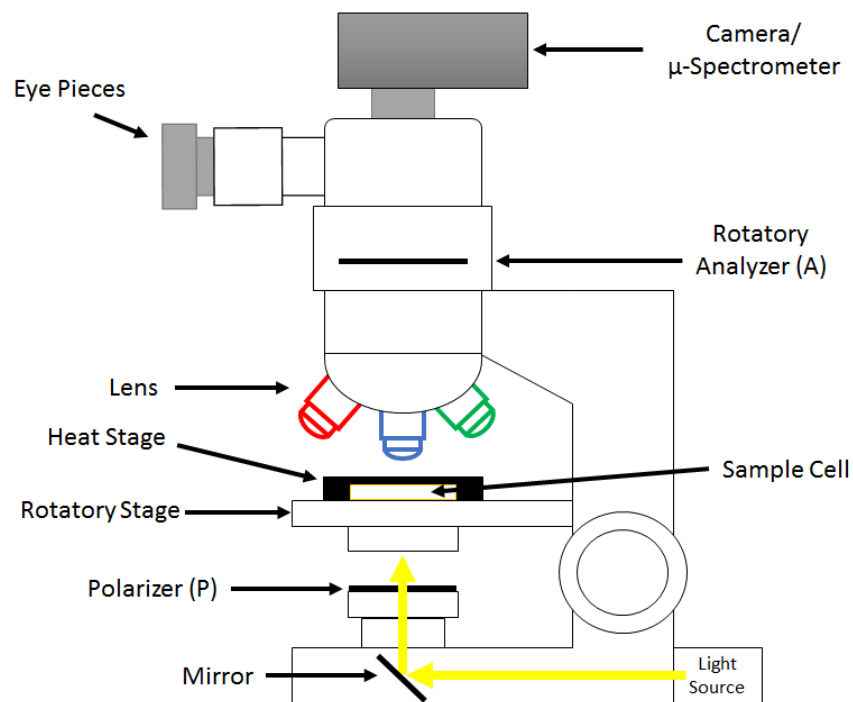
Fig. 4.4 Depolarized Transmitted Light Microscope. Unpolarized light passes through the polarizer, sample cell, and analyzer. The polarized light is detected through eye pieces and a camera or a μ-spectrometer only when the sample is birefringent.

The LC phases were observed under various configurations of the microscope (by

rotating the analyzer or removing the polarizer) to measure various optical effects of the LCs,

such as LD of SSY (Sec. 3.2). Light from a small area on the image plane of the microscope was

collected by an optical fiber, and the spectrum was recorded using a spectrometer. By measuring the intensity of light with the spectrometer, without the presence of the sample, it was found that the original light from the source was slightly polarized by the mirror that reflects the light from the light source. This initial polarization made it difficult to measure samples that have very small birefringence or LD.

4.5 Thermocycle (Thermal Dispersion)

The sample mixtures of two LCLCs in water tend to be inhomogeneously mixed in a cell shortly after it was prepared because of the evaporation of water. If the sample was inhomogeneously mixed, the observation didn't represent the most accurate picture of the phases at the expected concentration. Therefore, it was important to homogenize the concentration in a cell by dispersing the molecules with Brownian motion. The temperature change was one way to disperse the molecules in a short time period. Therefore, the heat stage of the microscope was utilized.

The dispersive method was applied twice, before and after the sample cell is made. The sample was heated when it was prepared in a plastic vial and after it was placed on a cell (Fig. 4.5 and 4.6). At high temperatures, the samples dissolved or became isotropic, as expected from the previous works [22] (Fig. 4.7). However, the high concentration samples that had columnar phase or solid crystals tended to keep their phases even at high temperature, 90 °C.
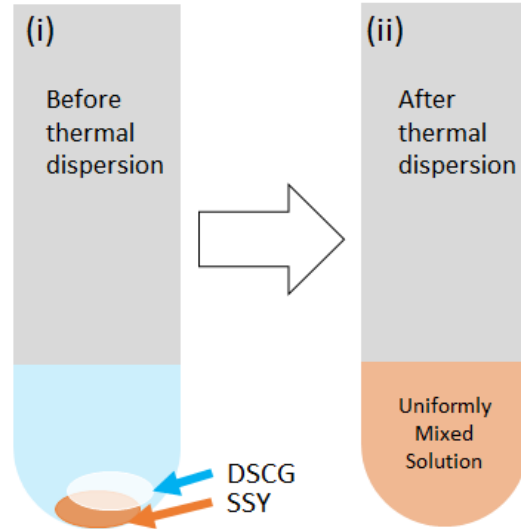
Fig. 4.5 A schematic of SSY and DSCG in water. Powdered state of SSY and DSCG were weighted in a plastic vial. These powders did not mix well in water initially. They were typically condensed at the bottom of the conical plastic vial. After it was placed in a warm oven at around 60 to 70 °C for 5 to 10 minutes, the reagents became more uniformly mixed in water due to the Brownian motion of the molecules. An ultrasonic bath sonicator was also used to mix the reagents.

Even though the sample looks homogenized in a plastic vial after applying the dispersive method, centrifugation of the vial destroys the homogeneity and separates SSY-rich and DSCG-rich domains for all the samples except uniform I or N phase samples. This disruption of uniform concentration indicates that the uniformity of the sample can easily be disturbed by external effect, such as centrifugal force.

The separation between SSY-rich and DSCG-rich domains were better observed under DTLM (Fig. 4.6 and 4.7). The dispersive method for the sample in the cell homogenized the mixture at high temperature, but the sample exhibited separation between SSY-rich and DSCG-rich regions at room temperature.

29
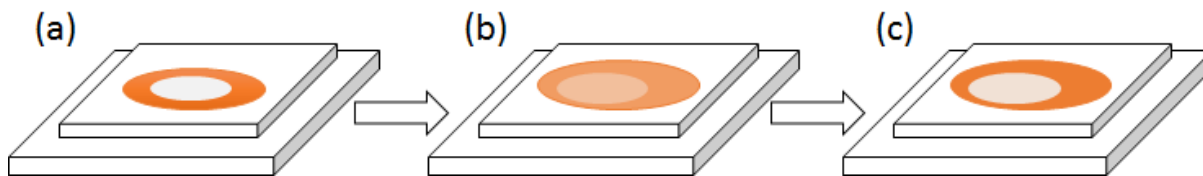
Fig. 4.6 Thermocycle of a mixed sample in a glass cell. (a) Right after the mixture was put on the glass cell, (especially when the sample exhibits I+N or I+M phase) clear phase separation and the concentration gradient was observed at room temperature (20 ~ 25 °C). (b) By raising the temperature, the LC phase of the sample dissolved and started mixing at higher temperature (60 ~ 90 °C). If the sample was thick and pressed by the glass plate on top of it, the sample spread over the cell as it melted and decrease its viscosity. (c) Birefringence reappeared by cooling the temperature down to the initial temperature (room temperature).
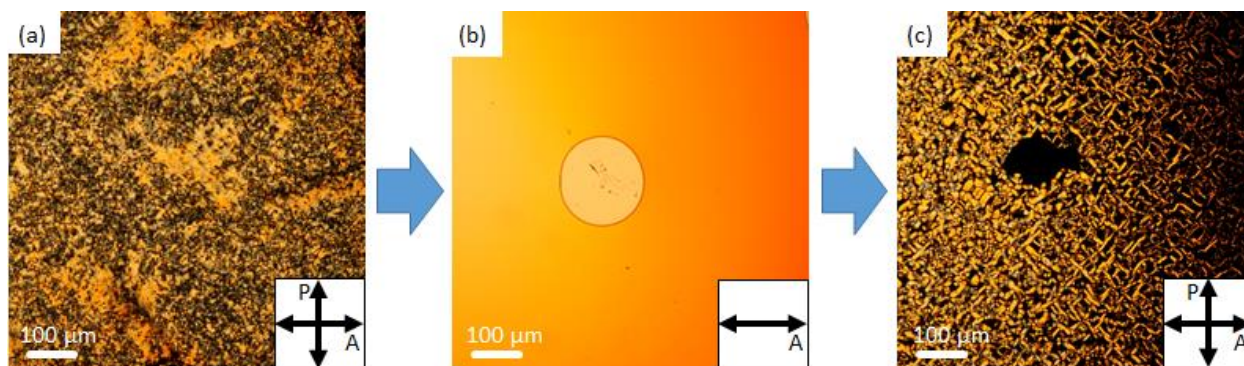
Fig. 4.7 Process of thermocycle for the mixture of SSY and DSCG that exhibits I+M biphase. (a) The micrograph taken shortly after the sample cell was prepared under a crossed polarizer and analyzer. The micrograph shows I+M biphase but the M phase domains are not well ordered. (b) By increasing the temperature of the heat stage, the sample dissolved into the I phase. (c) By cooling the temperature down to room temperature, the sample exhibited clear separation between SSY-rich and DSCG-rich domains. A little color gradient was observed in (b), which is considered as a concentration gradient of DSCG-rich and SSY-rich regions. Inside of the circular region around the center in (b) is an air bubble.

Moreover, for the samples with very high concentrations of the reagents (i.e., the total concentration of the reagents higher than 30 or 40 wt%), longer time and the higher temperature were required to homogenize the mixture. Some samples with very high concentrations (i.e., the total reagent concentration above 50 wt%) cannot be mixed well even at higher temperature.

4.6 Macro- and Micro (μ)-UV-Vis Spectroscopy

Ultraviolet-Visible (UV-Vis) spectroscopy measures the spectrum of light with the wavelength ranges from ultraviolet to visible spectrum. The measurement of the spectrum enabled the analysis of various characteristics of LCs. In particular, the spectrum measurement

of SSY was necessary because the difference in the intensity of the spectrum could provide

important information about the LCs, such as the order parameter and the concentration of SSY

LCs. This measurement was effective for SSY but not DSCG because SSY exhibits a clear effect

on the measured spectrum in the visible range due to LD (described in Sec. 3.2.1) with its

absorption peak at around 480 nm.

Two types of UV-Vis spectrometers (macro: Fig. 4.8 and micro: Fig. 4.9) were used in

order to determine the absorption coefficient of SSY, to measure the concentration of the sample

based on the Beer-Lambert Law (Sec. 2.2), to verify LD, and to determine the order parameter of

SSY (Sec. 2.1 and 5.4). The absorption coefficient was determined with several diluted solutions

of pure SSY (the concentrations below 1 wt%) using a crystal cuvette with the path length of 1.0

cm (Fig. 4.8).

The μ-spectrometer system was developed using DTLM and computer software,

OOIBase32 (developed and distributed by Ocean Optics, Inc.). The Beer-Lambert Law holds for

both macro- and μ-UV-Vis spectroscopies. The μ-spectrometer was used to measure the local

absorbance of the transmitted light through samples.
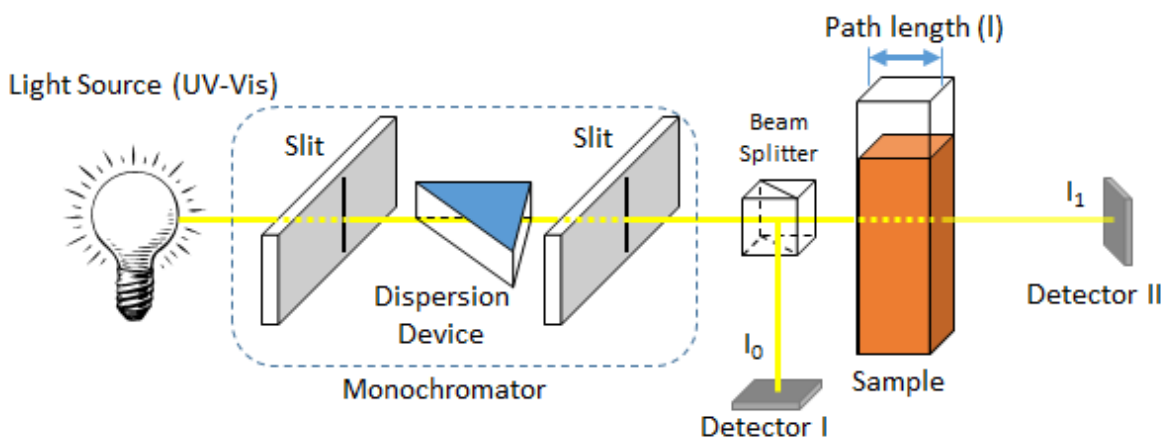
Fig. 4.8 UV-Vis spectroscopy. Incident light (I_0) and transmitted light through sample (I_1) were detected by Detector I and Detector II, correspondingly. The intensity of transmitted light (I_1) is inversely proportional to the path length and/or concentration of the sample, as described in Sec. 2.2. As the intensity of I_1 decreases, the absorption increases, as shown in equation 2.4 (in Sec. 2.2).

31
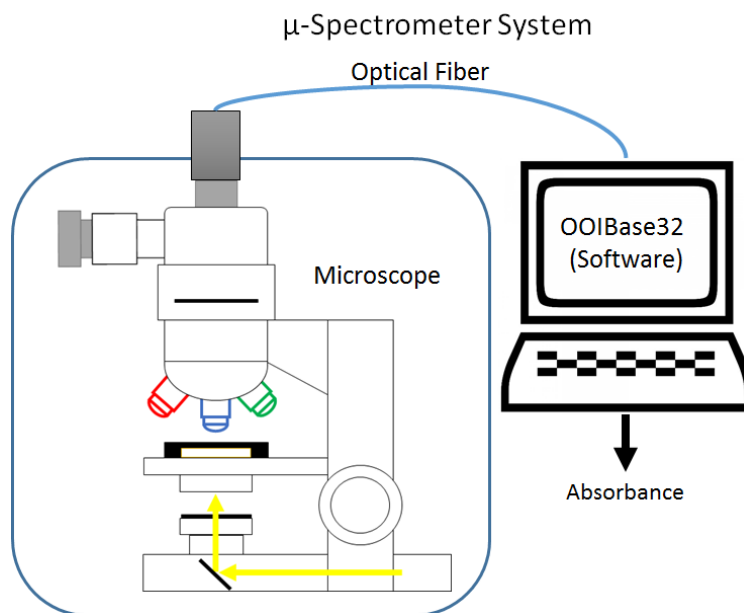
Fig. 4.9 A schematic of μ-UV-Vis spectroscopy (μ-spectrometer). A camera on top of the microscope was replaced by an optical fiber with a resolution of 50 μm, which was connected to a computer system to measure the absorption of the transmitted light through the sample. Computer software called OOIBase32, a spectrometer operating software (developed and distributed by Ocean Optics, Inc.), was installed for the measurements and data analysis.

The μ-spectrometer was very sensitive to the concentration and the path length of the sample (thickness of the cell) because the intensity of the transmitted light could easily be attenuated or blocked by the sample molecules at high concentration. Therefore, the measurement could easily be saturated, and this saturation limits the concentration and the thickness of the sample. For example, when the concentration of SSY was very high or the thickness of the cell was very thick, the incoming light was largely attenuated by the sample cell and the spectrometer indicates that the sample absorbs more light than was expected.

The saturation can be seen in a plot that shows the relationship between the absorbance versus the concentration of SSY. The absorption curve tended to be flattened or saturated if the concentration was high compared to the thickness of the cell (Fig. 5.5 (c-1) in Sec. 5.4.1). When a flat curve or no change in absorbance regardless of the change in concentration was observed, the sample cell was considered to have reached the limit of the measurement and the thickness of

the cell needs to be thinner to determine the concentration in high accuracy. In addition, the extinction coefficient for SSY was determined, and the relative concentration to the thickness of the cell within the saturation range was measured (See Appendix III and IV).

Chapter 5

Experimental Results: SSY and DSCG

5.1 Introduction

This chapter summarizes the results of the observations of the mixture of SSY and DSCG and the results of four additional analyses on these mixtures. All the observed phases or phase coexistences are shown and explained in Sec. 5.2. Sec. 5.3 explains the ternary phase diagram, which was made from the observations (Sec. 5.2). In Sec. 5.4, the alignment effect of DSCG domains called template effect on SSY domains is shown and explained. The further study on the template effect or the verification of linear dichroism is described in Sec. 5.5. Sec. 5.6 describes the stripe textures and their developments. Finally, the exclusion effect of DSCG-rich domains is explained in Sec. 5.7. The results and the modeling of the observed phases are discussed in further detail in Chapter 6.

5.2 Observed Phases and Phase Coexistences

Based on the visual observation with a DLTM (as described in Sec. 4.4), the total of eight different phases or phase coexistences were observed as follows: Isotropic (I), Isotropic + Nematic (I+N), Isotropic + Columnar (I+M), SSY-dominant Nematic (N_S), DSCG-dominant Nematic (N_D), Nematic + Columnar (N+M), Columnar + Columnar (M+M), and Isotropic + Nematic + Columnar (I+N+M). The observed phases are shown in Fig. 5.1 (a) – (h). The notation such as Isotropic + Columnar or I+M indicates the phase coexistence of isotropic and columnar phase in one sample cell. The samples shown in Fig. 5.1 (a) – (h) were prepared by the methods described in Section 4.2 and 4.3.

If both concentrations of SSY (c_S) and of DSCG (c_D) were low in water, uniformly mixed I phase, which has no birefringence and very little color gradient in the sample, was observed, as shown in Fig. 5.1 (a1) – (a3). In contrast, if c_S were larger than 1 wt%, the DSCG-dominant uniform N phase became biphasic (I+N phase), as shown in Fig. 5.1 (d). Under this condition, the phase coexistence was visually determined based on the clear color difference between I domains and N domains, depending on the c_S. On the other hand, if c_D is larger than ~3 wt%, the SSY-dominant uniform N phase turns into triphasic (I+N+M phase) or biphasic (N+M phase), as shown in Fig. 5.1 (e) and (g), respectively. In this case, c_S of a lower order domain (such as I phase domain) was larger than that in a higher order domain (such as N or Mphase domains), as shown in Fig. 5.1 (b) and (d).

Fig. 5.1 (a) – (h): Optical microscope images of the mixtures of SSY and DSCG showing various phases taken under DTLM. The images in the left columns (a1 – h1) exhibit the observed phases under a crossed polarizer and analyzer. The center and right columns exhibit the observed phases under only an analyzer without the polarizer. All the images were taken when the samples were at room temperature (21 ~ 25 °**C).** The white scale bars shown on the lower left in the figures represent 100 μm.
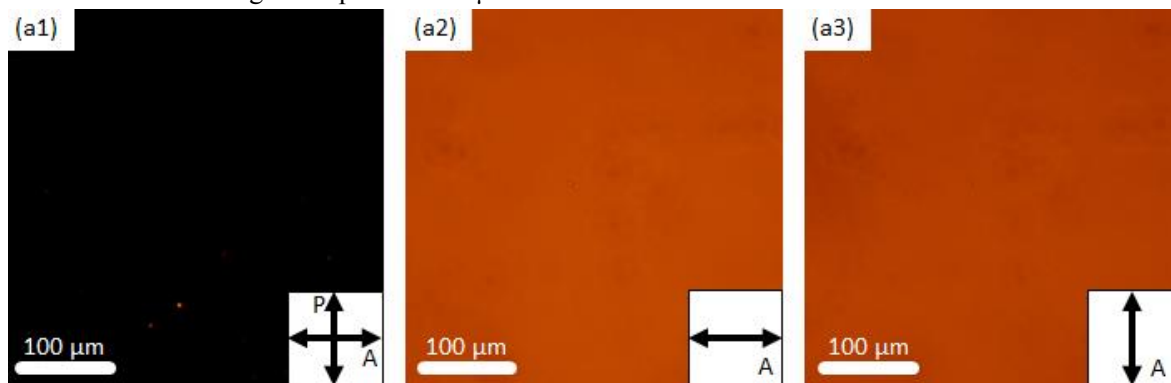
Fig. 5.1 (a). Isotropic (I) phase of a mixed sample at concentrations of (22.17 wt%, 3.05 wt%)[5]. No birefringence was observed under a crossed polarizer and analyzer (a1). No linear dichroism, or color change, was observed under different angles of the analyzer (a2 and a3).

Two types of uniform N phases were found when the concentration of one of the materials was very low compared to the other reagent; and the concentration of the other material

---

[5] The notion such as (0.5, 15) indicates the weight concentrations of SSY is 0.5 wt% and DSCG 15 wt% respectively. In other words, this notation is also defined as (c_S, c_D).

was near the concentration of its pure nematic phase. For example, one of the uniform N phase was observed when the c_S is much smaller than c_D and when c_D is near the nematic phase of DSCG, such as ($c_S = 0.2$ wt%, $c_D = 20$ wt%), as shown in Fig. 5.1 (b1). Similarly, the other uniform N phase was observed when c_D is much smaller than c_S and c_S is near the nematic phase of SSY, such as (35, 5), as shown in Fig. 5.1 (c1).

However, a mixture with the concentration of ($c_S = 0.2$ wt%, $c_D = 20$ wt%) initially exhibited apparent uniform N phase but produced small I domains after the thermal cycle, as shown in Fig. 5.16. In addition, SSY-abundant N phases were also observed for low c_D, (i.e., the mixtures (35, 0.5), (33, 1), (35, 2), and (35, 3)), as shown in Fig. 5.1 (b) and (c).
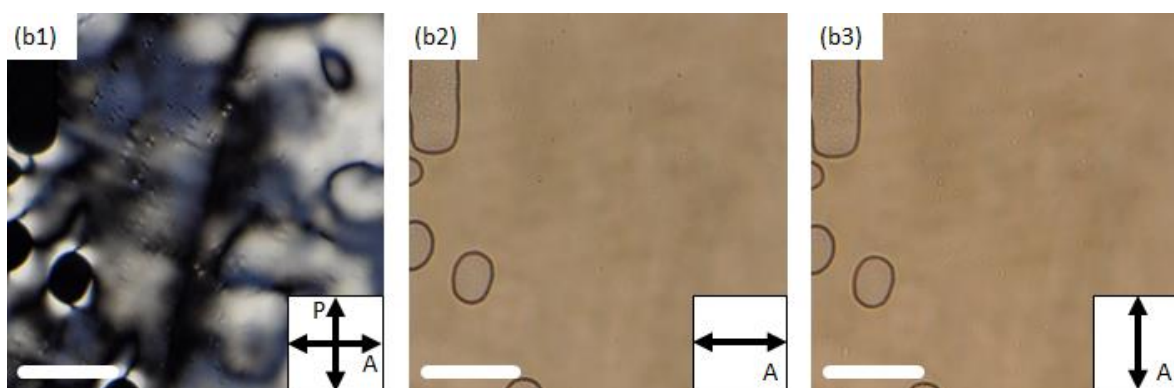
Fig. 5.1 (b). DSCG-rich Nematic Phase (N_D). Schlieren texture and birefringence of DSCG were observed under the crossed polarizer and analyzer. Very small color chance can be seen at different analyzer angles (b2 and b3). The concentrations of the sample were (0.20 wt%, 20,12 wt%).
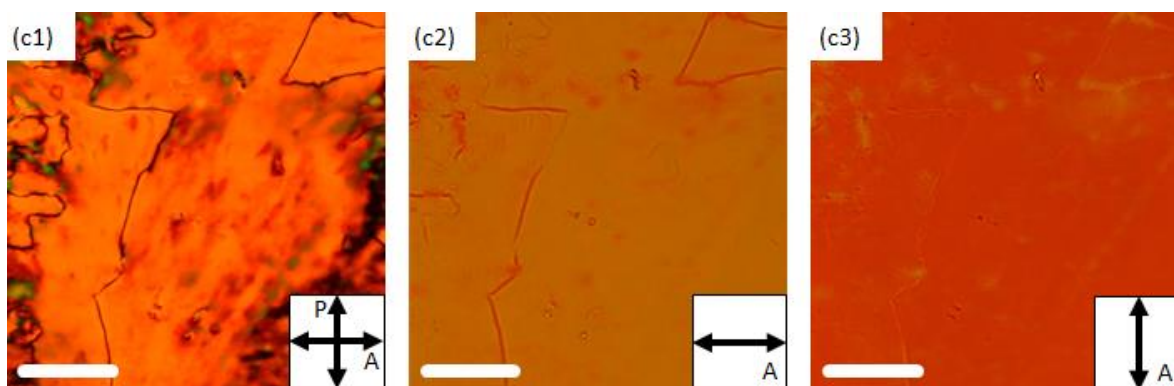
Fig. 5.1 (c). SSY-rich Nematic Phase (N_S). Birefringence of SSY was observed under the crossed polarizer and analyzer (c1). Linear dichroism of SSY was clearly observed by rotating the angle of the analyzer 90 degrees (c2 and c3). The concentrations of the sample were (35.47 wt%, 3.06 wt%).

The biphase of I+N phases were observed near the two ends of the I-region in the phase diagram (Fig. 5.1 (d)). The spectrum difference between I- and N phase domains indicates that N phase domains have relatively higher c_D than I phase domains in both SSY-rich and DSCG-rich cases (see Fig. 5.1.1). This difference in the c_S can be seen from the color differences in the micrographs without the polarizer (see Fig. 5.1 (d2) and (d3)).
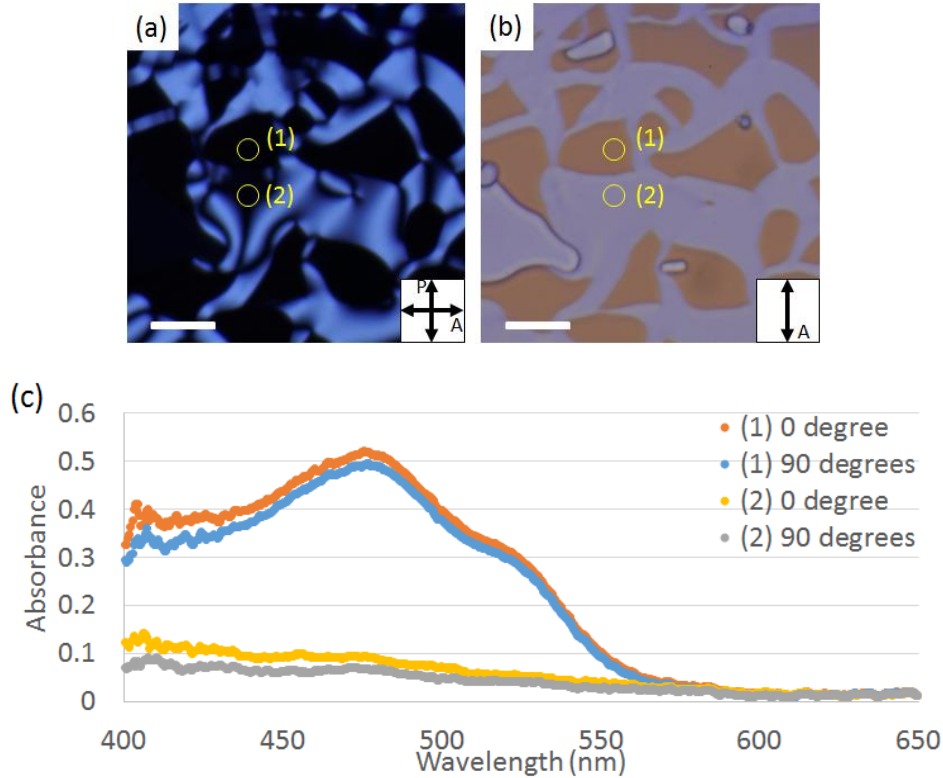
Fig. 5.1.1 Isotropic (I) + Nematic (N) Biphase and Absorption Spectra measured at DSCG-rich N domain vs. SSY-rich I domain (a) and (b) are micrographs observed under DTLM. White bars in (a) and (b) represent the length of 100 μm. The absorption spectra were measured at two positions indicated by (1) and (2) in (a) and (b). The measured spectra of each position at different angles are shown in (c). As can be seen in (c), the differences in absorbance between (1) at 0 and 90 degrees and (2) at 0 and 90 degrees are small. These small differences indicate that SSY exhibits no birefringence and was isotropic in both points. Moreover, the spectrum curves measured at (2) show very little peak at around 480 nm. This indicates that little SSY was present at position (2).
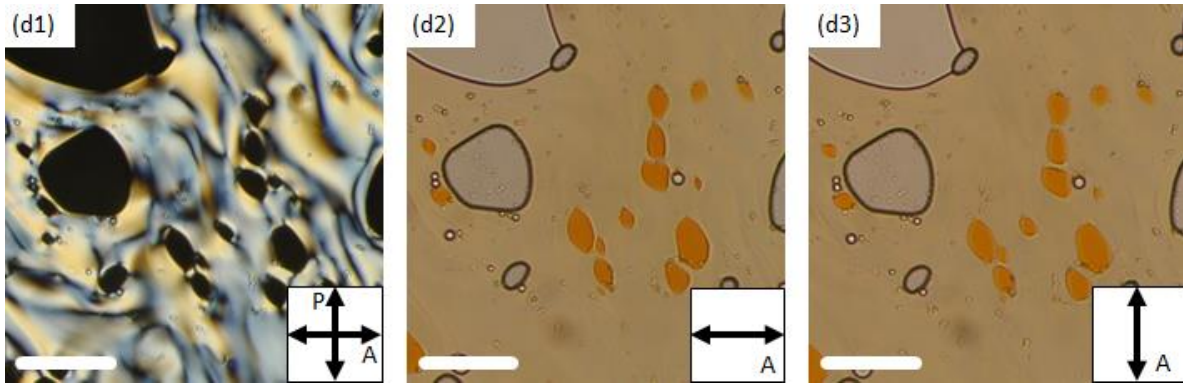
Fig. 5.1 (d). Isotropic (I) + Nematic (N) Biphase. Both I phase and N phase (Schlieren texture) were observed in a sample at once. The white regions in (d2) and (d3) with clear borders represent air bubbles in the cell. By comparing d1 and d2, it is clear that SSY is rich in the isotropic regions compared to the nematic regions. Moreover, little color change was observed in the sample by rotating the analyzer 90 degrees (d2 and d3). The concentrations of the sample were (2.01 wt%, 18.20 wt%).

Triphase of I+N+M was observed when the concentrations were (15.41 wt%, 20.78 wt%) (See Fig. 5.1 (e-i)). The micrographs (Fig. 5.1 (e2) and (e3)) were taken without a polarizer and they reveal the relative c_S among different phase domains. The color difference in (e2) and (e3) indicates that SSY was abundant in I phase domains while c_S was less abundant in M phase domains. This suggests that DSCG molecules expel water more strongly than SSY molecules. Because of this, DSCG molecules form higher order phases, such as N or M phases, more easily than SSY molecules.
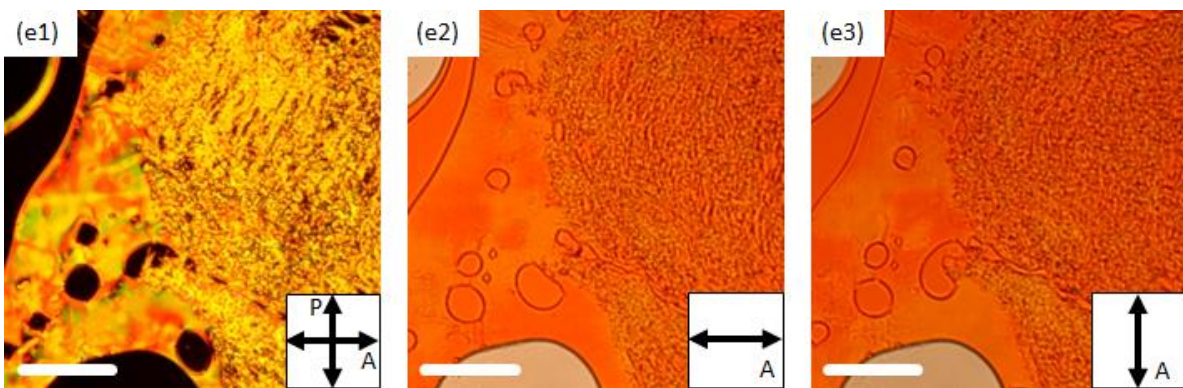
Fig. 5.1 (e-i) Micrographs of Isotropic (I) + Nematic (N) + Columnar (M) triphase. I phase (in a circular regions and regions on the left side), N phase (next to I phase with smooth texture), and M phase (mainly in right half of the figures with the cluster of small domains) were observed. LD was observed in N phase domain but not observed clearly in M phase domain. The concentrations of the sample were (15.41 wt%, 20.78 wt%).

Fig. 5.1 (e-ii) also shows the triphase of I+N+M but exhibits different texture than Fig. 5.1 (e-i). As shown in (e5) and (e6), clear separation between N phase SSY domain and M phase DSCG domain was observed.
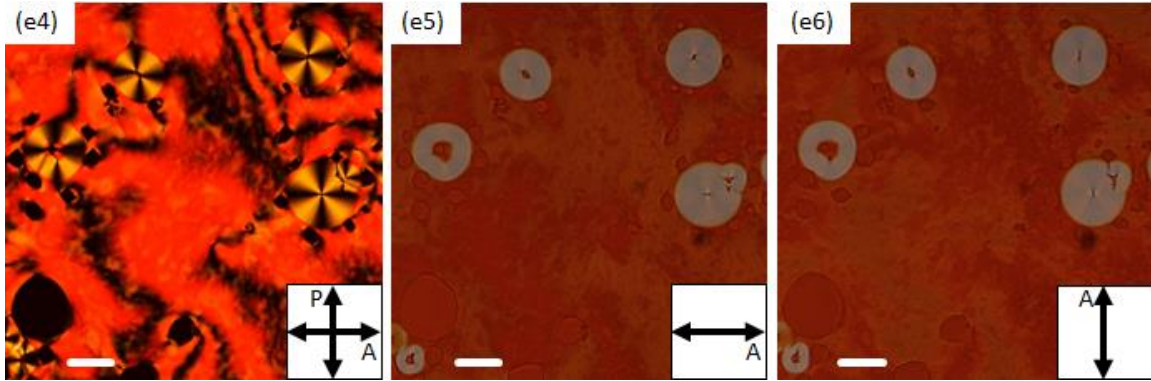
Fig. 5.1 (e-ii) Micrographs of Isotropic (I) + Nematic (N) + Columnar (M) Triphase. I phase (in circular regions and regions on the left side), N phase (next to the isotropic phase with smooth texture), and M phase (light-colored circular domains in the upper half of the figures) were observed. LD was clear in N domain but not as clear in M domain. The concentrations of the sample were (18.67 wt%, 10.79 wt%).

The I+M biphase, such that the coexistence of SSY-rich I phase and DSCG-rich M phase, was found in various concentrations (see Fig. 5.1 (f)). The observation of the color difference between I and M phase domains indicates that the DSCG-rich M domains strongly expel SSY aggregates.
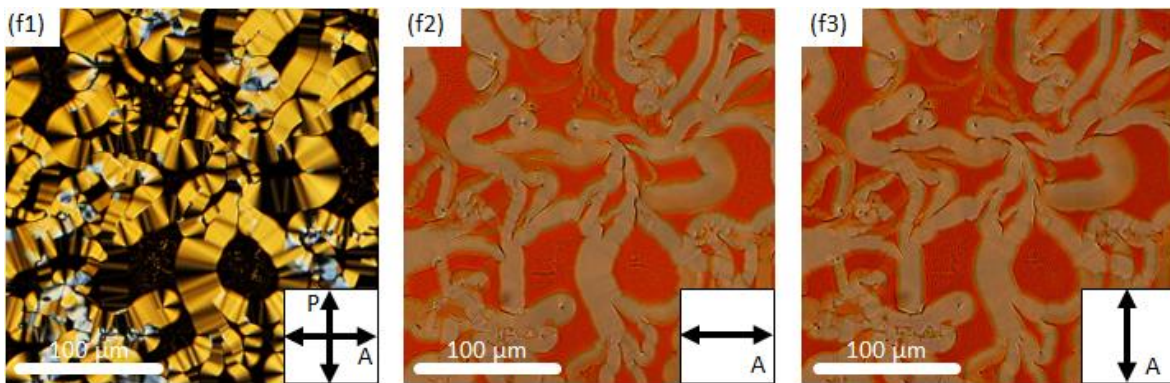
Fig. 5.1 (f). Isotropic (I) + Columnar (M) biphase. M phase was determined by comparing the texture with the pure DSCG M phase domains. I phase exhibits neither birefringence under the crossed polarizer and analyzer nor linear dichroism under only the analyzer. The concentrations of the sample shown above were (9.65 wt%, 13.42 wt%).

The biphase of N+M was observed at the concentrations of (20.51 wt%, 13.50 wt%) at room temperature (Fig. 5.1 (g)). M domain can be seen at the regions where straight lines and crossed brushes appear in Fig. 5.1 (g1). Schlieren texture or N phase domains were observed around the crossed brushes and the straight lines with greenish colors.
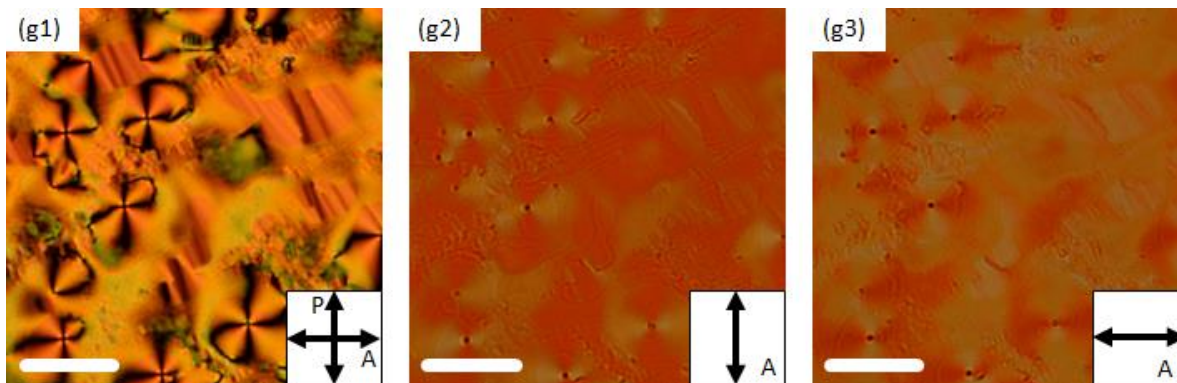
Fig. 5.1 (g). Nematic (N) + Columnar (M) biphase. M phase was observed at the round-shaped crossed brush textures and where there were straight lines. N phase can be seen around the M phase with greenish color in (g1). Under the analyzer, LD of SSY was observed in the entire region. These images do not show any clear separation between SSY and DSCG. The concentrations of the reagents were (20.51 wt%, 13.50 wt%).

The biphases of M+M were prepared in two different preparation techniques. One technique was performed by preparing the sample by mixing each reagent and water for their target concentration as it was described in Sec. 4.2. If the concentration of water was low, or if the concentration of total reagents was higher than 45 wt%, it was typically hard to observe the separation between SSY-rich and DSCG-rich domains because of the difficulty in dispersing the molecules by Brownian motion of the molecules (Fig. 5.1 (h)).
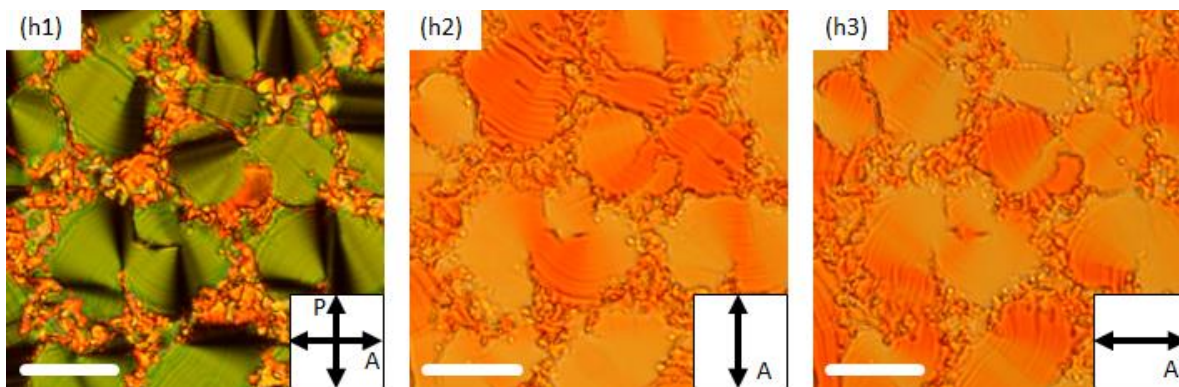
Fig. 5.1 (h). Columnar (M) + Columnar (M) biphase. The distinction between SSY and DSCG was not clear because LD was observed in the entire region of the image. This phase was determined as M + M coexistence since the texture shown in (h1) exhibits similar texture of M domain that is shown in Fig. e and g, and there was no Schlieren texture or N phase domain. The concentrations of the samples were (30.99 wt%, 13.16 wt%).

The other preparation technique applied the natural evaporation of water in the sample. In other words, the M+M biphase sample could also be prepared by water evaporation from I+N or I+M biphase samples. The speed of evaporation of water and the phase evolution were controlled by applying thermal-dispersion on an M+M biphase sample or by using different glass cells (as described in Sec. 4.3). Such samples exhibit clear separation between the SSY-rich M phase and the DSCG-rich M phase, as shown in Fig. 5.3 in Sec. 5.4.1.

Based on the visual observations shown above, there are two major findings as follows: 1) SSY and DSCG tend to expel each other and exhibit clear separations between SSY-rich and DSCG-rich regions or domains, 2) SSY tends to stay in lower order phase (I phase) when it was mixed with DSCG. In other words, SSY is more hydrophilic than DSCG.

Also noticeable was that essentially no LD of SSY was observed when the concentration of SSY was low, as shown in micrographs of the mixtures, (6 wt%, 11 wt%) and (6 wt%, 24 wt%) (Fig. (a), (b), (d), and (f)). However, LD of SSY was observed in the entire region of the sample in the cell when the concentration of the sample reagents were high, as shown in micrographs of the mixtures (29 wt%, 11 wt%) and (31 wt%, 13 wt%) (Fig. (g) and (h)).

The results of the observations are summarized as a ternary phase diagram in the next section. Furthermore, there were other phases with different preparation processes observed as the water in the sample cell evaporates over a long period of time. These phases exhibits very different textures than the phases shown in this section, which are shown in the later sections (See Sec. 5.4 and 5.5).

5.3 Ternary Phase Diagram

As described in the previous section, DTLM was used to identify various phases in a glass cell for over 100 combinations of various SSY and DSCG concentrations at room temperature (20 ~ 25°C). The birefringence observed under DTLM were identified as either I, N, or M phases or combinations of those. Based on the determined phases and the concentration of the reagents and water, a ternary phase diagram (TPD) was made as shown in Fig. 5.2. The TPD shows an overview of the LC phases of the mixtures of SSY and DSCG that exhibit I phase at a low concentration of the reagents in water and LC phases at a high concentration of the reagents in water.
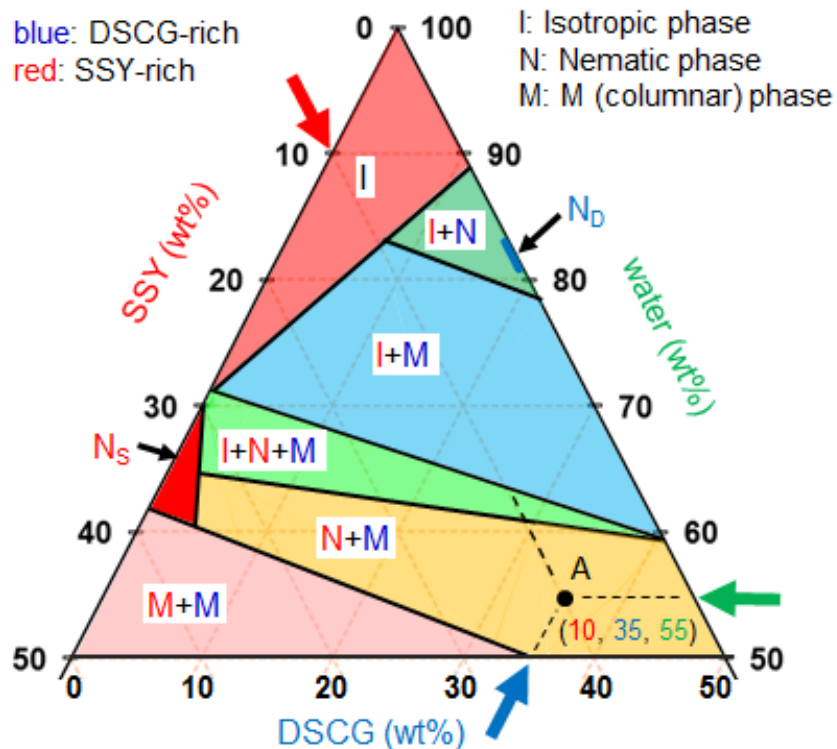
Fig. 5.2 Ternary Phase Diagram[6] of the mixture of SSY, DSCG, and water. Over 100 samples were prepared and observed under DTLM. Total of eight different combinations of the phases of SSY and DSCG LC were found. Uniform N-phases were identified in very limited regions indicated with the black arrows and the following letter 'N'. Blue letters represent DSCG-rich phases and red letters represent SSY-rich phases. (For example, at point A, which is represented by a black dot on lower right, c_S = 10 wt%, c_D = 35 wt%, and c_w (concentration of water) = 55 wt%.) The linear boundaries among different phases were identified based on the tendency of the phases corresponding to each concentration. Therefore, the boundary is not definite, and thus the observed phase can vary at the concentrations near the phase boundary.

Since a little amount of water in the sample can evaporate while preparing the cells, there was a little uncertainty in the recorded concentrations. In addition, the distinction between the N and M phases were less clear for some samples than the difference between I and N or M phase because the difference in the observed textures were not always comparable to the known textures of the LC phases in pure SSY or DSCG. However, this TPD reveals an overall tendency of the LC phase transition at various concentrations of SSY and DSCG.

---

[6] In order to improve the visibility of the TPD, not every axis shows all the concentrations, that is 0 to 100 wt%. Another triphase of I+N+M, where I phase is SSY-dominant and N and M phases are DSCG-dominant, was expected but hardly observed. The original TPD and the details of this triphase is further described in Appendix V.

Compared to the phase diagrams of pure SSY and pure DSCG, the TPD indicates that the mixture of SSY and DSCG form LCs at lower concentrations of water than when they were mixed with water separately. Moreover, the TPD shows that the mixtures can exhibit biphase or triphase in the same cell except when the mixture was uniform I or N phases at low concentrations of both or one of the reagents.

The TPD were made based on the observations of the samples with known amounts of each reagent and water. A total of eight phase coexistences were observed under this preparation method. However, different phases were observed based on the different preparation techniques with indefinite concentration. These phases are described in Sec. 5.4, 5.5, and 5.6.

5.4 Template Effect of DSCG-rich domains

For I+N or I+M biphase samples, as shown in Fig. 5.1 (d) and (f), the lower order phase (i.e., I phase) of SSY domains were observed to lose water by evaporation and became higher order phases such as N or M phases over time. Moreover, the SSY-rich domains seemed to follow the direction of the aggregates of DSCG, as shown in Fig. 5.3. In other words, the N or M phase of DSCG-rich domains seemed to affect the directions of the SSY aggregates as they evolved to form higher order phases.

5.4.1 Template Effect in M+M Biphase

As shown in Fig. 5.3 (a) – (d), these new M+M coexistence phases exhibit clear phase separation that cannot be seen in Fig. 5.1 (g) or (h) in Sec. 5.2. Moreover, the orientation of SSY aggregates follow the orientation of the DSCG aggregates. From Fig. 5.3, I call this orientational effect of DSCG-rich M domain the *template effect* since DSCG-rich domains seem to act as a template for SSY aggregates and affect their orientations. This effect can be observed by looking

44

at the same patterns of the dark brushes on and outside of the circular domains under a crossed

polarizer and analyzer and LD under only an analyzer (See Fig. 5.3).
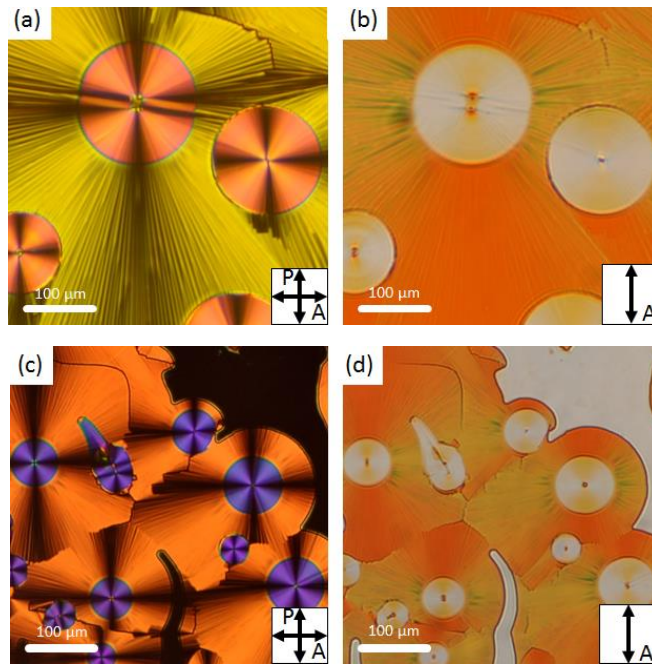
Fig. 5.3 Columnar (M) + Columnar (M) biphase of SSY and DSCG mixture. The clear separation between SSY and DSCG can be observed from these images. LD can also be seen in the micrographs on the right column. LDs in (b) and (d) indicate that SSY-aggregates were present on the surface of the DSCG-rich domain and follow the orientation of DSCG aggregates. The colors of circular domains and their surroundings observed under the crossed polarizer and analyzer (for figures (a) and (c)) are different due to the birefringence of DSCG with the index of refraction that would change depending on the thickness of the sample.

In order to verify the presence of SSY and LD on and outside of DSCG-rich circular

domain, µ-spectroscopy was used to measure the spectrum difference at different angles of the

analyzer. Two positions were selected (as shown in (1) and (2) in Fig. 5.4), and the absorption

spectra were measured (Fig. 5.5).
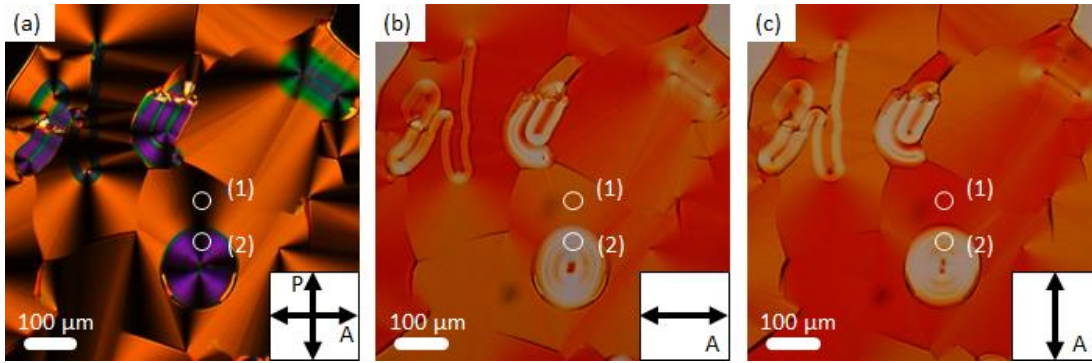
Fig. 5.4 Micrographs of Columnar (M) + Columnar (M) biphase. LD was visually observed by comparing the color difference between (b) and (c). The color in DSCG-rich M domain, position (2), was also changed by rotating the analyzer 90 degrees. This was an indication of the presence of well-ordered SSY aggregates on the DSCG-rich domain. Similar to Fig. 5.3, the template effect was observed.
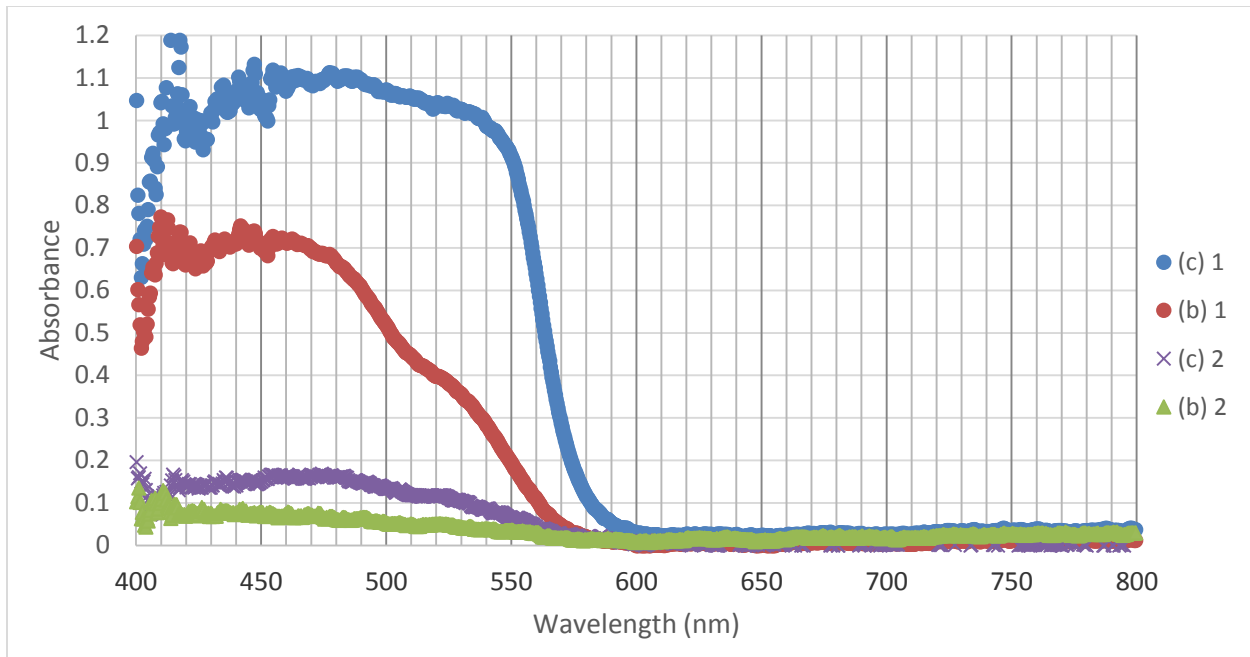
Fig. 5.5 Absorption spectra measured at two positions in M+M biphase. The labels (c1, b1, c2, b2) correspond to the labels and the positions in Fig. 5.4. For example, (b2) and (c2) represent the measured absorption spectrum at position (2) in figure (b) and (c), respectively. The absorbance at position (2) was less than that of position (1) because the c_S was much less on the DSCG-rich domain, as can be expected from the visual observation. Moreover, this plot shows evidence of the presence of LD of SSY from the different absorbance values between (b2) and (c2) at 480 nm.

The absorption spectrum of *(b) 1* shows a similar absorption peak as the one measured in Horowitz *et al.*, as shown in Fig. 3.8 [6]. However, the spectrum curve of *(c) 1* did not exhibit as clear of a peak as *(b) 1*. This is clue to the fact that *(c) 1* represents the saturated spectrum

curve because the curve shows little difference in absorbance in the range from 450 to 550 nm, which hides the characteristic curve of SSY (a peak at 480 nm).

5.4.2 Analysis of Order Parameters

Based on the absorption of light measured at two positions, one for the SSY-rich M phase domain and the other for the DSCG-rich M phase domain, the order parameter (S) (described in Sec. 2.1, eq. 2.3), for SSY was determined. Figure 5.6 shows the plot of S for SSY-rich and DSCG-rich domains based on the absorption measurement in Fig. 5.5.
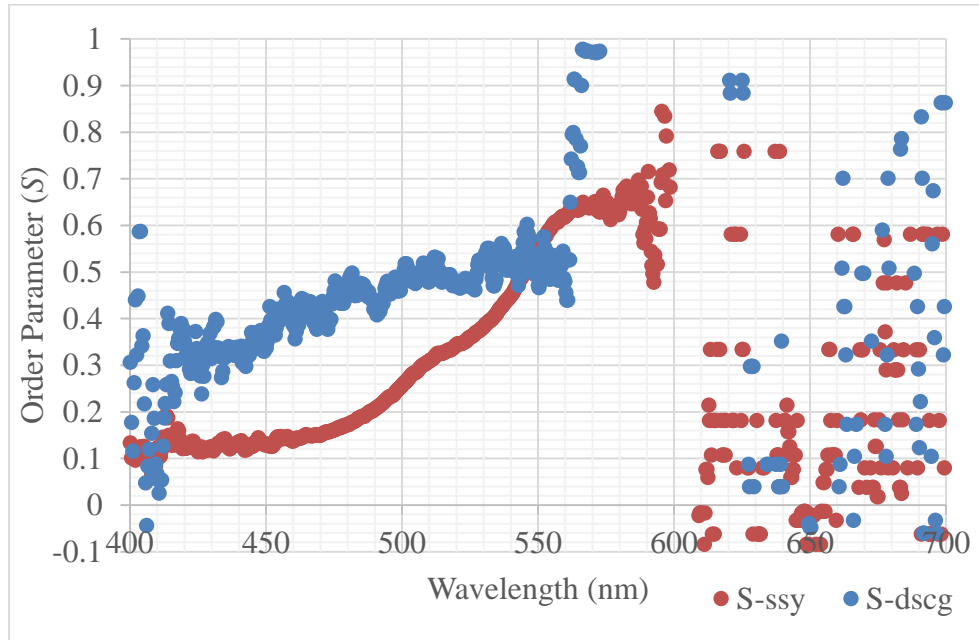
Fig. 5.6 The order parameter (S) vs. wavelength. S for the SSY-rich region is illustrated by red dots and S for DSCG-rich region is illustrated by blue dots. S above 600 nm become erratic because the absorption of light was very small as shown in Fig. 5.5.

Fig. 5.6 shows the increase in the order parameter of SSY-rich and DSCG-rich regions (point (1) and (2) in Fig. 5.4, respectively) under the wavelength ranges from 400 to around 600 nm. Since the absorption spectrum of the SSY-rich region, which is shown in Fig. 5.5, was saturated, the S_{SSY} was less than that of S_{DSCG} under the wavelength of 550 nm. This is consistent with the absorption spectrum shown in Fig. 3.8 by Horowitz *et al.* [6]. In addition, Fig. 3.8 and 5.5 show that the absorption of light was very small above 600 nm for SSY and 550 nm for

DSCG, and this indicates that the absorbance above these wavelengths is less likely to be saturated. Because the saturation effect is very small for S above 550 nm, the wavelength of 560.25 nm and 570.33 nm were selected to calculate S_{SSY}. Furthermore, because the absorption spectrum was not saturated for DSCG-rich domains at 480.11 nm, the absorbance at this wavelength was also used to calculate S_{DSCG}. Table 1 shows the absorption of light and the order parameter for the SSY-rich and DSCG-rich domains at the three selected wavelengths.

Table 5.1 Absorbance and the order parameter of the SSY-rich and DSCG-rich M phase domains. S for SSY-rich and DSCG-rich domains for a wider range of wavelengths are plotted in Fig. 5.6. S_{DSCG} at 570.33 nm (lower-right in the table) exceeds 1.0, which is theoretically impossible based on Eq. 2.1. This is because the absorption of light at the wavelength at 570.33 nm was very small and affected by the random measurements. Contrary to physical possibility and Eq. 2.4, negative absorbances were observed for 560.25 nm and 570.33 nm. These incomparable values are shown in red, and the reasonable values of the order parameter are highlighted in yellow.

Wavelength	SSY-rich			DSCG-rich		
	$A_\parallel$	$A_\perp$	S_{SSY}	$A_\parallel$	$A_\perp$	S_{DSCG}
480.11 nm	1.072	0.658	0.173	0.162	0.043	0.480
500.15 nm	1.046	0.513	0.257	0.043	0.012	0.463
560.25 nm	0.601	0.102	0.620	0.025	-0.001	1.130
570.33 nm	0.253	0.040	0.641	0.022	-0.005	2.250

The analyzer angles for the absorption measurement for $A_\parallel$ and $A_\perp$ were determined based on the visual observation of when the sample was dark or bright in comparison to different analyzer angles. If the absorptions were measured when the analyzer angle was slightly off (within 5 degrees) from the director of the aggregates ($A_\parallel$ and $A_\perp$), $A_\parallel$ would be lower than its maximum possible value and $A_\perp$ would be higher than its minimum possible value. Therefore, the values of the order parameter for both SSY-rich and DSCG-rich domains can be lower than their most accurate values.

However, compared to the typical values for the order parameter that ranges from 0.3 to 0.9 [1], the order parameter for both the SSY-rich ($S_{SSY} \approx 0.63$) and DSCG-rich ($S_{DSCG} \approx 0.47$)

domains fall within the range of the given values. Moreover, these results indicate that SSY aggregates are better aligned in the SSY-rich domains than in the DSCG-rich domains.

5.4.3 Potential Template Effect in I+N and I+M Biphases and Linear Dichroism

The previous section describes the alignment of the DSCG-rich domains affect on the alignment of the SSY aggregates on and around the DSCG-rich LC domains. In addition to the M+M biphase samples, the similar color changes were observed in the I+N and I+M biphase samples under DTLM without a polarizer. Due to the potential to gain further information about the molecular interaction between SSY and DSCG, the cause of these color changes were studied in further detail. This section describes the study on this potential template effect in the I+N and I+M biphase samples.

The color change was limited but observed in DSCG-rich nematic or columnar domain in I+N and I+M when the analyzer was rotated 90 degrees with no presence of a polarizer. Based merely on the visual observation with DTLM, SSY on DSCG-rich N or M phase domains seemed to exhibit LD (Fig. 5.7 and 5.8).
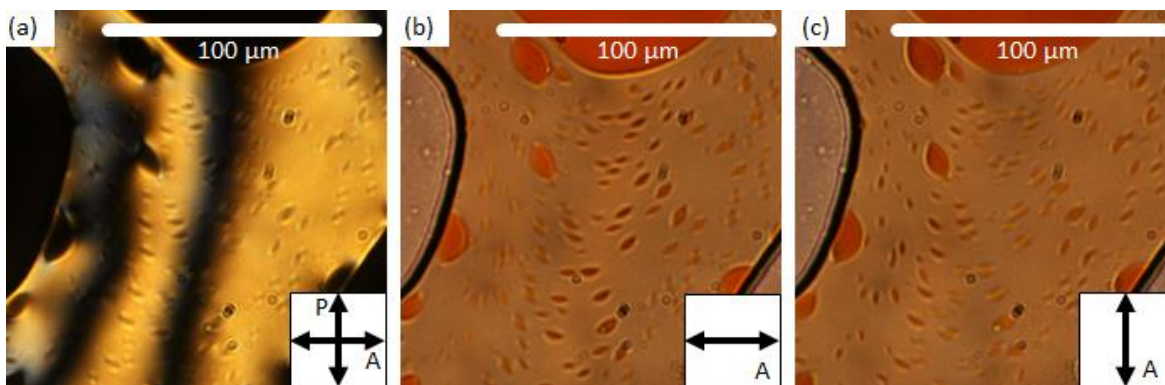
Fig. 5.7 I+N biphase of SSY and DSCG mixture. Color difference was observed when the analyzer was rotated 90 degrees. Notice that the brightness of the color around the center changes between the images (b) and (c). Moreover, the contrast at the boundary of isotropic domains in the DSCG-rich nematic region also changed significantly. Therefore, the color change in the DSCG-rich N phase domain was assumed to be due to LD of SSY. However, this change could also be due to the birefringence of DSCG.
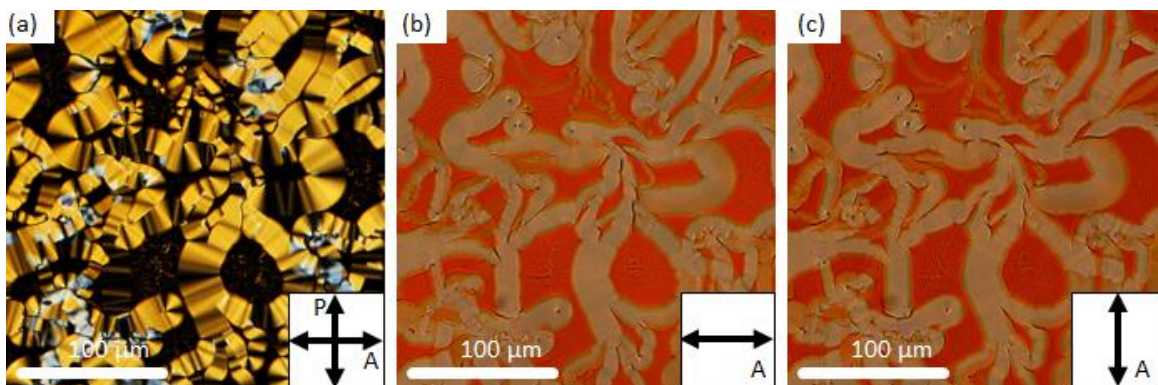
Fig. 5.8 I+M biphase of a SSY and DSCG mixture. Similar to the I+N mixture in Fig. 5.7, the color of the DSCG-rich M phase domain was changed when the analyzer was rotated 90 degrees. Since the contrast of the boundary between the DSCG-rich domain and the isotropic SSY regions was also changed, birefringence effect was expected.

However, since the visual observation did not give enough evidence for the presence of the template effect on very short SSY aggregates, the absorption spectra of these domains were measured with μ-spectroscopy in order to verify LD on DSCG-rich N or M phase domains.

5.4.4   Absorption Spectra of I+M and I+N+M Samples

Another sample mixture of SSY and DSCG (18.67 wt%, 10.79 wt%) that exhibits I+M biphase was prepared. The observed LC phase and the measured positions are shown in Fig. 5.9. The absorption spectrum of each position at different analyzer angles is shown in Fig. 5.10.

By comparing the color of the circular DSCG-rich M phase domain around the upper center of the Fig. 5.9 (b) and (c), the color change was visually observed. Moreover, the color and/or the brightness at the positions labeled by (1) and (2) also changed. However, in contrast to the visual observation of the color change of the DSCG-rich M phase domains, no significant change was measured in the absorption spectrum to conclude the presence of LD (Fig. 5.10).
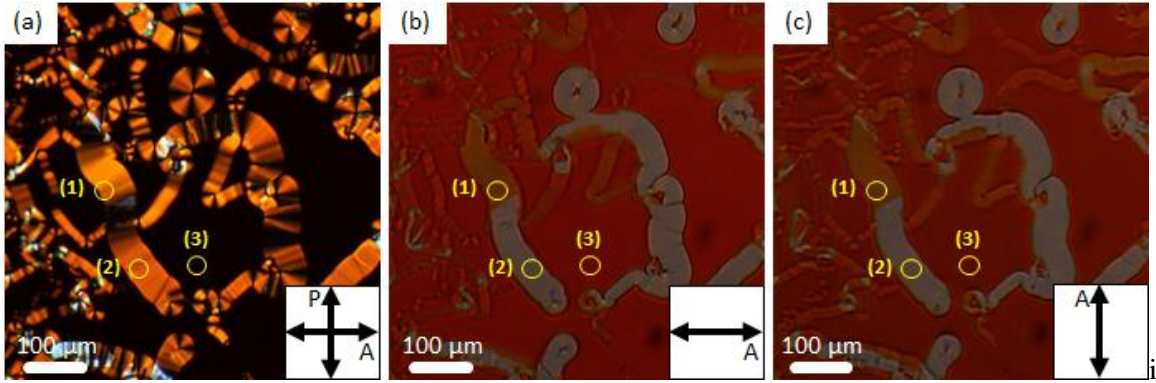
Fig. 5.9 DTLM images of I+M biphase sample. Absorbance spectrum at points (1), (2), and (3) were measured. Point (1) is the DSCG-rich M domain covered with SSY-rich I phase. Point (2) is a DSCG-rich M phase domain with little presence of SSY. Point (3) is considered a SSY-rich I phase. The spectrum curves are shown in Fig. 5.10.
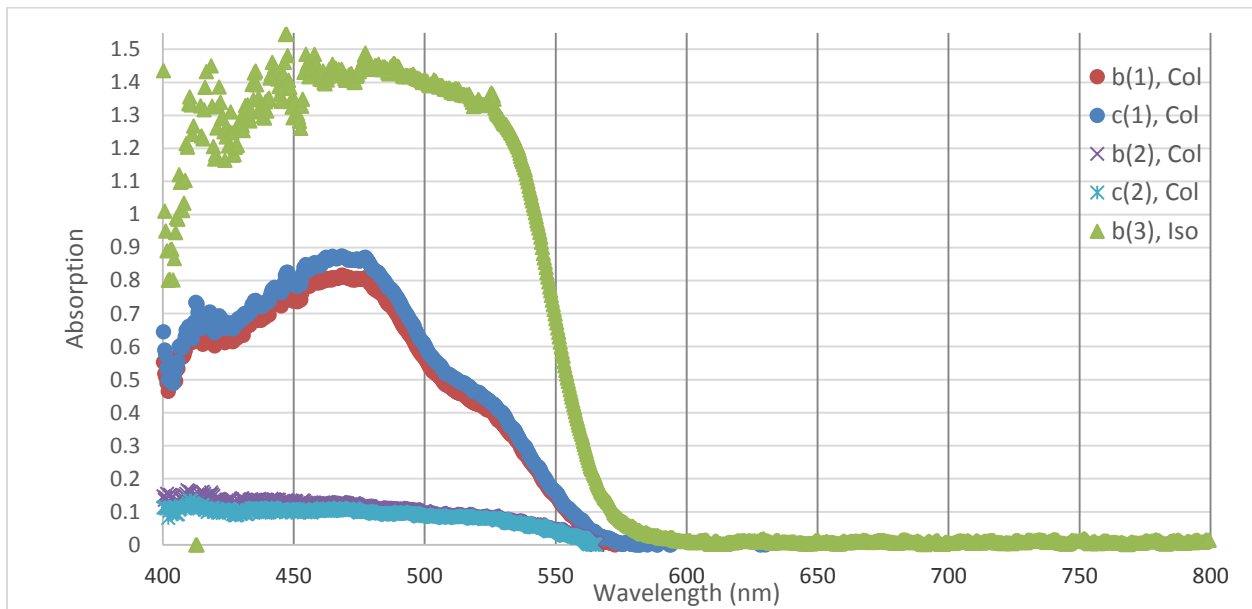
Fig. 5.10 Absorption spectra at three positions of the I+M biphase sample. The labels on the upper right represent the positions of the measurements. For example, *b(1), Col* was measured at point (1) when the analyzer was oriented horizontally (as in Fig. 9 (b)). The spectrum curve measured at the SSY-rich I phase domain (labeled as b(3)) is saturated since the absorbance does not change in the range from 450 to 500 nm, or the absorption peak of SSY is no longer clear at this high value of the absorbance.

Based on the results in Fig. 5.10, no LD was confirmed on the DSCG-rich M phase domain. However, in order to verify the presence of LD in other samples, an additional sample that exhibits I+N+M triphase was prepared. The observed LC phase and the measured positions are indicated in Fig. 5.11, and the measured spectra are shown in Fig. 5.12.
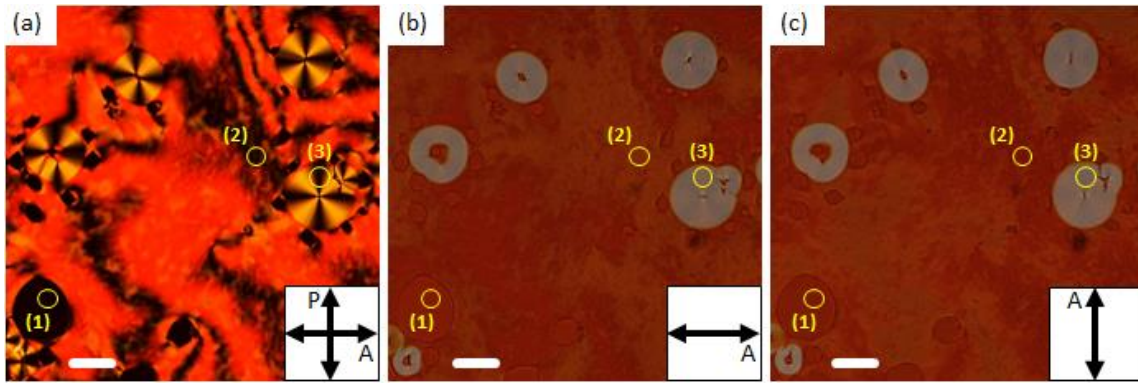
Fig. 5.11 I+N+M triphase sample with initial concentration of (18.67%, 10.79%). The absorption of light was measured at points (1), (2), and (3). Point (1) is SSY-rich I phase domain. Point (2) is SSY-rich N phase domain. Point (3) is DSCG-rich M phase domain with a little presence of SSY. The spectrum curves are shown in Fig. 5.12.
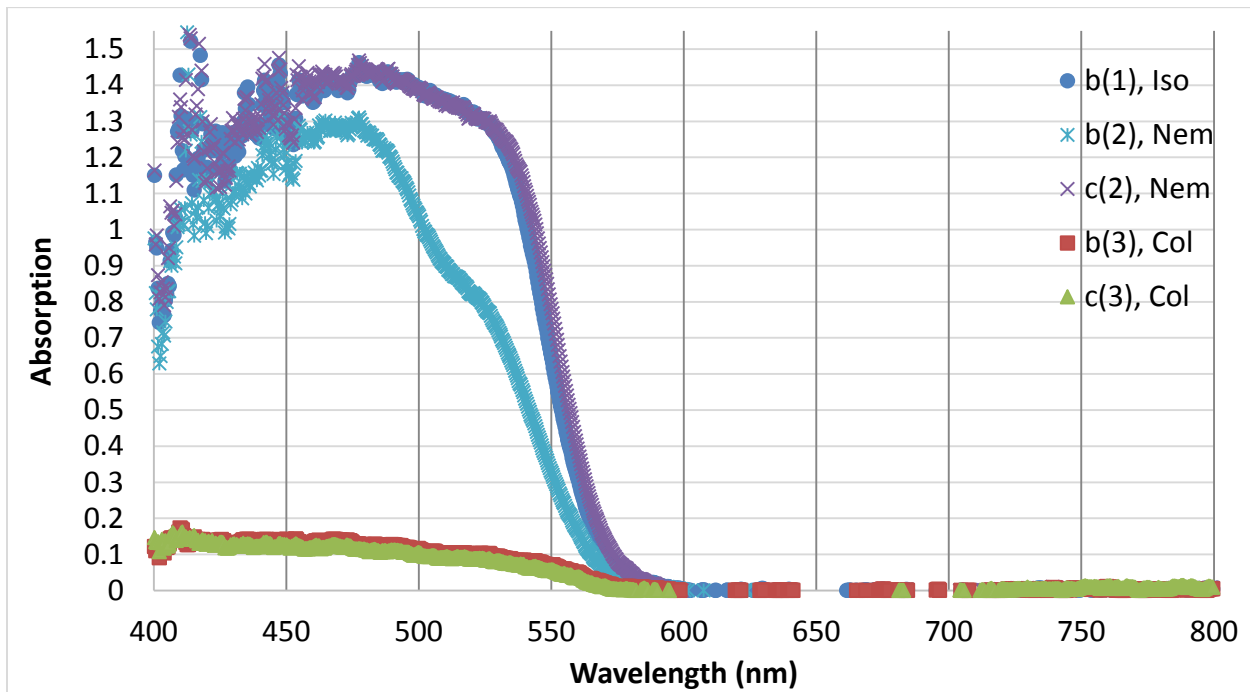
Fig. 5.12 The absorption spectrum for I+N+M triphase. The labels on the upper right represent the measured positions and the phases under different angles of the analyzer, as shown in Fig. 5,11 (b) and (c). For example, "*b(1), Iso*" was measured at point (1) when the analyzer was oriented horizontally, as shown in Fig. 5.11 (b).

As well as the I+M biphase sample described above, this I+N+M triphase sample also exhibited no LD on DSCG-rich M phase domain. Since no LD was verified in DSCG-rich LC domains, the color difference was assumed to be due to the birefringence of DSCG. In order to verify the birefringence of DSCG, the next section describes the absorption spectra measurements of a DSCG-rich uniform N phase domain.

5.4.5 Verification of Linear Dichroism in DSCG-rich N phase domains

In addition to the I+N and I+M biphase samples, a DSCG-rich uniform N phase sample was prepared, as shown in Fig. 5.13. The absorption spectra of this sample were measured in order to check LD of SSY in DSCG-rich N phase domain.
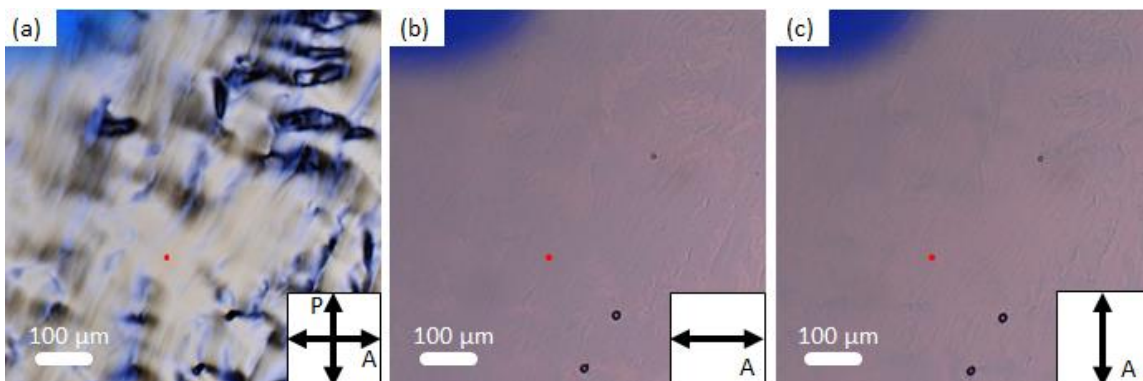
Fig. 5.13 Absorption spectra curves of DSCG-rich nematic domain were measured with a μ-spectroscope. The sample mixture had concentrations of (0.21 wt%, 12.53 wt%) and formed uniform N phase. The spectrum was measured at the position with a red dot around the center of the images. The spectra curves are shown in Fig. 5.14.
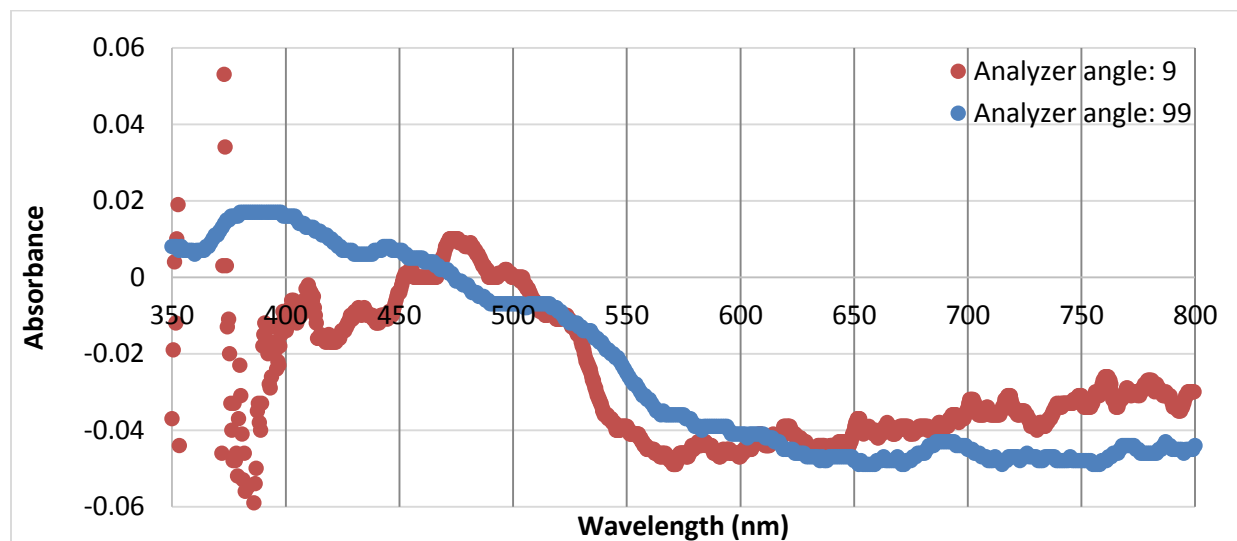
Fig. 5.14 Original absorption spectra for DSCG-rich N phase. The absorption spectra of DSCG-dominant N phase were measured at two different analyzer angles. The difference in the absorbances between the two plots is very small (within the range of 0.01). This indicates that SSY didn't exhibit LD. Moreover, the very small values of absorbance indicate that little SSY was present in the sample, as expected by the concentrations of (0.21 wt%, 12.53 wt%). Also the values of absorbance are much smaller than the absorbance range of 0.5 ~ 1.3 that was shown in LD on columnar DSCG domain (Fig. 5.4 and 5.5). In addition, the absorbance values are negative in wide ranges of the wavelength. This is due to the initial calibration of the spectrometer. This effect was compensated for by setting the average absorption value to be zero above 650 nm when analyzing the order parameter in Sec. 5.4.2.

Based on the measurements above, the limitations of the μ-spectrometer became clear as follows: (1) the diameter of the optical fiber of about 50 μm limits the resolution and the accuracy in position of the absorption measurements. This limitation can be easily overcame by selecting a large and uniform LC domain. However, if a position of the measurement contains very small domain of SSY in I phase (as we can see in Fig. 5.7), then the absorption measurement becomes more uncertain. (2) As shown in Fig. 5.14, if the absorbance of the transmitted light is very small, the relative uncertainty becomes large.

5.5 Stripe Texture (evolution of phase in SSY-dominant uniform N phase sample)

In addition to the eight phases (phase coexistences) that were reported in Sec. 5.2, a unique phase development in the mixture of SSY and DSCG was observed. This new phase exhibited the separation between SSY and DSCG over time. Initially, the sample was a SSY-dominant uniform N phase (as shown in Fig. 5.1 (c) 1-3 in Sec. 5.2), but the separation of SSY-rich and DSCG-rich domain was observed over time as shown in Fig. 5.15.
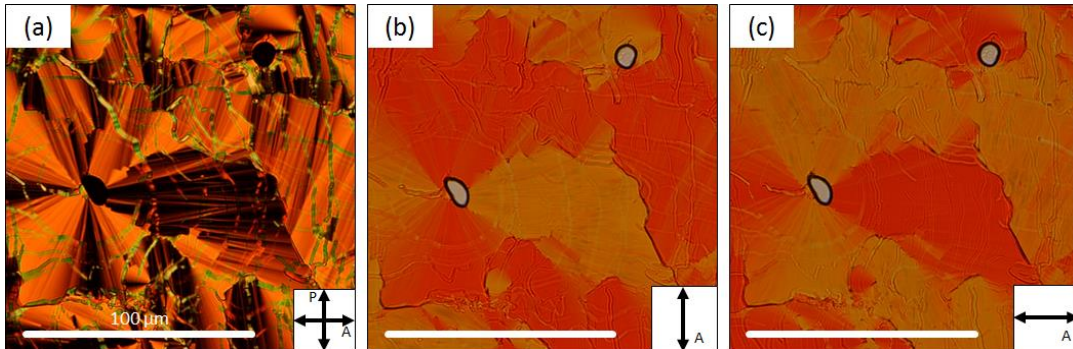
Fig. 5.15 Stripe Texture. (a) The texture observed under a crossed analyzer and polarizer. (b) The texture observed under an analyzer and without a polarizer. (c) The texture observed under only an analyzer rotated 90 degrees from (b). LD was confirmed by comparing the color change between (b) and (c). The change in color in the DSCG-rich columnar regions follow LD of SSY.

The texture shows narrow stripes of different colors (yellow or green in Fig. 5.15 (a)) compared to their surroundings. Therefore, by comparing Fig. 5.15 with Fig. 5.1 (h) and Fig. 5.4, it was assumed that the concentration of DSCG in those striped regions are higher than in their

surroundings. It was expected that DSCG molecules are slowly excluded from SSY domains and form in islands or lines, as shown in Fig. 5.4 (a) or 5.15, (a), respectively.

The small DSCG aggregates tend to stack together to form longer aggregates due to Brownian motion. Moreover, these longer aggregates reach an energetically favorable state over time. Possible model of the mixed aggregates of the stripe texture and template effect are proposed later in Sec. 6.3.

5.6 Exclusion Effect (DSCG-dominant uniform N phase)

In addition to the stripe texture that was observed in SSY-dominant uniform N phase described in the previous section, the phase evolution of DSCG-dominant uniform N phase was also observed. In contrast to the SSY-dominant uniform N phase sample, the DSCG-dominant uniform N phase sample excludes SSY as time evolves (see Fig. 5.16, 5.17, and 5.18).

By continuing the observation of the same sample over a few days, it was seen that water in the sample slowly evaporated and the phase developed into an I+M biphase. The separation between SSY-rich I phase and DSCG-rich M phase became clear as shown in Fig. 5.18 below.
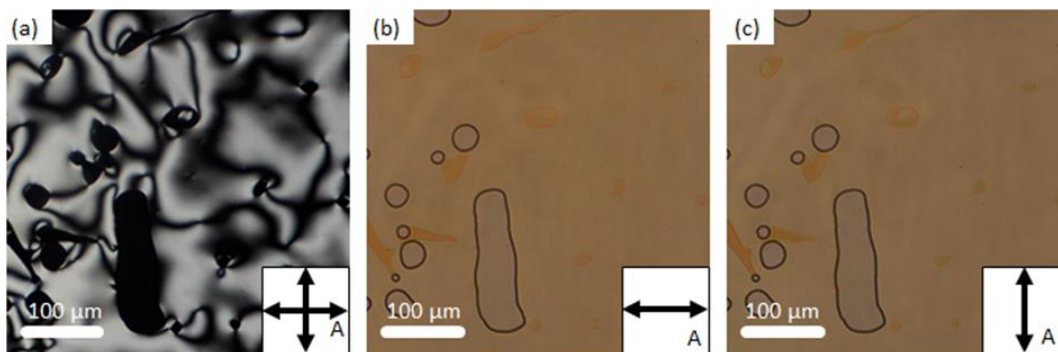
Fig. 5.16 DSCG-rich uniform N phase sample of the concentration (0.20 wt%, 20.12 wt%). This sample initially exhibited uniform texture with no separation between SSY-rich I phase and DSCG-rich N phase. The images (a) ~ (c) are taken during the process of cooling after thermal dispersion. As time evolved, the separation between these I and N phases got smaller and finally became uniform N phase, as shown in Fig. 5.17.
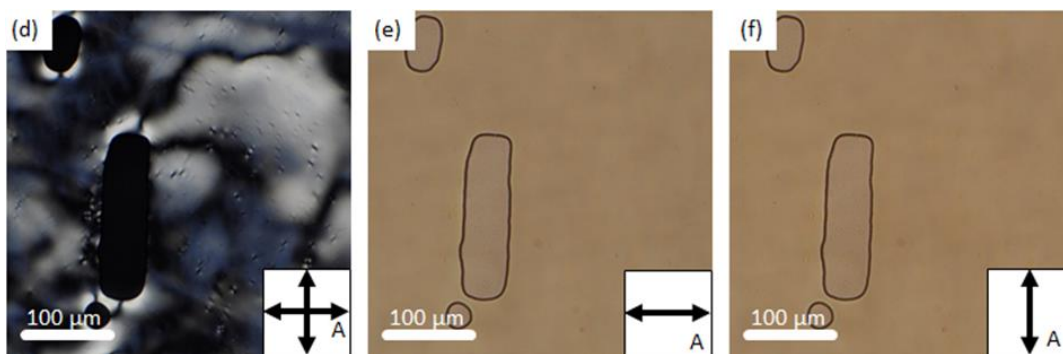
Fig. 5.17 Micrographs of DSCG-rich uniform N phase sample. This uniform phase was observed in the same sample cell as in Fig. 5.16. Many small domains can be seen in (d). Magnified observation indicates that SSY-rich I phase is present in these small domains. It was easy to distinguish the difference between I or N phase when the domain size was large enough to be observed, as shown in Fig. 5.7. However, it became harder to distinguish the difference between the SSY-rich and DSCG-rich domains as the I domain size became smaller.
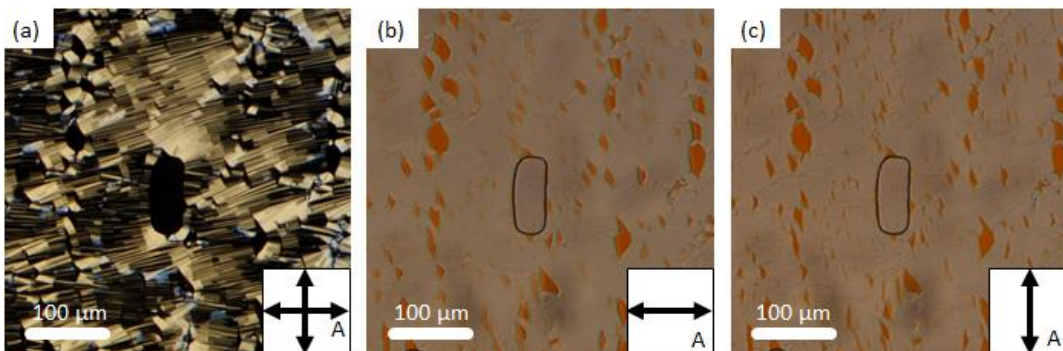
Fig. 5.18 Micrographs of I+M biphase. The I+M phase evolved from DSCG-dominant uniform N phase sample (Fig. 5.17). Compared to Fig. 5.17, clear separations between SSY-rich I phase and DSCG-rich M phase were observed in (b) and (c).

It is likely that minority aggregates (i.e. SSY in DSCG-rich uniform N phase sample) coexist in the majority aggregates in N phase, as long as the size of the minority aggregates are small enough and the interaction with the majority aggregate is insignificant (Fig. 5.17). As the concentration of SSY and DSCG increases above a certain concentration[7], the size of aggregates of the minority material becomes larger and likely to be expelled from the domains of the majority aggregate. In M phase domains, even very small minority aggregates were expelled (Fig. 5.18). Further discussion on this exclusion behavior is described in Sec. 6.6.

---

[7] The concentration of the sample increased due to natural evaporation of water. Therefore, the accurate concentrations for SSY and DSCG to exhibit the clear separation was undetermined. However, it is assumed that the concentration of each reagent is higher than their initial concentrations (0.20 wt%, 20.12 wt%).

Chapter 6

Discussions

This chapter introduces further analysis and findings based on the results described in Chapter 5. The limits of visual observation are discussed in Sec. 6.1. The ternary phase diagram is discussed in Sec. 6.2. Moreover, based on the computer simulated model of pure SSY proposed by Chami and Wilson [8] and pure DSCG aggregate model by Agra-Kooijman *et al.* [18], renewed models of the molecular and aggregate interactions between SSY and DSCG are proposed in Sec. 6.3. LD of SSY and the inherent polarization effect of DTLM is described in Sec. 6.4. The template effect and the stripe textures that were shown in Sec. 5.4 and 5.6 are discussed in Sec. 6.5. Finally, the exclusion effect of DSCG-rich domain is discussed in Sec. 6.6.

6.1. Visual Observation

Based on visual observations, a total of eight phase coexistences were found. Within each, we observed the tendency of SSY and DSCG's partial mixing in both M and N phases to form SSY-rich and DSCG-rich domains as described in Chapter 5 (Sec. 5.2). In addition, different sample and cell preparation techniques allowed the mixtures to exhibit different LC textures than the textures shown in Chapter 5, such as the template effect of DSCG (Sec. 5.4) and stripe texture (Sec. 5.5).

While the visual observation with DTLM was a quick way to observe the samples and determine the phase or phase coexistences, the nature of this technique limits the accuracy because the sample can exhibit complicated texture, as shown in Fig. 5.1 (e) and (h). Therefore, an additional test was necessary to verify the presence of LD in I+N or I+M biphase samples using μ-spectroscopy, as described in Sec. 5.4. However, there was a difficulty in determining

the phase when the separation between DSCG- and SSY-rich phases was not clear, especially when the concentration of the sample was very high compared to the amount of water. Furthermore, it was difficult to determine the phase to be either N or M because the sequence of the phase formation was counterintuitive especially for DSCG (since DSCG exhibits M phase before N phase during the cooling process after thermal cycling), which was reported by Agra-Kooijman et al. [18].

Therefore, in addition to the visual observation, spectroscopic analysis was necessary in order to make an accurate determination of the phases. Moreover, X-ray crystallography may allow us to determine the phases with less confusion if the diffraction pattern is clear and comparable to the diffraction of the well-known phases that have already been shown by Agra-Kooijman et al. [18] and Horowitz et al. [6].

6.2. Ternary Phase Diagram

The ternary phase diagram (TPD) was made based on the visual observation of over 100 samples and the corresponding data of concentrations of each reagent. Compared to the phase diagram of pure SSY reported by Horowitz et al. [6], TPD shows that SSY remains in I phase even at higher concentrations when DSCG is added (Sec. 5.3, Fig. 5.2). This is probably because the volume fraction of DSCG aggregate is larger than that of SSY aggregate. Furthermore, it became clear from the TPD that SSY is more hydrophilic than DSCG because SSY tends to remain in I phase while DSCG tends to become higher order phases (i.e., N or M phase) when they are mixed in water.

Although the separation between SSY and DSCG was not as clear as we can see in I+N or I+M biphases, the mixture of SSY and DSCG can exhibit M phase (Sec. 5.2, Fig. 5.1 (h)) and the coexistence of M+M biphase (Sec. 5.4, Fig. 5.3). However, no sample was observed that

exhibited N+N biphase, or a clear separation between SSY-rich N phase and DSCG-rich N phase domains. The possible reason the mixture does not exhibit N+N biphase is because the concentrations for SSY and DSCG to exhibit N phase are different, and because SSY tends to retain water from DSCG-rich domains and remain lower order phases.

6.3. Molecular Models

Based on the previous works by Chami and Wilson's computer simulated model of SSY [8] and the DSCG aggregate model by Agra-Kooijman *et al.* [21], the models of molecular interaction between SSY and DSCG aggregates were made (Fig. 6.1 (a)-(h)). In order to make these models, the relative size of SSY and DSCG molecules and the aggregate structures were considered. In particular, head-to-tail (antiparallel) stacking of SSY and head-to-head (parallel) stacking of DSCG molecules were taken into account.

Figures 6.1 (a) – (h) show the structures and the arrangement of SSY and DSCG aggregates in I, N, and M phases as well as the observed combinations of these phases. The observed phase coexistences show the separation of SSY and DSCG aggregates and the invariance of the stacking distance of the aggregates without linear dichroism of SSY in DSCG M phase.

Fig. 6.1 (a) – (h). Sketches of the modeled structures of mesophases of the mixtures. DSCG molecules are represented by blue colored objects and SSY molecules are represented by orange colored objects. Water molecules are not illustrated in the figure but they are assumed to be present.
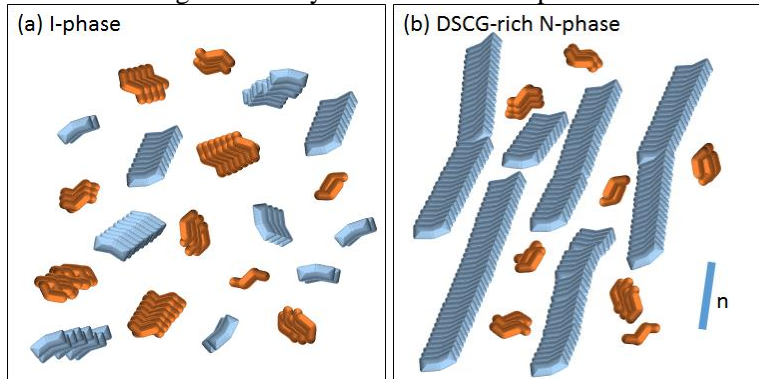
Fig. 6.1 (a) I phase. When concentrations of both materials are low in water, the aggregates are short and have no preferred orientation. Hence, the mixture exhibits I phase.

(b) DSCG-rich uniform N phase. When the concentration of DSCG is dominantly higher than that of SSY and the concentration of DSCG is close to the concentration to form pure-DSCG nematic phase, such as (0.5 wt%, 20wt%), the mixture exhibits uniform N phase. In this mixture, DSCG aggregates become much longer than that of SSY and align in a preferred direction, **n**, while very short SSY aggregates reside in the DSCG-rich N phase domain in random directions.
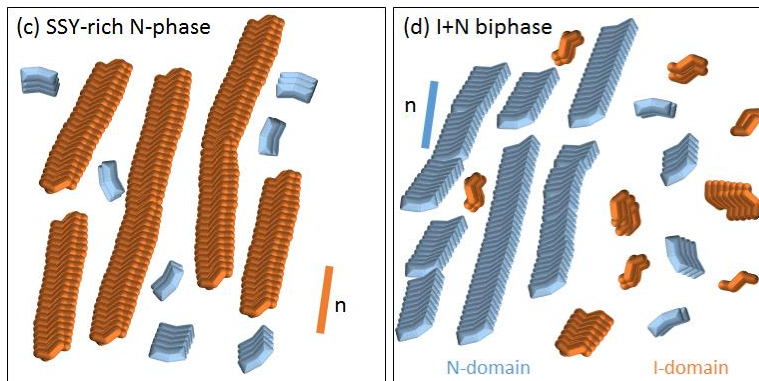
(c) SSY-rich uniform N phase. When the c_S is dominantly higher than the c_D and is close to the pure-SSY nematic phase concentration, such as (30 wt%, 0.5 wt%), the mixture exhibits uniform N phase. Under this condition, SSY aggregates become longer than that of DSCG and are aligned in a preferred direction, **n**, while very short DSCG aggregates reside the N phase domain in random directions.

(d) I+N biphase. As the ratio between c_S and c_D decreases (or becomes closer to the ratio of 1:1), the mixture exhibits I+N biphase. It is expected that the DSCG-rich N phase domain has a limitation in containing SSY aggregates in the amount and size because the small packing-distance of DSCG aggregates exclude SSY aggregates. Therefore, I and N phase domains are separated.
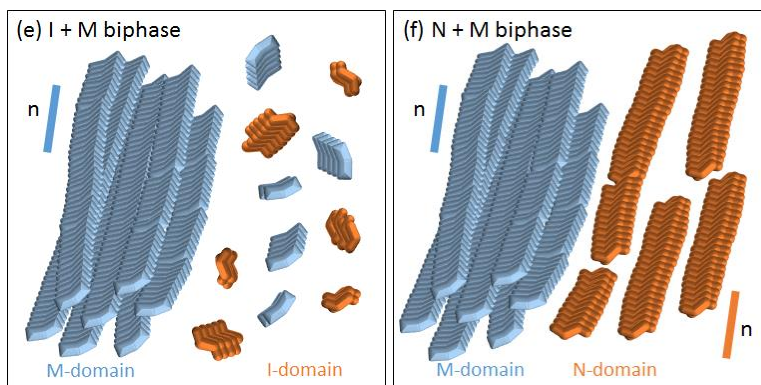
(e) I+M biphase. As c_D in the mixture further increases from I+N biphase, the DSCG aggregates become longer and better aligned to form a columnar structure by expelling more of the short SSY aggregates over time. Therefore, I and M phase domains are separated as shown.

(f) N+M biphase. As c_S in the mixture increases from I+N or I+M biphases, the SSY aggregates become longer and better aligned to form a nematic structure. The direction of SSY aggregates tend to be aligned parallel or perpendicular to the direction of the DSCG aggregates.
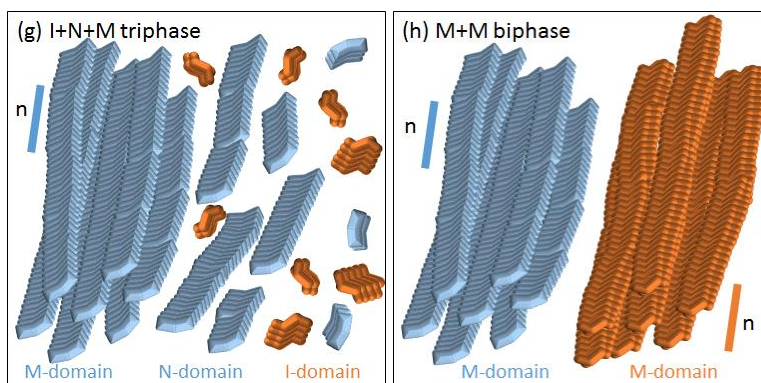
(g) I+N+M triphase. This model is made based on the DSCG-rich triphase that can be seen in Fig. 5.1 (e) in Sec. 5.2. However, there is another type of I+N+M triphase observed in SSY-rich triphase, as shown in Fig. 5.10 in Sec. 5.4.2. In the case of the SSY-rich triphase, SSY is rich in I and N phase domains while DSCG is rich in M phase.

(h) M+M biphase. As the concentration of the mixture increases from I+N or I+M biphases, SSY aggregates become longer and better aligned to form a columnar structure over time. Different textures of M+M biphase were observed based on the different cell preparation techniques as described in Sec. 5.2 and 5.4. The separation between the SSY-rich and DSCG-rich domains was not clear[8], as shown in Fig. 5.1 (h). The molecular model of the template effect of DSCG is discussed in detail in Sec. 6.5.

The basis of the models drawn above are as follows: for the I phase, the molecules are stacked and form short aggregates that are randomly oriented. For the N phase, the aggregates become longer than the aggregates in I phase, and they obtain directional ordering. For the M phase, the aggregates become even longer than when they are at N phase, and the aggregates

---

[8] See Sec. 5.4 (Fig. 5.3) for the case when the cell is prepared with thermal dispersion and the template effect

obtain positional ordering in addition to orientational ordering.

6.4. Linear Dichroism of SSY on DSCG-rich LC Domains

Based on visual observation of the color change of I+N and I+M biphase samples under DTLM, LD was predicted to be present on DSCG-rich N or M phase domains because the short SSY aggregates were expected to align parallel to the longer aggregates of DSCG. However, the spectrum analyses of DSCG-rich N and M phase domains confirmed that there was no LD as described in Sec. 5.4.2. In addition, by measuring the spectrum of the pure DSCG N and M phase samples, it was confirmed that the color change was because of the birefringence of DSCG as described in Sec. 5.4.2.

On the other hand, while LD of SSY was not detected in both I+N and I+M biphases, LD was detected in DSCG-rich LC domains by both visual observation and μ-spectroscopy measurements when both concentrations of SSY and DSCG were high in water and formed the M+M biphase (Sec. 5.4.1).

Further optical spectroscopic measurements of the mixtures will be important to determine the local concentration of SSY and the orientational order parameter of each chromonic material accurately. Furthermore, X-ray scattering analyses are expected to provide useful information to elucidate the structure of the self-assembled LC phases of the two chromonics in water, such as the aggregate structure and the molecular spacing.

6.5. Molecular Models of the Template Effect and Stripe Textures

In contrast to I+N and I+M biphases, LD of SSY on DSCG-rich M phase domain was observed as shown in Fig. 5.3 and 5.4 in Sec. 5.4.1. Based on the relative orientation of the sample and the analyzer of DTLM, the direction of SSY aggregates were determined. The molecular models of the alignment of the aggregates were made and shown in Fig. 6.2 (c)
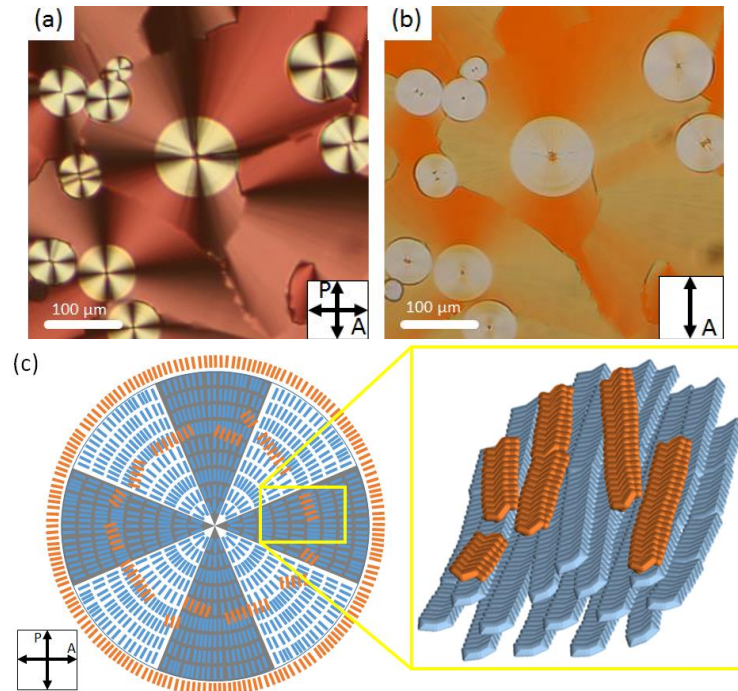
Fig. 6.2 Micrographs and the molecular model of the template effect. (a) M+M biphase observed under crossed polarizer and analyzer with DTLM. (b) An observed texture without the presence of the polarizer. The LD of SSY is present on DSCG-rich circular M phase domain and LD. Moreover, LD in the surrounding SSY-rich domains exhibit the same aggregate directions as the SSY aggregates in DSCG-rich domains. (c) An illustration of the expected directions of SSY and DSCG aggregates, which was viewed from the top, on DSCG-rich circular domain. The SSY aggregates are drawn by a set of orange bars that represent SSY molecules. The DSCG molecules are illustrated by blue bars. In this illustration, the direction of DSCG aggregates is expected to be parallel to the direction of SSY aggregates.

In addition to the template effect of DSCG on surrounding SSY aggregates, the template effect and LD on DSCG-rich domain were observed. Fig. 6.2 (a) and (b) shows the observed phase under different orientation of the analyzer. The Fig. 6.2 (c) shows the illustration of the models of each molecule on the DSCG-rich domain and surrounding SSY molecules.

This section described possible models of the template effect of DSCG aggregates on SSY aggregates. The effect was observed when there were clear boundaries between SSY-rich and DSCG-rich domains but they were in contact with each other. In order to better understand the behavior of the aggregates that separate each other, a possible molecular model of the exclusion effect is described in the next section.

63

6.6. Exclusion Effect of DSCG-rich domains

Short aggregates of SSY can dissolve into DSCG-rich N phase domains when there is enough space in DSCG-rich domains. By decreasing the concentration of water (c_W), the space among DSCG aggregates is decreased and it is likely that the aggregate size of SSY is increased. Thus SSY is excluded from the DSCG-rich domains and this will lead the short SSY-aggregates to form small SSY-rich I phase domains. This process of the exclusion effect is shown in Fig. 6.3. Furthermore, the molecular model of this dissolution and exclusion of short SSY-aggregates is illustrated in Fig. 6.4.
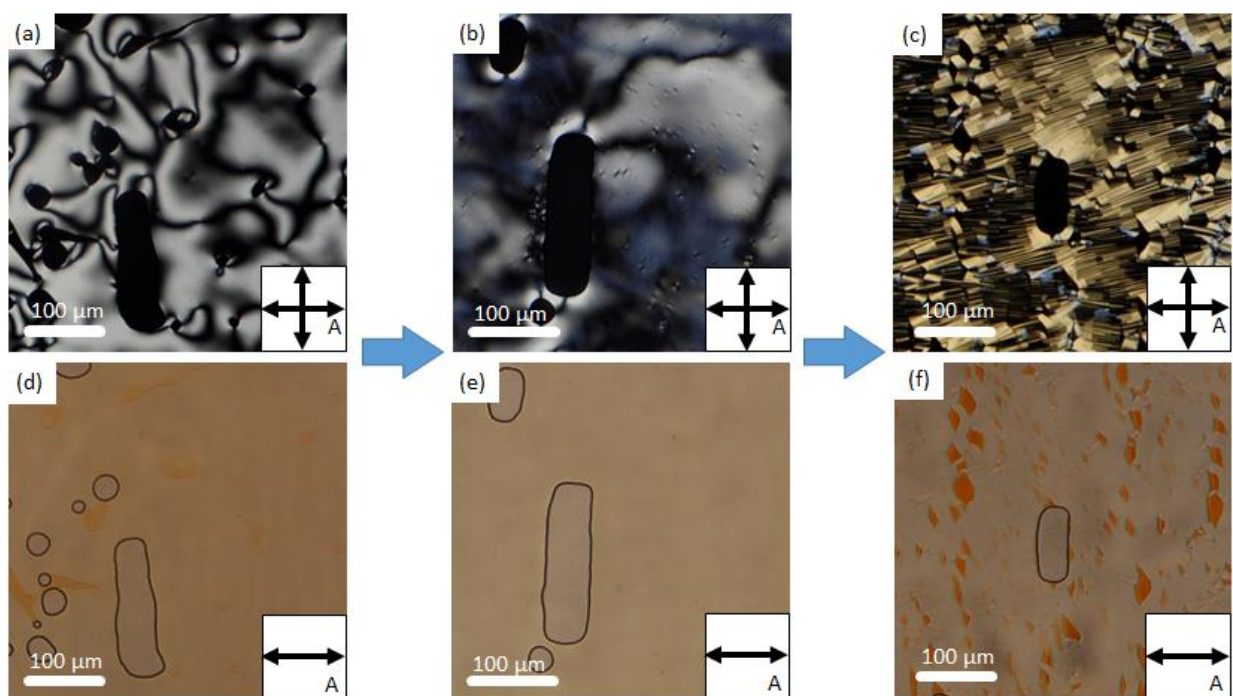
Fig. 6.3 Micrographs of the time evolution of DSCG-rich uniform N phase sample. The micrographs (a) and (d) are observed during the process of cooling after thermal dispersion. After 0.5 ~ 1 hour, the temperature of the sample cooled down to room temperature and the SSY-rich I phase domains dissolved into DSCG-rich N phase domains as shown in (b) and (e). The micrographs (c) and (f) show the same sample observed a few days after the sample was made. The micrographs (c) and (f) show I+M biphase. The water in this cell was expected to evaporate over time. By increasing the concentration of the sample, the DSCG-rich N phase domain turned into M phase and excluded SSY aggregates. The clear white regions in (d), (e), and (f) within the clear black boundaries are air bubbles.
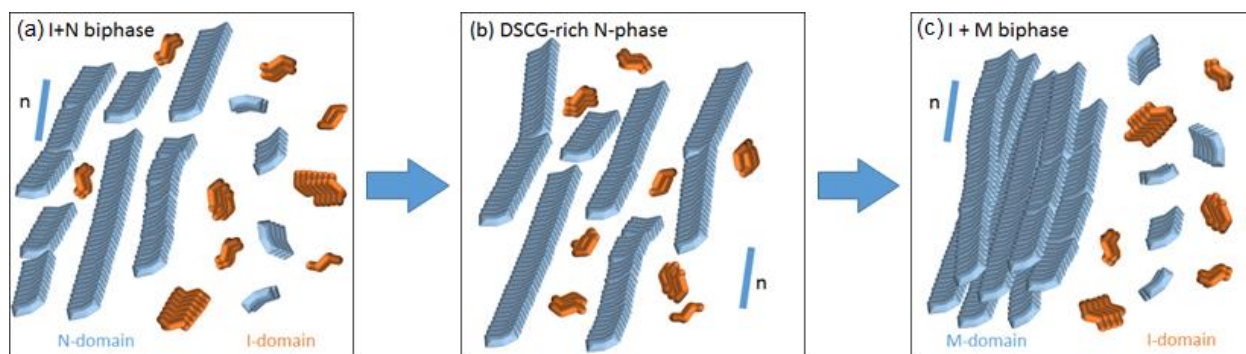
Fig. 6.4 Molecular model of the dissolution and exclusion of short SSY-aggregates in the DSCG-rich N phase domains. Figures (a), (b), and (c) correspond to (a, d), (b,e), and (c,f) in Fig. 6.3, respectively.

Based on the observations of various phase evolutions such as the stripe texture, exclusion effect, and template effect, it became clear that the mixture of SSY and DSCG in water exhibits various degrees of separation and phase coexistences depending on the concentration, age, and thermal history. It is expected that these phase behaviors of the mixture are due to the separation of the molecules in the formation of the aggregates and the separation of aggregates by their slow diffusion.

The processes of evolution are summarized in Table 2. The initial phase depends on the initial concentration of the samples. These initial phases evolve to form higher order phases (i.e., the transition from I to N and finally to M phase) over time by losing water. This time evolution, or age, changes the concentration of the sample and LC phases. For the samples that were initially prepared as higher ordered phase or phase coexistence exhibited a less ordered texture as shown in Fig. 4.7 (a) and Fig. 5.1 (h). By applying additional thermal dispersion[9], the samples exhibited a well-ordered texture as shown in Fig. 4.7 (c), while the sample with a high initial concentration couldn't be dispersed well enough to exhibit clear separation between SSY-rich and DSCG-rich domains. As more water was lost from the M+M biphase, the samples started becoming solid crystals.

---

[9] An additional thermal history was added by deliberately raising and cooling the temperature of the sample.

Table 6.1 Summary of the initial phase(s), their processes of phase evolution, and the final equilibrium phase(s). The ninth phase, I+(N+M) (DSCG-rich), is a hypothetical phase that was not observed but expected to be observed.

	Initial Phase(s)	Steps of Evolution	Equilibrium Phase(s)
1	I	→ I+M → N+M → M+M	M+M
2	N_S	→ N+M → M+M	M+M (Stripe Texture)
3	N_D	→ I+M → N+M → M+M	M+M
4	I+N	→ I+M→ N+M → M+M	M+M
5	I+M	→ N+M → M+M	M+M
6	N+M	→ M+M	M+M Template if thermally controlled.
7	M+M	Very little change	M+M Template if thermally controlled.
8	(I+N)+M (SSY-rich)	→ N+M → M+M	M+M
9	I+(N+M) (DSCG-rich)	→ N+M → M+M	M+M

Most samples exhibited the template effect when they became M+M biphase, except the sample no. 6 and 7 in Table 6.1. The samples that were initially prepared to be M+M biphase had very high viscosity and it seemed hard for the samples to rearrange their molecules to reform the template texture. Furthermore, only one sample (N_S) exhibited the stripe texture, as shown in Fig. 5.15.

Chapter 7

Conclusions

Throughout the project, we studied LC phases of the mixtures of two well-known LCLC materials, Sunset Yellow FCF (SSY) and Disodium Cromoglycate (DSCG) in water using a depolarized transmitted light microscopy and an UV-Vis spectroscopy. Mixtures of the two LCLCs (SSY and DSCG) in water exhibit diverse mono-, bi-, and tri-phasic micro-textures. A phase diagram of the mixtures was made based on visual observations, as shown in Fig. 5.2.

Furthermore, the details of the molecular interaction between SSY and DSCG were studied. Specifically, based on the measurements of the absorption spectrum of SSY, SSY was found to have no linear dichroism in DSCG-rich N or M phase domains in I+N and I+M biphase samples. Moreover, in biphasic or triphasic mixtures, a tendency of SSY to stay in relatively lower ordered phases was observed while DSCG tends to stay in higher ordered phases.

A total of eight phase coexistences were observed. In addition to these phases, the novel LC phases called stripe texture and DSCG's template effect were found. Based on the visual observation of the template effect, DSCG was found to affect the alignment of SSY aggregates when SSY became N or M phases from I phase. Based on the detailed analysis of the absorption spectrum of the phase coexistences and the template effect, the molecular models of the mixture were proposed in Ch. 6. These models are expected to be accurate in terms of relative size of the molecules, aggregate structures, and their ordering to describe the behavior of the molecules when two chromonics are mixed in water. Finally, the various degrees of phase separation were explained depending on the concentration, age, and thermal history of the sample.

References

[1] P. J. Collings, *Liquid Crystals: Nature's Delicate Phase of Matter* (Princeton University Press, Princeton, N.J, 1990).

[2] M. Nakata, G. Zanchetta, B. D. Chapman, C. D. Jones, J. O. Cross, R. Pindak, T. Bellini, and N. A. Clark, Science **318**, 1276 (2007).

[3] T. P. Fraccia, G. P. Smith, G. Zanchetta, E. Paraboschi, Y. Yi, D. M. Walba, G. Dieci, N. A. Clark, and T. Bellini, Nat. Commun. **6**, (2015).

[4] T. K. Attwood and J. E. Lydon, Mol. Cryst. Liq. Cryst. **108**, 349 (1984).

[5] Y. A. Nastishin, H. Liu, T. Schneider, V. Nazarenko, R. Vasyuta, S. V. Shiyanovskii, and O. D. Lavrentovich, Phys. Rev. E **72**, 041711 (2005).

[6] V. R. Horowitz, L. A. Janowitz, A. L. Modic, P. A. Heiney, and P. J. Collings, Phys. Rev. E **72**, 041710 (2005).

[7] J. P. de Almeida Martins, F. V. Chávez, and P. J. Sebastião, Magn. Reson. Chem. **52**, 540 (2014).

[8] F. Chami and M. R. Wilson, J. Am. Chem. Soc. **132**, 7794 (2010).

[9] N. H. Hartshorne and G. D. Woodard, Mol. Cryst. Liq. Cryst. **23**, 343 (1973).

[10] J. E. Lydon, Mol. Cryst. Liq. Cryst. **64**, 19 (1980).

[11] J. Lydon, Curr. Opin. Colloid Interface Sci. **3**, 458 (1998).

[12] J. Lydon, J. Mater. Chem. **20**, 10071 (2010).

[13] P.-G. de Gennes, *The Physics of Liquid Crystals*, 2nd ed (Clarendon Press ; Oxford University Press, Oxford : New York, 1993).

[14] S. Chandrasekhar, *Liquid Crystals*, 2 edition (Cambridge University Press, Cambridge England ; New York, NY, USA, 1993).

[15] S. Shoarinejad and M. S. Zakerhamidi, Mol. Cryst. Liq. Cryst. **613**, 149 (2015).

[16] J. Lydon, Liq. Cryst. **38**, 1663 (2011).

[17] J. S. G. Cox, G. D. Woodard, and W. C. McCrone, J. Pharm. Sci. **60**, 1458 (1971).

[18] D. M. Agra-Kooijman, G. Singh, A. Lorenz, P. J. Collings, H.-S. Kitzerow, and S. Kumar, Phys. Rev. E **89**, 062504 (2014).

[19] L. Wu, J. Lal, K. A. Simon, E. A. Burton, and Y.-Y. Luk, J. Am. Chem. Soc. **131**, 7430 (2009).

[20] D. J. Edwards, J. W. Jones, O. Lozman, A. P. Ormerod, M. Sintyureva, and G. J. T. Tiddy, J. Phys. Chem. B **112**, 14628 (2008).

[21] M. R. Tomasik and P. J. Collings, J. Phys. Chem. B **112**, 9883 (2008).

[22] H.-S. Park, S.-W. Kang, L. Tortora, Y. Nastishin, D. Finotello, S. Kumar, and O. D. Lavrentovich, J. Phys. Chem. B **112**, 16307 (2008).

[23] L. Joshi, Phys. Rev. E **80**, (2009).

[24] L. Joshi, S.-W. Kang, D. M. Agra-Kooijman, and S. Kumar, Phys. Rev. E **80**, 041703 (2009).

Appendix I

Apparatus and Sample Information

The following list shows the sources and the identification numbers of materials and the instruments used throughout the project.

Lyotropic Chromonic Liquid Crystals (Sigma-Aldrich Products Information)

Sunset Yellow FCF – Dye content 90%, Product number: 465224

Cromolyn sodium salt – Content $\geqq$ 95%, Product number: C0399 SIGMA

Water (HPLC): W5-4 (CAS 7732-18-5), Fisher Chemical

Cell Components

Glass plates (Slide Glass):

➢ VWR Micro Slides, 25×75 mm, 1.0 mm thick (Cat. No. 48300-25)

➢ VWR micro cover glass, 18×18 mm (Cat. No. 48366 205)

Mineral Oil, Heavy: O122-1 (CAS 8042-47-5), Fisher Chemical

Epoxy: unknown

Spacers: unknown

Instruments for Optical Measurements and Analysis

Microscope: Nikon OPTIPHOT – POL (ID No. UCB 116159 RPHC)

Temperature Controller: INSTEC STC 200D (Serial Number: 88990116)

Computer: Dell Dimension 3000 (Serial Number: CN-0UC283-70821-54C-O3VW)

Camera: Nikon D5000 (Serial Number: 3564107)

UV-Vis spectrometer: Evolution 60S, Thermo Scientific

(Serial Number: 2R1S167209) (CAT 840-208500)

Other Instruments

Centrifuge: Biofuge A, Model 1217, Baxter

(Serial Number: 161312) (ID No. University of Colorado at Boulder 141660)

Pipettes: 2.5 ul and 10 ul pipettes, Eppendorf Research

Plastic Vial: 1.7 ml Micro Tubes, OmniSeal

Appendix II

Mathematica Codes for Extinction Coefficient Analysis

In order to determine the extinction coefficient (also known as absorption coefficient) from the data obtained from the absorption measurement of SSY solutions, *Mathematica* was used. Based on the weighted-average method, a linear fit curve with the errors associated with each measurement was found. The following *Mathematica* codes or inputs and outputs of [1] ~ [25] show the *Mathematica* functions that were used to generate the linear fit, errors, and the plot. The original codes for the absorption coefficient analysis were obtained and modified from http://nano-optics.colorado.edu/index.php?id=60 (*Mathematica* file: *Wlinfit.nb*).

Initialize *Mathematica*.

```
In[1]:=      Clear["Global`*"]
```

Load a file to make error bar plots.

```
In[2]:=      Needs["ErrorBarPlots`"]
```

Import the data from the excel file (in CSV format).

```
In[3]:=      s480 = Import["[directory of the data file].csv"];

In[4]:=      ss480 = s480[[1]];

In[5]:=      x = ss480[[All, 1]]; (*Absorption*)

In[6]:=      y = ss480[[All, 2]]; (*Concentration*)

In[7]:=      σ = ss480[[All, 3]]; (*Standard Deviation*)

In[8]:=      L = Length[σ];
```

Set the error bars on the plot.

```
In[9]:=      yerror = Table[ErrorBar[σ[[i]]], {i, 1, L}];

In[10]:=     xydata = Thread[{x, y}];

In[11]:=     xyerrordata = Thread[{xydata, yerror}];
```

Make a plot.

```
In[12]:=     P2   =   ErrorListPlot[xyerrordata,   PlotStyle   →   {Red,
         PointSize[Medium]}, PlotRange → {{xmin, xmax}, {ymin, ymax}}, Frame → True,
```

```
FrameLabel → {"Concentration of SSY (wt%)", "Absorbance/Thickness"},
LabelStyle → 18, FrameStyle → Bold,  ImageSize → Large, GridLines →
Automatic, PlotRange → All]
```

Out[12]:=
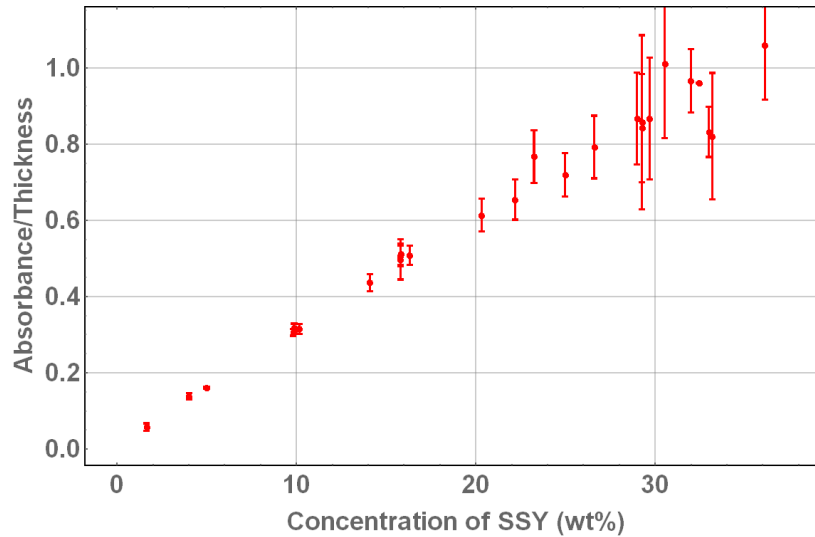
In[13]:= $J = \sum_{i=1}^{L} (\frac{x[i]}{\sigma[[i]]})^2 ;$

In[14]:= $M = \sum_{i=1}^{L} (\frac{x[i]}{\sigma[[i]]^2}) ;$

In[15]:= $P = \sum_{i=1}^{L} (\frac{y[i]*x[i]}{\sigma[[i]]^2}) ;$

In[16]:= $G = \sum_{i=1}^{L} (\frac{1}{\sigma[[i]]^2}) ;$

In[17]:= $H = \sum_{i=1}^{L} (\frac{y[i]}{\sigma[[i]]^2}) ;$

In[18]:= $\Delta = J * G - M^2 ;$

Set the slope of the best-fit line, *m*.

In[19]:= $m = \frac{P*G - M*H}{\Delta} ;$

Set the intercept of the best-fit line, *b*.

In[20]:= $b = \frac{J*H - P*M}{\Delta} ;$

Calculate the uncertainty of the slope *m*.

In[21]:= $\delta m = (\frac{1}{\Delta}) \sqrt{\sum_{i=1}^{L} (\frac{G*x[[i]] - M}{\sigma[[i]]})^2} ;$

Calculate the uncertainty of the intercept b.

```
In[22]:=
```
$$\delta b = \left(\frac{1}{\Delta}\right)\sqrt{\sum_{i=1}^{L}\left(\frac{J-M*x[[i]]}{\sigma[[i]]}\right)^2} \ ;$$

Display the slope, intercept, and their uncertainties.

```
In[23]:=      Grid[{{"m", m}, {"δm",δm}, {"b", b}, {"δb",δb}}, Frame → All]
Out[23]:=
```

m	0.029104
δm	0.0000702649
b	0.0161932
δb	0.00227911

Make a plot of the best fit.

```
In[24]:=      P1 = Plot[m*x + b, {x, xmin, xmax}, PlotRange → {{xmin, xmax}, {ymin,
         ymax}}, Frame → True, FrameLabel → {"Concentration of SSY (wt%)",
         "Absorbance/Thickness", "λ = 480.11 nm"}, LabelStyle → 18, FrameStyle →
         Bold, ImageSize → Large, GridLines → Automatic, PlotRange → All];
```

Make a combined plot of the plots *P1* and *P2*.

```
In[25]:=      Show[P1, P2]
Out[25]:=
```
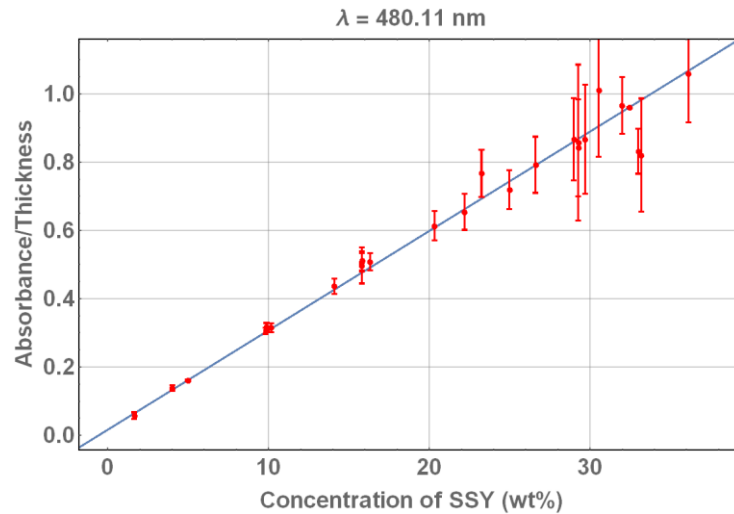
Appendix III

Absorption Coefficient Analysis

Based on the measurements of the peak absorption of SSY at the wavelength of 480.11 nm, the plot of the absorption vs. the weight concentration of SSY was made (Fig. III-1). The slope of the linear curve is the absorption coefficient (ε) and was determined to be $\varepsilon = 0.029$ (wt%$^{-1}$μm^{-1}). The uncertainty of the absorption coefficient is $\delta\varepsilon = 7.02\times10^{-5}$ (wt%$^{-1}$μm^{-1}). Furthermore, the intercept of the slope is b = 0.016 (μm^{-1}) with the uncertainty of δb = 0.002 (μm^{-1}).
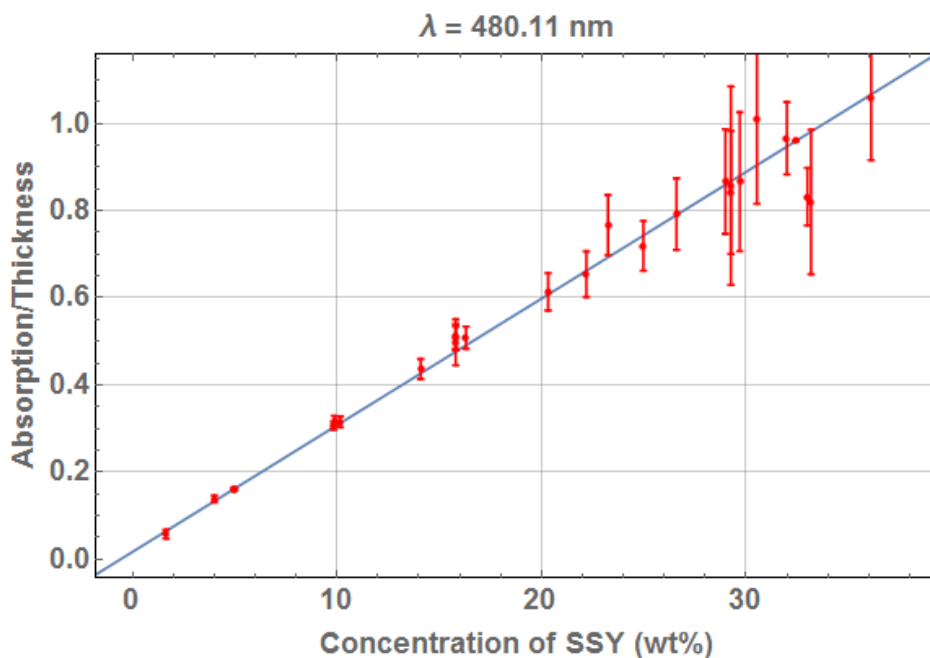
Fig. III-1 A plot of concentration versus absorption per unit path length of 1 μm. Based on the plot, the extinction coefficient was determined by analyzing the slope of the linear fit. The extinction coefficient ε is 2.9 $\times 10^{-2} \pm 7.02 \times 10^{-5}$ (wt%$^{-1}$μm^{-1}) and the intercept b is 0.016 ± 0.002 (μm^{-1}). The uncertainty of the curve is proportional to the concentration of the solution because the absorption spectrum tends to saturate at the higher c_S as described in Sec. 4.6.

Appendix IV

Absorption Spectra, Concentration, and Cell Thickness

In Section 4.6, we stated that in order to measure the absorption spectrum without saturation using μ-spectrometer, either the concentration of SSY must be lowered or the path lengths (or thickness of the cell) must be shortened. Furthermore, in order to make measurements of the absorption spectrum to calculate the order parameter, it was important to measure the spectrum without saturation. However, since LC phases of SSY have very high concentrations (i.e., above 27 ~ 30 wt%), it was necessary to make a thin cell to measure the spectrum without saturation, as shown in Fig. 4.3 (b) Standard Cell in Sec. 4.3.

Based on the measurements of the absorption spectrum of SSY by varying the thickness of the cell, the following table was made that illustrates the relation between the weight concentration of SSY (c_S) and the cell thickness with the indications of saturation of the spectra.

Table III-1 List of the weight concentrations of SSY, sample thickness, absorption of light, and saturation.

c_S (wt%)	Thickness (μm)	Absorption intensity at 480 nm (a.u.)	Saturation
1.65	5.0 ~ 6.0	0.20 ~ 0.34	No
4.01	2.0 ~ 3.0	0.30 ~ 0.40	No
5.54	5.0 ~ 6.0	0.70 ~ 0.80	No
9.83	5.5 ~ 6.5	1.70 ~ 1.85	Yes
9.87	3.0 ~ 3.5	0.65 ~ 0.85	No
14.09	2.0	0.90 ~ 1.10	No
17.42	5.0 ~ 5.5	2.10 ~ 2.80	Yes
23.25	1.0 ~ 1.5	0.90 ~ 1.40	No
26.40	2.0 ~ 3.0	1.00 ~ 2.00	Yes

As shown on the table, a cell with a thickness of less than 5 μm can be used for absorption measurement for the c_S of less than 6 ~ 7 wt%. When using a cell with the thickness of 2 ~ 3μm, the absorption spectrum is not saturated for the sample with 10 ~ 20 wt% of SSY. Moreover, a cell with the thickness of 1 μm can be used up to 29 wt% of SSY.

Appendix V

Ternary Phase Diagram

The ternary phase diagram (TPD) of the mixture of SSY and DSCG is shown in Sec. 5.3 (Fig. 5.2). This shows the total of eight phase coexistences at various concentrations of SSY, DSCG, and water. Although the triphase of I+N (SSY-rich) +M (DSCG-rich) was observed (as shown in Fig. 5.1 (e-i) and (e-ii)), the triphase of I (SSY-rich) +N+M (DSCG-rich) was not observed. This phase was expected to be (but was not) observed during the process of phase transition from DSCG-rich uniform N phase (N_D) to I+M biphase, in between the phases shown in Fig. 5.17 and 5.18. Moreover, the biphase of N+M (SSY-rich) +M (DSCG-rich) was expected to be (but was not) observed during the process of phase transition from N+M phase to M+M phase. If the biphase of N+M+M and the triphase of I+N+M were observed and taken into account, the TPD would be expected to be as shown in Fig. V-1.

Although the coexistence of SSY-dominant I phase and DSCG-dominant N and M phase were expected, the I+N+M triphase was not observed. The difficulty in the observation of this biphase and triphase can be expected to be due to abrupt and counterintuitive phase behavior of DSCG. As described by Agra-Kooijman *et al.* [18], we also observed the phase transition from I to M and eventually to N phase without the transition of I to N phase between I to M phase during the process of cooling, as shown in Fig. V-2.

The original ternary phase diagram was made before simplification. This phase diagram is shown in Fig. V-3.
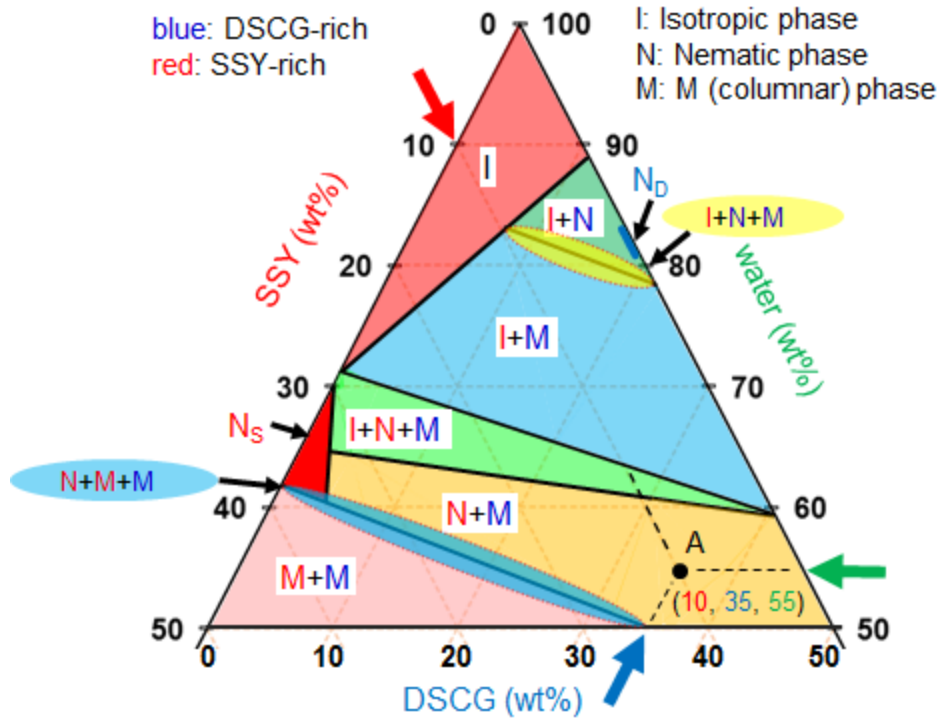
Fig. V-1 Alternative Ternary Phase Diagram. In this phase diagram, two phases (triphase of I+N+M, a coexistence of SSY-dominant I phase and DSCG-dominant N and M phase, and biphase of N+M+M) were taken into account and shown in the yellow and blue shaded area at the boundary between I+N and I+M biphases and between N+N and M+M biphases, respectively.
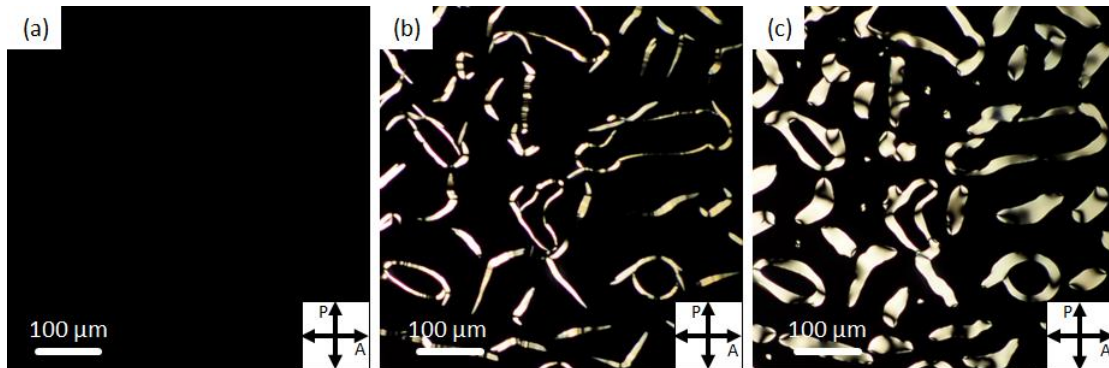
Fig. V-2 Micrographs of pure DSCG during thermal cycling (cooling-process). (a) The sample exhibited I phase at high temperature. (b) (I+M biphase) By lowering the temperature of the sample, M phase of DSCG started appearing. (c) (I+N biphase) As the temperature of the sample further lowered down, the M phase domain got larger and became N phase. By lowering the temperature of the sample further at room temperature, the sample exhibited uniform N phase. The initial concentration of DSCG in water was 21.7 wt%. This behavior was not illustrated by Lydon in the phase diagram shown in Fig. 3.1 [11].
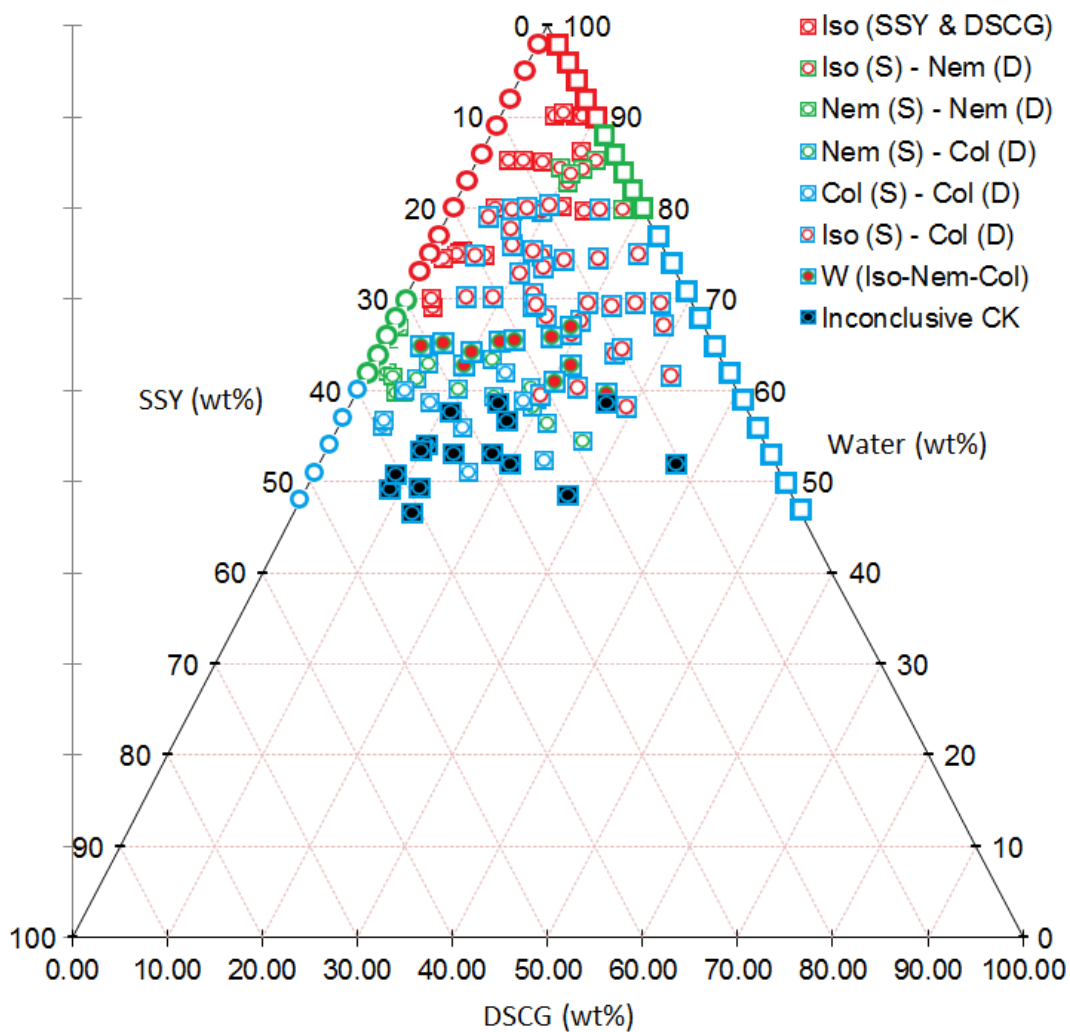
Fig. V-3 Original Phase Diagram. The axes of the phase diagram range from 0 to 100 weight %. More than 100 samples were observed and plotted on the TPD. The overall phase behavior was simplified and shaded for better visibility, as shown in Fig. V-2 or Fig. 5.2. No sample was prepared for the reagent concentration higher than 55 wt%, or the concentration of water lower than 45 wt% because the sample became very viscous and the sample cell could not be prepared properly for visual observation.

Appendix VI

Publication and Conference Poster

The portion of this research focusing on the mixture of Sunset Yellow and Disodium Cromoglycate was submitted in October 2015 with title: *Phase and Structures of Sunset Yellow and Disodium Cromoglycate Mixtures in Water* to the journal *Soft Matter*.

The following pages show a poster presented at the International Liquid Crystal Conference of the International Liquid Crystal Society in Trinity College in Dublin, Ireland in 2014.

Phase Behaviour of Chromonic Liquid Crystal Mixtures

A. Yamaguchi,[1] C. Xu,[1] G. Smith,[1] Y. Yi,[1] S. Biffi,[2] F. Serra,[2] T. Bellini,[2] and N. Clark[1]

1. Liquid Crystal Materials Research Center, University of Colorado, Boulder, Colorado, U.S.A

2. Dipartimento di Chimica, Biochimica e Biotecnologie per la Medicina, Università degli Studi di Milano, Milan, Italy

Introduction

Nearly planar molecules with hydrophobic cores and hydrophilic peripheries stack into aggregates in water, forming chromonic liquid crystals (CLCs). Sunset yellow (SSY) and disodium cromoglycate (DSCG) are well-known CLCs and their phases and alignment are well studied.[1-4] Exploring self-assembly of the two molecules, which is roughly comparable to DNA, is of interest. We study the phase behavior of the CLCs of ternary mixtures of SSY and DSCG in water using polarized light microscopy. We present a ternary phase diagram of the mixtures including isotropic(I), nematic(N), and M (also called columnar), biphasic and tri phasic regions depending on species ratio and concentration at room temperature. Various degrees of phase separation of SSY and DSCG are observed. There is a tendency of DSCG-rich regions show higher order phases while SSY-rich regions show lower order phases due to the apparently higher affinity of SSY for water. Quantitative measurement of the local concentration in phase separation supportS the SSY-rich and DSCG-rich phase separation and the structure of the meso phases of the mixtures.

Self-Assembly and Phases of SSY

Molecular Structure
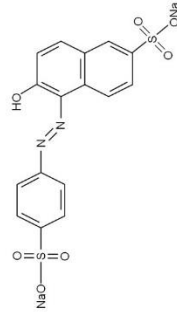
Self Assembly of SSY in Water
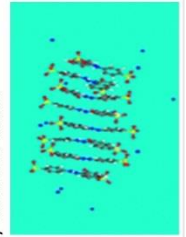
Chami and Wilson,
J Am Chem Soc
(2010)

Ternary Phase Diagram of SSY and DSCG Mixtures

Depolarized transmission light microscopy (pictures taken by this method are shown in the left column) was used to identify phases in over 90 combinations of SSY and DSCG with varying concentrations and ratios, all confined in glass cells. The phase diagram shows that the mixtures are biphasic and triphasic except at low concentrations, which only show isotropic phases.

M: M (columnar) phase
N: Nematic phase
I: Isotropic phase

blue letter: DSCG-rich
red letter: SSY-rich

water (wt%)

SSY (wt%)

DSCG (wt%)

At room temperature

I+N, I, I+M, I+N+M, N+M, M+M, E, (10, 35, 55)

[6,11] [6,24] [29,11] [31,13]

0.5 mm
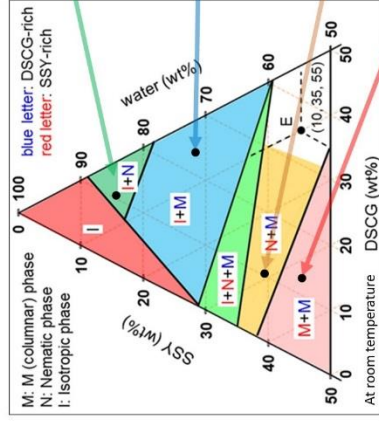
To guide reading of the diagram, point E, which represents 10, 35, and 55 wt% of SSY, DSCG, and water, respectively, is placed in the lower right of the diagram. The numbers on the pictures in the left column represent wt% of SSY and DSCG, respectively.
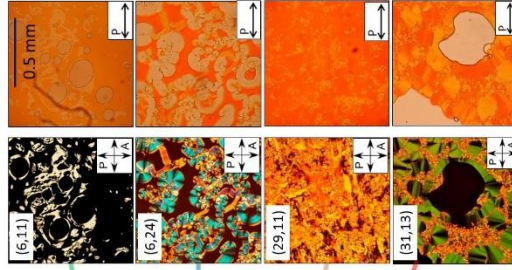
Micrographs taken without analyzer (right column) reveal the relative concentration of SSY between the domains because SSY absorbs blue and green light while DSCG is completely transparent in the visible light spectrum. The pictures in the right column of the first two rows reveals that SSY-poor (or DSCG-rich) domains have N and M phases while SSY-rich domains have I phase. This suggests that DSCG expels water more strongly and forms higher order phases more easily than SSY.

Also noticeable is that essentially no linear dichroism of SSY is observed when the concentration of SSY is low as shown in micrographs of the mixtures, (6,11) and (6,24). However, SSY linear dichroism is everywhere when its concentration is high, as shown in micrographs of the mixtures (29,11) and (31,13).

Relative Concentration of the Phases Messured using Spectroscopy

I. Spectroscopy of Bulk Phase Separation by Centrifugations

Glass Capillary — Mixture of SSY and DSCG — SSY + DSCG

Centrifugation — Phase Separation — SSY Rich / DSCG Rich

Cut off

Concentration Measurement (Spectrophotometry)

SSY Rich →
DSCG Rich →
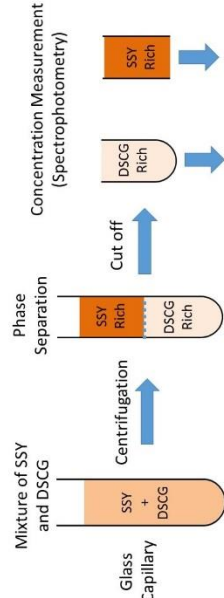
2. μ-Spectroscopy using Fiber Optic Spectrometer

CCD camera, Image plane, Relay lens, Analyzer, Objective lens, Sample plane, Scan, Optical fiber, Spectrometer

This setup enables us to measure local spectrum of

thin cells with a resolution of ~10 μm.

The absorbance of micro domains in the cells shows higher absorbance in the isotropic phase than in the nematic of a (2, 18) mixture. The absorbance of the isotropic phase is larger than absorbances of the nematic phase measured with the sample oriented such that the director is parallel and perpendicular to the polarizer. The measurement indicates that SSY does not show any linear dichrosim in the nematic phase of the mixture and the birefringence comes from DSCG.

Spectroscopic measurements of the separated phases in the mixtures confirm that the concentrations of SSY in lower order phases are always larger than those of relatively higher order ones. For an example, the SSY concentration in the isotropic phase of the mixture of 2.3 wt% SSY and 12.7 wt% DSCG is about 30% higher than that of the nematic phase. On the other hand, the concentration of DSCG of the mixtures of lower order phases are always smaller than those of relatively higher order ones. Note: significant amounts of water were lost during the procedures to separate and measure the phases.

Initial wt% (SSY, DSCG) of SSY and DSCG mixture	Relative SSY Concentration of SSY-Rich and DSCG-Rich Phases	Relative DSCG Concentration of SSY-Rich and DSCG-Rich Phases
(2.3, 12.7)	1.3 (C_{Iso}/C_{Nem})	0.7 (C_{Iso}/C_{Nem})
(10, 10)	2.4 (C_{Nem}/C_M)	0.5 (C_{Nem}/C_M)

Discussions

We observe a tendency of SSY and DSCG partial mixing in both M and N phases to form SSY-rich and DSCG-rich phases. Linear dichroism of SSY is undetectable in the DSCG-rich phases when its concentration is low. However, it is detected in both SSY-rich and DSCG-rich phases when its concentration is high. More careful optical spectroscopic measurements of the mixtures is necessary to precisely determine the amount and orientational order of each chromonic material in the CLC phases of the mixtures. X-ray scattering as well as theoretical work will be also needed to elucidate the structure of the self-assembly of the two chromonics in water.

Summary

We study phases of the mixtures of SSY and DSCG dissolved in water. A variety of biphasic states, coexistence of three phases, and isotropic phase of the ternary mixtures is observed by optical microscopy and spectroscopy. A phase diagram of the mixtures is made based on this study. We find a tendency that SSY prefers to stay in relatively lower order phases while DSCG, in relatively higher order phases, confirmed by spectroscopy of separated phases of the mixtures. We also find that SSY is isotropic in DSCG-rich nematic phase of a mixture with low concentration of SSY. The mixing and separation of the chromonics and their structure in the mixtures is studied using precise measurement of local concentration of each material in each phases.

References

[1] N. H. Hartshorne, G. D. Woodward, Molecular Crystals and Liquid Crystals 23, 343-368 (1973).

[2] V. Horowitz, L. Janowitz, A. Modic, P. Heiney, P. Collings, Physical Review E 72, 041710 (2005).

[3] K. Simon, E. Burton, F. Cheng, N. Varghese, N. Falcone, L. Wu, Y. Luk, Chemistry of Materials 22, 2434-2441 (2010).

[4] Y. Yi and N. Clark, Liquid Crystals 40, 1736-1737 (2013).

Acknowledgements

Phases of SSY in Water

| Isotropic (I) 25 wt% | Nematic (N) 28 wt% | M or Columnar (C) 40 wt% | Linear Dichroism |

Modified from Park et al., J Phys. Chem. B (2008)

Phases of DSCG

Molecular Structure of DSCG

Phases of DSCG

| I 5 wt% | N 10 wt% | M (or C) 22 wt% |

Phase Diagram of DSCG

Lydon, Curr. Opin. Colloid Sci. (1998)